

Radiative corrections to decays of the 125 GeV Higgs boson in the complex Higgs triplet model

Masashi Aiko,^a Shinya Kanemura,^b Mariko Kikuchi,^c Kodai Sakurai,^{d,e} Sora Taniguchi^b and Kei Yagyu^f

^a*National Institute of Technology, Miyakonojo College, Miyakonojo, Miyazaki 885-8567, Japan*

^b*Department of Physics, University of Osaka, Toyonaka, Osaka 560-0043, Japan*

^c*Department of Physics, Saga University, 1 Honjomachi, Saga 840-8502, Japan*

^d*Department of Physics, Tohoku University, Sendai, Miyagi 980-8578, Japan*

^e*National Institute of Technology, Tsuruoka College, Tsuruoka, Yamagata 997-0842, Japan*

^f*Department of Physics, Tokyo University of Science, 1-3, Kagurazaka, Shinjuku-ku, Tokyo 162-8601, Japan*

E-mail: m-aiko@miyakonojo.kosen-ac.jp,
kanemu@het.phys.sci.osaka-u.ac.jp, mkikuchi@cc.saga-u.ac.jp,
kodai.sakurai@tsuruoka-nct.ac.jp,
taniguchi@het.phys.sci.osaka-u.ac.jp, yagyu@rs.tus.ac.jp

ABSTRACT: The extension of the Higgs sector with an additional complex triplet field is often considered for generating the neutrino mass by the Type-II seesaw mechanism. Such an extension generally predicts $\rho \neq 1$, where ρ is the electroweak rho parameter at the tree level, so that the renormalization of the electroweak parameters is different from models like the standard model (SM) and two Higgs doublet models. In this paper, we present a full set of radiative corrections to decays of the 125 GeV Higgs boson (h) in this model. One-loop contributions of the extra Higgs bosons as well as SM fermions and gauge bosons to the decay rates of h are calculated in the on-shell scheme. Gauge dependence appearing in the counter terms of mixing angles is eliminated by the pinch technique. Higher-order QCD corrections are also implemented. We find that the decay rates can significantly deviate from the predictions in the SM and other extensions such as the two Higgs doublet models and the singlet model. For example, the decay rates of $h \rightarrow WW^*$ and $h \rightarrow ZZ^*$ can be a few percent larger than the SM value under current experimental and theoretical constraints. In this case, deviations in $h \rightarrow \gamma\gamma$ and Higgs self-coupling can reach about -20% and 100% , respectively. The pattern of the deviations is different from the other extended Higgs models. These characteristic predictions are expected to be detected at the High-Luminosity LHC or future Higgs factories.

Contents

1	Introduction	1
2	The complex Higgs triplet model	3
2.1	The Higgs potential	4
2.2	The kinetic term and Yukawa interaction	5
2.3	Theoretical constraints	7
2.4	Decoupling limit	7
3	Renormalization and electroweak precision observables	8
3.1	Renormalization of the complex Higgs triplet model	8
3.2	The G_F input scheme	9
3.3	Electroweak precision observables	10
4	Gauge invariant scalar two-point functions	11
4.1	CP-even sector	12
4.2	CP-odd sector	16
5	Decays of the SM-like Higgs boson	20
5.1	Renormalized vertex functions	20
5.1.1	$h f \bar{f}$ vertex	20
5.1.2	$h VV$ vertex	21
5.1.3	$h VV'$ vertex	22
5.2	Decay rates of the SM-like Higgs boson	22
5.2.1	$h \rightarrow f \bar{f}$	22
5.2.2	$h \rightarrow ZZ^* \rightarrow Z f \bar{f}$	23
5.2.3	$h \rightarrow WW^* \rightarrow W f' \bar{f}$	25
5.2.4	$h \rightarrow gg, \gamma\gamma, Z\gamma$	27
5.3	Theoretical behaviors of radiative corrections	28
6	Deviations from the SM predictions in the Higgs boson decays	30
6.1	Constraints on the parameter space	30
6.2	Numerical results in the heaviest $H^{\pm\pm}$ scenario	33
6.2.1	Correlations in the decay rates of h	33
6.2.2	Correlations of the branching ratios of h	38
6.3	Numerical results in the lightest $H^{\pm\pm}$ scenario	40
7	Conclusions	43
A	Tree level scalar-vector couplings	44
B	1PI diagrams for $h f \bar{f}$ vertex	44

1 Introduction

The Standard Model (SM) has been confirmed as a successful theory explaining physics at the electroweak scale. However, there remain various mysteries that cannot be explained in the SM, such as neutrino oscillations, dark matter, the baryon asymmetry of the Universe, and inflation. Constructing new physics models to solve these unsolved problems is a goal in high-energy physics. While the Higgs boson with a mass of 125 GeV has been discovered, the structure of the Higgs sector has not been determined yet. The dynamics of electroweak symmetry breaking and the nature of the electroweak phase transition are also to be understood. Extensions of the Higgs sector of the SM are often introduced in new physics models, in which additional Higgs bosons are predicted. Although there are various types of extended Higgs sectors, many of them can be described by the simplest extensions with an additional scalar field at least approximately.

One of the simplest extensions is the model with an additional isospin triplet field with $Y = 1$, which we call the complex Higgs triplet model (CHTM). This model may be motivated by generating neutrino masses via the Type-II seesaw mechanism [1–5], for which allowed parameter regions consistent with current neutrino data are discussed in Ref. [6]. The triplet field can also be introduced for radiative seesaw models [7–10]. The CHTM can also appear in the low-energy theory of the left-right symmetric model [11–14]. Another motivation of this model is that the electroweak phase transition can be realized in this model, leading to characteristic predictions such as stochastic gravitational waves [15, 16] and deviations from the SM in the Higgs boson self-coupling [17, 18].

The experimental value of the electroweak rho parameter (ρ) is close to unity, which strongly constrains extended Higgs models. While $\rho = 1$ is guaranteed at tree level in the model with doublets and singlets, $\rho \neq 1$ is generally predicted in the CHTM¹. In order to satisfy the data, the vacuum expectation value (VEV) of the triplet field (v_Δ) has to be taken to be small. The fact that the CHTM predicts $\rho \neq 1$ at tree level requires a different framework of renormalization for electroweak parameters from the models with $\rho = 1$ at tree level [18, 21, 22].

The CHTM provides rich phenomenology in collider experiments because it contains multiple extra Higgs bosons such as two neutral Higgs bosons, singly charged Higgs bosons (H^\pm), and doubly charged Higgs bosons ($H^{\pm\pm}$). Direct searches for $H^{\pm\pm}$ are a definite way to distinguish the CHTM from other extensions like multi-doublet models at collider

¹In the Georgi-Machacek model [19, 20], in which the CHTM is included as a part of the particles content, $\rho = 1$ is predicted at tree level.

experiments. The decay pattern of $H^{\pm\pm}$ largely depends on the mass spectrum of additional Higgs bosons and the VEV of the triplet field. For example, the mass of $H^{\pm\pm}$ is strongly constrained from below by the leptonic decays ($H^{++} \rightarrow \ell^+ \ell^+$) when v_Δ is smaller than $\mathcal{O}(1)$ MeV [23]. On the other hand, for larger values of v_Δ , $H^{\pm\pm}$ mainly decays to $W^\pm W^\pm$. In Ref. [24], constraints for the mass of $H^{\pm\pm}$ via diboson searches have been investigated. In the case where mass differences among the additional Higgs bosons are relatively large, cascade decays of additional Higgs bosons become important. Such a case has been studied in Ref. [25]². In the triplet extension models, H^\pm can, in general, decay into $W^\pm Z$ with a large branching ratio [27–29], while such a decay process is suppressed in the model with a multi-doublet structure [30].

Apart from the direct searches for additional particles in extended Higgs sectors, measurements of the discovered Higgs boson with a mass of 125 GeV (h) have been intensively performed. In general, new physics effects deviate the couplings of h from the SM predictions, which are strongly model-dependent. Therefore, one can test various new physics models by precision measurements of the Higgs boson observables by detecting the pattern of deviations. The current measurement accuracy for the Higgs boson couplings is expected to be improved at the High-Luminosity LHC (HL-LHC) [31, 32] and future Higgs factories such as the International Linear Collider (ILC) [33–36], the Circular Electron-Positron Collider (CEPC) [37, 38], $e^+ e^-$ collisions of the Future Circular Collider (FCC-ee) [39, 40]. For example, the hWW coupling is measured with an accuracy of 1.6 (0.35)% at the HL-LHC (at the International linear collider) while the current measurement uncertainty at the LHC is 6% for ATLAS [41] and 8% for CMS experiments [42]. In order to determine the shape of the Higgs sector by utilizing such future high-precision data, the theoretical predictions for h observables also should be accurately evaluated in a variety of extended Higgs models, including higher-order corrections.

There are many previous works discussing radiative corrections in the context of the simple extended Higgs models with $\rho = 1$ at tree level. In two-Higgs doublet models (2HDMs), the influence of one-loop corrections to the Higgs boson couplings [43–47], the decays of h [48–50] and heavy Higgs bosons [51–58] are investigated. Similar studies have also been performed in the framework of the Higgs singlet model (HSM) [59–63]. Recently, two-loop corrections to h observables are also discussed in Refs. [64–71]. As a public tool to perform the numerical evaluations of higher-order corrections in the above extended Higgs models, the authors of this paper have developed the `H-COUP` program [72–74]. Apart from this program, other public tools such as `2HDECAY` [75], `ewN2HDECAY` [76], `EWsHDECAY` [63], `profecy4f` [77], and `FlexibleDecay` [78] are also available. The difference between these programs and `H-COUP` is the following. `H-COUP` evaluates the full one-loop corrections to all major decay modes of h and additional Higgs bosons within a common renormalization scheme for various extended Higgs models, thereby enabling a systematic comparison of predictions among different models.

The importance of precision calculations is also applied to the models with triplet scalar extensions. In Ref. [21], a renormalization scheme was proposed to evaluate higher

²From the recent CDF II results, large mass differences are strongly indicated in the CHTM [26].

order corrections to the electroweak precision parameters in the model with a real triplet scalar field. The renormalization scheme was extended to the CHTM in Ref. [22]. In Refs. [17, 18], the authors proposed an on-shell renormalization scheme for the Higgs sector in the CHTM, and clarified the importance of one-loop corrections of Higgs boson couplings to weak gauge bosons and Higgs self-couplings. However, radiative corrections to the Yukawa interactions were not studied in Refs. [17, 18]. Furthermore, the scalar mixing angles were not determined in a gauge independent way [79–81].

In this paper, we present a full set of radiative corrections to decays of the 125 GeV Higgs boson (h) in this model. One-loop contributions of the extra Higgs bosons as well as SM fermions and gauge bosons to the decay rates of h are calculated in the on-shell scheme. We first remove the gauge dependence of the scalar mixing angle by using the pinch technique [82–87]³ We then investigate in detail the decays of the Higgs boson, including NLO EW corrections and higher-order QCD corrections. Furthermore, we analyze the deviations from the SM predictions appearing in the Higgs boson decays. After taking into account theoretical and experimental constraints, we show that a characteristic pattern of deviations can be obtained, which allows us to distinguish the CHTM from other extended Higgs models. Compared to earlier works on the renormalization of the CHTM, this paper has the following new points. (1) We construct, for the first time in the CHTM, a gauge-invariant renormalization scheme by removing the gauge dependence from the on-shell renormalization of the scalar mixing angle. (2) Analytic formulae for the renormalized $h f \bar{f}$ vertex function are provided. (3) In the CHTM, the full one-loop corrections to the Higgs boson decay rates are calculated for the first time, and this includes not only the two-body decays of the Higgs boson but also the three-body decays.

This paper is organized as follows. In Sec. 2, we describe the Lagrangian of CHTM and discuss features of this model. After presenting how we perform renormalization in Sec. 3, we devote ourselves to discussions about the gauge dependence on the scalar mixing angles and the procedure to remove it in Sec. 4. We then describe the analytical formulae of decay rates of h in Sec. 5, and discuss numerical results for the deviations from the SM in h decays in Sec. 6. Conclusions are given in Sec. 7.

2 The complex Higgs triplet model

In this section, we define the Lagrangian of the CHTM and discuss theoretical constraints as well as the decoupling limit. We follow the notation of Refs. [17, 18]. The CHTM consists of a scalar doublet field Φ with hypercharge $Y = 1/2$ and a complex scalar triplet field Δ with $Y = 1$. After electroweak symmetry breaking, the scalar fields are parameterized as

$$\Phi = \begin{pmatrix} \phi^+ \\ \frac{1}{\sqrt{2}}(v_\phi + \phi + i\chi) \end{pmatrix}, \quad \Delta = \begin{pmatrix} \frac{1}{\sqrt{2}}\Delta^+ & \Delta^{++} \\ \Delta^0 & -\frac{1}{\sqrt{2}}\Delta^+ \end{pmatrix} \quad \text{with} \quad \Delta^0 = \frac{1}{\sqrt{2}}(v_\Delta + \delta + i\eta), \quad (2.1)$$

³Other gauge invariant renormalization schemes for extended Higgs sectors are discussed in e.g., Refs. [88, 89]. Focusing on two-body scattering processes, we demonstrate how the appropriate pinch terms can be extracted.

where v_ϕ and v_Δ denote the VEVs, which satisfy $v^2 = v_\phi^2 + 2v_\Delta^2 \simeq 246$ GeV.

2.1 The Higgs potential

The most general Higgs potential constructed from Φ and Δ is given by

$$\begin{aligned} V(\Phi, \Delta) = & m^2 \Phi^\dagger \Phi + M^2 \text{Tr}(\Delta^\dagger \Delta) + \left[\mu \Phi^T i\sigma_2 \Delta^\dagger \Phi + \text{h.c.} \right] \\ & + \lambda_1 (\Phi^\dagger \Phi)^2 + \lambda_2 \left[\text{Tr}(\Delta^\dagger \Delta) \right]^2 + \lambda_3 \text{Tr}[(\Delta^\dagger \Delta)^2] \\ & + \lambda_4 (\Phi^\dagger \Phi) \text{Tr}(\Delta^\dagger \Delta) + \lambda_5 \Phi^\dagger \Delta \Delta^\dagger \Phi, \end{aligned} \quad (2.2)$$

where m^2 , M^2 and λ_{1-5} are real parameters, whereas μ is in general complex. Since the relative phase between Φ and Δ only affects the μ term in the Higgs potential, the phase of μ can be removed by an appropriate field redefinition. Thus, all parameters in the Higgs potential can be taken as real without loss of generality [90]. In the following, we work in the basis where μ is real.

From the stationary conditions of the Higgs potential, we obtain

$$m^2 = -\lambda_1 v_\phi^2 - \frac{1}{2}(\lambda_4 + \lambda_5)v_\Delta^2 + \sqrt{2}\mu v_\Delta, \quad (2.3)$$

$$M^2 = -(\lambda_2 + \lambda_3)v_\Delta^2 - \frac{1}{2}(\lambda_4 + \lambda_5)v_\phi^2 + \frac{\mu v_\phi^2}{\sqrt{2}v_\Delta}. \quad (2.4)$$

The mass matrices for the singly charged states (\mathcal{M}_\pm^2), the CP-odd states ($\mathcal{M}_{\text{odd}}^2$), and the CP-even states ($\mathcal{M}_{\text{even}}^2$) are obtained as

$$\mathcal{M}_\pm^2 = \left(\frac{\mu v_\phi^2}{\sqrt{2}v_\Delta} - \frac{\lambda_5}{4}v_\phi^2 \right) \begin{pmatrix} 2v_\Delta^2/v_\phi^2 & -\sqrt{2}v_\Delta/v_\phi \\ -\sqrt{2}v_\Delta/v_\phi & 1 \end{pmatrix}, \quad (2.5)$$

$$\mathcal{M}_{\text{odd}}^2 = \frac{\mu v_\phi^2}{\sqrt{2}v_\Delta} \begin{pmatrix} 4v_\Delta^2/v_\phi^2 & -2v_\Delta/v_\phi \\ -2v_\Delta/v_\phi & 1 \end{pmatrix}, \quad \mathcal{M}_{\text{even}}^2 = \begin{pmatrix} \mathcal{M}_{11}^2 & \mathcal{M}_{12}^2 \\ \mathcal{M}_{21}^2 & \mathcal{M}_{22}^2 \end{pmatrix}, \quad (2.6)$$

where the components of $\mathcal{M}_{\text{even}}^2$ are given by

$$\begin{aligned} \mathcal{M}_{11}^2 &= 2\lambda_1 v_\phi^2, \quad \mathcal{M}_{22}^2 = \frac{\mu v_\phi^2}{\sqrt{2}v_\Delta} + 2(\lambda_2 + \lambda_3)v_\Delta^2, \\ \mathcal{M}_{12}^2 &= \mathcal{M}_{21}^2 = (\lambda_4 + \lambda_5)v_\phi v_\Delta - \sqrt{2}\mu v_\phi. \end{aligned} \quad (2.7)$$

We define the mass eigenstates as

$$\begin{pmatrix} \phi^\pm \\ \Delta^\pm \end{pmatrix} = R(\beta) \begin{pmatrix} G^\pm \\ H^\pm \end{pmatrix}, \quad \begin{pmatrix} \chi \\ \eta \end{pmatrix} = R(\beta') \begin{pmatrix} G^0 \\ A \end{pmatrix}, \quad \begin{pmatrix} \phi \\ \delta \end{pmatrix} = R(\alpha) \begin{pmatrix} h \\ H \end{pmatrix}, \quad (2.8)$$

where G^\pm and G^0 denote the Nambu–Goldstone (NG) bosons. The rotation matrix is given by

$$R(\theta) = \begin{pmatrix} c_\theta & -s_\theta \\ s_\theta & c_\theta \end{pmatrix}, \quad (2.9)$$

with the shorthand notation $c_\theta = \cos \theta$ and $s_\theta = \sin \theta$. In this paper, we identify h with the SM-like Higgs boson with a mass of 125 GeV. The mixing angles are given by

$$\tan \beta = \frac{\sqrt{2}v_\Delta}{v_\phi}, \quad \tan \beta' = \frac{2v_\Delta}{v_\phi}, \quad \tan 2\alpha = \frac{2\mathcal{M}_{12}^2}{\mathcal{M}_{11}^2 - \mathcal{M}_{22}^2}. \quad (2.10)$$

The mixing angles of the charged states (β) and the CP-odd states (β') differ because Φ and Δ belong to different representations of $SU(2)_L$. Nevertheless, they are not independent: $\tan \beta = \tan \beta'/\sqrt{2}$. The masses of the physical Higgs bosons are obtained as

$$m_{H^{\pm\pm}}^2 = \frac{\mu v_\phi^2}{\sqrt{2}v_\Delta} - \lambda_3 v_\Delta^2 - \frac{\lambda_5}{2} v_\phi^2, \quad (2.11)$$

$$m_{H^\pm}^2 = \left(\frac{\mu v_\phi^2}{\sqrt{2}v_\Delta} - \frac{\lambda_5}{4} v_\phi^2 \right) \left(1 + \frac{2v_\Delta^2}{v_\phi^2} \right), \quad m_A^2 = \frac{\mu v_\phi^2}{\sqrt{2}v_\Delta} \left(1 + \frac{4v_\Delta^2}{v_\phi^2} \right), \quad (2.12)$$

$$m_h^2 = \mathcal{M}_{11}^2 c_\alpha^2 + \mathcal{M}_{22}^2 s_\alpha^2 + 2\mathcal{M}_{12}^2 s_\alpha c_\alpha, \quad m_H^2 = \mathcal{M}_{11}^2 s_\alpha^2 + \mathcal{M}_{22}^2 c_\alpha^2 - 2\mathcal{M}_{12}^2 s_\alpha c_\alpha. \quad (2.13)$$

We note that the CP-odd Higgs boson becomes massless in the $\mu \rightarrow 0$ limit with nonzero v_Δ . This is because the Higgs potential respects a global $U(1)$ symmetry when $\mu = 0$, in which case the CP-odd Higgs boson becomes an additional NG boson.

The original seven parameters in the Higgs potential can be expressed in terms of the masses of the Higgs bosons and the mixing angles. The explicit relations are provided, for instance, in Ref. [18]. It is convenient to take λ_4 as an input parameter instead of the mixing angle α , which is related by

$$\sin(2\alpha) = \frac{2v_\phi v_\Delta}{m_H^2 - m_h^2} \left[\frac{4m_{H^\pm}^2}{v_\phi^2 + 2v_\Delta^2} - \frac{2m_A^2}{v_\phi^2 + 4v_\Delta^2} - \lambda_4 \right]. \quad (2.14)$$

Thus, we choose the following parameters as input:

$$v, \quad m_h^2, \quad m_H^2, \quad m_A^2, \quad m_{H^\pm}^2, \quad m_{H^{\pm\pm}}^2, \quad \lambda_4, \quad \beta'. \quad (2.15)$$

We note that the following condition must be satisfied since $\mathcal{M}_{\text{even}}^2$ is a real symmetric matrix.

$$(m_H^2 - m_h^2)^2 \geq 4(\mathcal{M}_{12}^2)^2. \quad (2.16)$$

This is equivalent to requiring $|\sin(2\alpha)| \leq 1$.

2.2 The kinetic term and Yukawa interaction

The kinetic terms are given by

$$\mathcal{L}_{\text{Kin}} = (D_\mu \Phi)^\dagger (D^\mu \Phi) + \text{Tr} \left[(D_\mu \Delta)^\dagger D^\mu \Delta \right], \quad (2.17)$$

where the covariant derivatives are defined as

$$D_\mu \Phi = (\partial_\mu - ig\tau^a W_\mu^a - ig'Y B_\mu) \Phi, \quad D_\mu \Delta = \partial_\mu \Delta - ig[\tau^a W_\mu^a, \Delta] - ig'Y B_\mu \Delta, \quad (2.18)$$

with the commutator $[a, b] = ab - ba$. Here, τ^a denotes the $SU(2)_L$ generators defined as $\tau^a = \sigma^a/2$ with the Pauli matrices σ^a .

The masses of the weak gauge bosons are obtained as

$$m_W^2 = \frac{g^2}{4}(v_\phi^2 + 2v_\Delta^2), \quad m_Z^2 = \frac{g_Z^2}{4}(v_\phi^2 + 4v_\Delta^2), \quad (2.19)$$

with $g_Z = g/c_W$ and $\tan\theta_W = g'/g$. At tree level, the electroweak ρ parameter is given by

$$\rho_0 = \frac{m_W^2}{m_Z^2 c_W^2} = \frac{v_\phi^2 + 2v_\Delta^2}{v_\phi^2 + 4v_\Delta^2}. \quad (2.20)$$

Thus, unlike in the SM, ρ_0 deviates from unity in the CHTM. The global fit result for the electroweak ρ parameter, $\rho_{\text{exp}} = 1.00031 \pm 0.00019$ [91], implies the bound $v_\Delta \lesssim 1.45$ GeV from Eq. (2.20). However, we note that the tree-level contribution is of the same order as loop corrections, i.e., $v_\Delta/v \simeq (16\pi^2)^{-1}$. Therefore, one-loop effects would modify the tree-level bound on v_Δ . The one-loop analysis of electroweak precision observables is discussed in Sec. 6.

The Yukawa sector of the CHTM consists of the Φ and Δ parts: $\mathcal{L}^Y = \mathcal{L}_\Phi^Y + \mathcal{L}_\Delta^Y$. The Φ part is identical to the Yukawa sector in the SM, while the Δ part is given by

$$\mathcal{L}_\Delta^Y = h_{ij} (\overline{L}_L^c)_i i\tau_2 \Delta (L_L)_j + \text{h.c.}, \quad (2.21)$$

where h_{ij} is a 3×3 complex symmetric matrix. The Δ part generates neutrino masses via the Type-II seesaw mechanism [1–5]. In the following analysis of the SM-like Higgs boson decays, we neglect contributions from the neutrino Yukawa couplings h_{ij} . These are sufficiently small to reproduce the observed neutrino oscillation data in the parameter region of interest in this paper.

From \mathcal{L}_Φ^Y , the Yukawa interactions in the mass basis are obtained as

$$\begin{aligned} \mathcal{L}_\Phi^Y \supset & - \sum_{f=u,d,e} \frac{m_f}{v} [\overline{f} f (\zeta_h h + \zeta_H H) - 2i I_f \overline{f} \gamma_5 f (\zeta_{G^0} G^0 + \zeta_A A)] \\ & + \left[\left(\frac{\sqrt{2}m_u}{v} V_{ud} \overline{u} P_L d - \frac{\sqrt{2}m_d}{v} V_{ud} \overline{u} P_R d \right) (\zeta_{G^\pm} G^\pm + \zeta_{H^\pm} H^\pm) + \text{h.c.} \right] \\ & - \left[\frac{\sqrt{2}m_e}{v} \overline{\nu} P_R e (\zeta_{G^\pm} G^\pm + \zeta_{H^\pm} H^\pm) + \text{h.c.} \right], \end{aligned} \quad (2.22)$$

where I_f denotes the weak isospin of a fermion f , and V_{ud} the CKM matrix. In the following analysis, we neglect the effects of quark mixing because they are small, and take the CKM matrix to be unity. The coupling modifiers ζ_X are given by

$$\begin{aligned} \zeta_h &= c_\alpha/c_\beta, & \zeta_{G^0} &= c_{\beta'}/c_\beta, & \zeta_{G^\pm} &= 1, \\ \zeta_H &= -s_\alpha/c_\beta, & \zeta_A &= -s_{\beta'}/c_\beta, & \zeta_{H^\pm} &= -s_\beta/c_\beta. \end{aligned} \quad (2.23)$$

2.3 Theoretical constraints

The potential parameters are required to satisfy theoretical constraints from vacuum stability and tree-level unitarity. Vacuum stability demands that the Higgs potential be bounded from below at large field values, thereby ensuring the stability of the electroweak vacuum. The necessary and sufficient conditions for vacuum stability are given [92]

$$\begin{aligned} \lambda_1 > 0, \quad \lambda_2 + \text{MIN}\left[\lambda_3, \frac{\lambda_3}{2}\right] > 0, \\ \lambda_4 + \text{MIN}[0, \lambda_5] + 2\text{MIN}\left[\sqrt{\lambda_1(\lambda_2 + \lambda_3)}, \sqrt{\lambda_1\left(\lambda_2 + \frac{\lambda_3}{2}\right)}\right] > 0. \end{aligned} \quad (2.24)$$

Tree-level unitarity requires that the eigenvalues of the two-to-two scalar scattering matrix do not exceed $\zeta_{\text{LQT}} = 1$ [93, 94] or $1/2$ [95, 96], depending on the choice of unitarity criterion. In the CHTM, there are twelve independent eigenvalues [92]⁴.

$$\begin{aligned} y_1 &= 2\lambda_1, \quad y_2 = 2(\lambda_2 + \lambda_3), \quad y_3 = 2\lambda_2, \\ y_{4,\pm} &= \lambda_1 + \lambda_2 + 2\lambda_3 \pm \sqrt{(\lambda_1 - \lambda_2 - 2\lambda_3)^2 + \lambda_5^2}, \\ y_{5,\pm} &= 3\lambda_1 + 4\lambda_2 + 3\lambda_3 \pm \sqrt{(3\lambda_1 - 4\lambda_2 - 3\lambda_3)^2 + \frac{3}{2}(2\lambda_4 + \lambda_5)^2}, \\ y_6 &= \lambda_4, \quad y_7 = \lambda_4 + \lambda_5, \quad y_8 = \frac{1}{2}(2\lambda_4 + 3\lambda_5), \\ y_9 &= \frac{1}{2}(2\lambda_4 - \lambda_5), \quad y_{10} = 2\lambda_2 - \lambda_3. \end{aligned} \quad (2.25)$$

For $a_i = y_i/(16\pi)$, the tree-level unitarity bound is given by $|a_i| \leq \zeta_{\text{LQT}}$. In this paper, we take $\zeta_{\text{LQT}} = 1$. In addition to tree-level unitarity, we impose the perturbativity constraint $|\lambda_i| \leq 4\pi$.

2.4 Decoupling limit

From Eq. (2.20), it follows that v_Δ must vanish in the decoupling limit of the triplet field. This requirement results from the stationary condition in Eq. (2.4), which yields

$$v_\Delta = \frac{\mu v_\phi^2}{\sqrt{2} \left[M^2 + (\lambda_2 + \lambda_3)v_\Delta^2 + (\lambda_4 + \lambda_5)v_\phi^2/2 \right]}. \quad (2.26)$$

Then, in the limit $M^2 \rightarrow \infty$, decoupling is realized with $v_\Delta \sim \mu v_\phi^2/(\sqrt{2}M^2) \rightarrow 0$. Alternatively, $v_\Delta \rightarrow 0$ can be realized by taking $\mu \rightarrow 0$, even if M^2 is of the order of the electroweak scale. In this case, Eq. (2.26) shows that $v_\Delta \sim \mu$. If one takes the limit $\mu \rightarrow 0$ while keeping nonzero v_Δ , an additional NG boson (A) emerges as mentioned earlier in this section.

From Eq. (2.23) and Table 1 in Appendix A, one finds that the coupling modifiers of $h\bar{f}f$, hZZ and hWW become unity when $v_\Delta = 0$. Thus, the SM-like Higgs boson couplings

⁴The similar analysis was performed in the context of the Georgi-Machacek model [97].

also approach their SM values in the $v_\Delta \rightarrow 0$ limit. We note that $\sin(2\alpha)$ is proportional to v_Δ (see Eq. (2.14)). Hence, as long as the λ_i couplings remain perturbative, $v_\Delta \rightarrow 0$ implies $\alpha \rightarrow 0$.

3 Renormalization and electroweak precision observables

In this section, we describe the renormalization of the CHTM and the G_F input scheme adopted in our calculation. We also discuss the electroweak precision observables, which are employed to constrain the CHTM parameters in numerical analysis.

3.1 Renormalization of the complex Higgs triplet model

In models with $\rho_0 = 1$ such as the SM, the electroweak sector is characterized by three independent input parameters, conventionally chosen to be α_{em} , m_W , and m_Z [98, 99]. In contrast, in models with $\rho_0 \neq 1$ including the CHTM, an additional input parameter is required to specify the electroweak sector.

Depending on the choice of the additional input parameter, several renormalization schemes can be defined. In Ref. [21], the effective weak mixing angle of the electron, s_e^2 , is adopted as the additional input in the real Higgs triplet model. This renormalization scheme was extended to the CHTM in Ref. [22]. It was pointed out that the existence of the decoupling limit is non-trivial in this scheme [22, 100–102]. The reason is that v_Δ becomes an output parameter, whose value is fixed at some nonzero value when one inputs $s_e^2 \neq (s_e^2)_{\text{SM}}$, where $(s_e^2)_{\text{SM}}$ denotes the SM prediction. As a result, the limit $v_\Delta \rightarrow 0$, which is required to realize the decoupling of the triplet field, cannot be freely taken. To make the decoupling behavior manifest, a renormalization scheme based on the $\overline{\text{MS}}$ -renormalized triplet VEV was proposed in Ref. [102] (see also Ref. [103]).

In this paper, we mainly follow renormalization scheme II of Ref. [18], in which the mixing angle β' is taken as an additional input parameter and is renormalized by imposing an on-shell condition on the G^0 – A mixing (see also Ref. [43]). In this scheme, all counterterms are fixed by the on-shell conditions, and the decoupling limit can be realized by taking $\beta' \rightarrow 0$. The conventional input parameters, α_{em} , m_W , and m_Z , are also used to specify the electroweak sector and are renormalized according to the on-shell conditions [98, 99].

Our calculation differs from that in Ref. [18] in two aspects. The first concerns the treatment of gauge dependence. Mixing counterterms depend on the gauge choice when these are renormalized using off-diagonal components of the two-point function [57]. To eliminate the gauge dependence, we employ the pinch technique [82–87] for the first time to the CHTM⁵, which will be discussed in Sec. 4⁶.

The second concerns the tadpole renormalization. There are two schemes for tadpole renormalization: the standard tadpole scheme [106] and the alternative tadpole scheme [107]. For convenience in the subsequent analysis, we adopt the alternative tadpole scheme,

⁵The similar analysis has been done in the Georgi–Machacek model [104].

⁶One may use physical processes to renormalize the mixing angles in a gauge-invariant way, and applications for extended Higgs models are discussed in, e.g., Refs. [57, 88, 89, 105].

whereas the standard tadpole scheme is employed in Ref. [18]. In the alternative tadpole scheme, tadpole-inserted diagrams are included in all self-energies.

$$\Pi_{ij}(p^2) = \Pi_{ij}^{\text{1PI}}(p^2) + \Pi_{ij}^{\text{Tad}}. \quad (3.1)$$

Then, the counterterms are determined with $\Pi_{ij}(p^2)$. We also include tadpole inserted diagrams in all vertex contributions. Although the expressions for the counterterms depend on the tadpole scheme, there is no scheme difference in the renormalized quantities in the CHTM⁷.

We here comment on the renormalization of the Yukawa Lagrangian. Since the doublet part, \mathcal{L}_Φ^Y , is identical to that in the SM, its renormalization is performed in the same manner as in the SM [98, 99, 106]. On the other hand, the triplet part, \mathcal{L}_Δ^Y , is irrelevant for the decays of the SM-like Higgs boson and is therefore neglected. It would become relevant when studying loop corrections to the decays of the additional Higgs bosons, but this is beyond the scope of this paper.

In the following, we discuss the input scheme for one-loop calculations and electroweak precision observables in the CHTM. We denote the renormalized two-point function of the gauge bosons by $\hat{\Pi}_{VV}(p^2)$, whose explicit expressions are given in Ref. [18].

3.2 The G_F input scheme

In our calculation, we use the Fermi constant G_F as an input instead of m_W . For this replacement, we employ the following relation.

$$G_F = \frac{1}{\sqrt{2}v^2(1 - \Delta r)} \quad \text{with} \quad v^2 = \frac{m_W^2}{\pi\alpha_{\text{em}}} \left(1 - \frac{m_W^2}{\rho_0 m_Z^2}\right). \quad (3.2)$$

The Δr parameter is determined by the muon decay process and is given by [109]

$$\Delta r = \frac{\text{Re } \hat{\Pi}_{WW}(0)}{m_W^2} + \delta_{VB}, \quad (3.3)$$

where δ_{VB} correction represents vertex and box contributions. At the one-loop level, it is expressed as [21]

$$\delta_{VB} = \frac{\alpha_{\text{em}}}{4\pi s_W^2} \left[6 + \frac{10(1 - s_W^2) - 3(R/c_W^2)(1 - 2s_W^2)}{2(1 - R)} \ln R \right] \quad \text{with} \quad R = \frac{m_W^2}{m_Z^2}. \quad (3.4)$$

The right-hand side of Eq. (3.2) is a function of $\alpha_{\text{em}}, m_W, m_Z$ and β' ⁸. Thus, the value of m_W that reproduces the observed value of G_F for given α_{em}, m_Z and β' can be determined by solving Eq. (3.2) iteratively [21, 99].

Instead of iteratively solving Eq. (3.2), we adopt an alternative approach introducing \bar{m}_W as [48]

$$\bar{m}_W^2 = \rho_0 m_Z^2 \bar{c}_W^2 \quad \text{with} \quad \bar{c}_W^2 = 1 - \bar{s}_W^2, \quad (3.5)$$

⁷Such a cancellation is non-trivial when $\overline{\text{MS}}$ renormalized counterterms are involved, as in the two Higgs doublet model and the Higgs singlet model [108].

⁸It also depends on the other inputs such as $m_h, m_t, m_{H^{\pm\pm}}$ and so on.

where \bar{s}_W is given as a function of $\alpha_{\text{em}}, G_F, m_Z$ and β' .

$$\bar{s}_W^2 = \frac{1}{2} \left(1 - \sqrt{1 - \frac{4A_0}{\rho_0 m_Z^2}} \right) \quad \text{with} \quad A_0 = \frac{\pi \alpha_{\text{em}}}{\sqrt{2} G_F}. \quad (3.6)$$

At the one-loop level, Δr can be evaluated using \bar{m}_W instead of m_W , since Δr is a one-loop quantity and the difference would only appear at the two-loop level. From Eq. (3.2), the weak mixing angle and the W boson mass are written as

$$s_{W,G_F}^2 = \frac{1}{2} \left[1 - \sqrt{1 - \frac{4A_0}{\rho_0 m_Z^2 (1 - \Delta r)}} \right], \quad m_{W,G_F}^2 = \rho_0 m_Z^2 c_W^2. \quad (3.7)$$

They coincide with s_W^2 and m_W^2 , which are obtained by iteratively solving Eq. (3.2), at the one-loop level. In subsequent analysis, we use \bar{m}_W and \bar{s}_W for loop calculations similar to Δr . Since \bar{m}_W is not the on-shell mass and is not the Lagrangian parameter in the on-shell scheme, we use m_{W,G_F} instead of \bar{m}_W for tree-level calculations. In addition, we use m_{W,G_F} for a kinematical factor involving processes with external W bosons, such as $h \rightarrow WW^*$.

Finally, we discuss the treatment of β' . Since β' is not convenient as an input for numerical analysis, we introduce \bar{v}_Δ defined by

$$\bar{v}_\phi^2 + 2\bar{v}_\Delta^2 = \bar{v}^2 \quad \text{with} \quad \bar{v}^2 = \frac{1}{\sqrt{2} G_F}, \quad (3.8)$$

and take $\tan \beta' = 2\bar{v}_\Delta / \bar{v}_\phi$ according to the tree-level relation in Eq. (2.10). From Eq. (3.2), v_Δ can be expressed as

$$v_{\Delta,G_F}^2 = \frac{s_{\beta'}^2}{2(1 + c_{\beta'}^2)} \frac{1}{\sqrt{2} G_F (1 - \Delta r)}. \quad (3.9)$$

Thus, similar to s_{W,G_F}^2 and m_{W,G_F}^2 , v_{Δ,G_F} can be calculated for given $\alpha_{\text{em}}, G_F, m_Z$ and β' . Since $\beta' = 0$ corresponds to $v_{\Delta,G_F} = 0$, the decoupling limit can be realized by taking the renormalized mixing angle β' to be zero in our scheme.

3.3 Electroweak precision observables

The electroweak precision observables, such as the effective mixing angle and Z -boson decay rates, can be expressed in terms of the effective Zff couplings. They are given by [21]

$$g_V^f = 2 \left(\frac{\rho_0 (1 - \Delta r)}{1 + \hat{\Pi}'_Z(m_Z^2)} \right)^{1/2} \times \left[\frac{I_f}{2} - Q_f s_W^2 \left(1 + \frac{c_W}{s_W} \frac{\hat{\Pi}_{Z\gamma}(m_Z^2)}{m_Z^2 + \hat{\Pi}_{\gamma\gamma}(m_Z^2)} \right) + \Gamma_{Zff}^{\text{V,loop}}(0, 0, m_Z^2) \right], \quad (3.10)$$

$$g_A^f = 2 \left(\frac{\rho_0 (1 - \Delta r)}{1 + \hat{\Pi}'_Z(m_Z^2)} \right)^{1/2} \left[\frac{I_f}{2} + \Gamma_{Zff}^{\text{A,loop}}(0, 0, m_Z^2) \right]. \quad (3.11)$$

where Q_f denotes the electric charge of a fermion.

$$\hat{\Pi}'_Z(p^2) = \text{Re} \left. \frac{d\hat{\Pi}_Z(p^2)}{dp^2} \right|_{p^2=m_Z^2} \quad \text{with} \quad \hat{\Pi}_Z(p^2) = \hat{\Pi}_{ZZ}(p^2) - \frac{\left[\hat{\Pi}_{Z\gamma}(p^2) \right]^2}{p^2 + \hat{\Pi}_{\gamma\gamma}(p^2)}. \quad (3.12)$$

The expressions for the loop-corrected vertices $\Gamma_{Zf\bar{f}}^{V/A,\text{loop}}(0,0,p^2)$ are the same as those in the SM in the massless limit of the external fermions. Explicit formulae can be found, for instance, in Ref. [48].

The effective weak mixing angle at the Z pole, s_f^2 , is defined as

$$s_f^2 = \frac{1}{4|Q_f|} \left(1 - \frac{\text{Re}(g_V^f)}{\text{Re}(g_A^f)} \right). \quad (3.13)$$

The leptonic decay rate of the Z boson is given by

$$\Gamma(Z \rightarrow \ell\bar{\ell}) = \frac{\sqrt{2}m_Z^3 G_F}{12\pi} \left[(g_V^\ell)^2 + (g_A^\ell)^2 \right] \left(1 + Q_\ell^2 \frac{3\alpha_{\text{em}}}{4\pi} \right). \quad (3.14)$$

We also introduce the loop-corrected ρ parameter

$$\rho = \rho_0 + \Delta\rho, \quad (3.15)$$

where $\Delta\rho$ is given by [18]

$$\Delta\rho = \text{Re} \left[\frac{\Pi_{ZZ}(0)}{m_Z^2} - \frac{\Pi_{WW}(0)}{m_W^2} + \frac{2s_W}{c_W} \frac{\Pi_{Z\gamma}(0)}{m_Z^2} - \frac{s_{2\beta'}}{1 + c_{\beta'}^2} \delta\beta' \right], \quad (3.16)$$

with the mixing counterterm $\delta\beta'$ given in Eq. (4.3). The analytical expressions for the transverse part of the gauge-boson two-point functions $\Pi_{VV'}(p^2)$ ($V, V' = \gamma, Z, W$) are given in Ref. [18]. We use these quantities to impose the experimental constraints. See the discussion in Sec. 6.

4 Gauge invariant scalar two-point functions

In this section, we discuss a prescription for removing the gauge dependence from the two-point functions of the scalar bosons. The unrenormalized two-point functions have the gauge dependence through 1PI diagrams involving gauge bosons, NG bosons, and Faddeev-Popov ghost fields. Thanks to the Nielsen identity [110] in the alternative tadpole scheme, the gauge-dependent part of the two-point function defined in Eq. (3.1) for a single scalar field $\Pi_{\phi\phi}$ is proportional to $(p^2 - m_\phi^2)$. Therefore, by imposing the on-shell condition for the renormalized two-point function, the gauge dependence vanishes. As a consequence, the mass counterterm becomes gauge-independent. In contrast, for the off-diagonal self-energy $\Pi_{\phi\phi'}$ ($\phi \neq \phi'$), the gauge dependence is not removed even under the on-shell condition. Because of this, counterterms of the mixing angles such as $\delta\alpha$, acquire the gauge dependence.

We employ the pinch technique [82–87], in which the gauge dependence in the two-point functions is canceled by adding the pinch terms extracted from the $f\bar{f} \rightarrow f\bar{f}$ scattering process. Namely, we extract the gauge dependent parts of the vertex corrections, the box corrections and the wave-function renormalization of the external fermions in the $f\bar{f} \rightarrow f\bar{f}$ process, and add them into the self-energy corrections such that the gauge dependence of the latter is canceled. We follow the procedure for extracting these pinch terms as described in Ref. [108], where the pinch terms of two-point functions in the 2HDMs and the HSM are discussed in detail. In this paper, the two-point functions of the CP-even and CP-odd scalar fields are used to determine the counterterms in the scalar sector, while those of the charged scalar fields are not used for the renormalization. We thus focus on the discussion of the pinch terms for the CP-even and CP-odd scalar sectors.

The pinch terms $\Pi_{ij}^{\text{PT}}(p^2)$ derived in this section are included in the self-energies as follows,

$$\tilde{\Pi}_{ij}(p^2) = \Pi_{ij}^{\text{1PI}}(p^2) + \Pi_{ij}^{\text{Tad}} + \Pi_{ij}^{\text{PT}}(p^2). \quad (4.1)$$

which is gauge independent. As a result, the pinch terms are also added in counterterms of the mixing angles as follows,

$$\delta\alpha = -\frac{1}{2(m_H^2 - m_h^2)} \left(\tilde{\Pi}_{Hh}(m_H^2) + \tilde{\Pi}_{Hh}(m_h^2) \right), \quad (4.2)$$

$$\delta\beta' = -\frac{1}{2m_A^2} \left(\tilde{\Pi}_{AG^0}(m_A^2) + \tilde{\Pi}_{AG^0}(0) \right). \quad (4.3)$$

Since β is related to β' as given in Eq. (2.10), $\delta\beta$ can be written as $\delta\beta = (1 + s_\beta^2) \delta\beta' / \sqrt{2}$. We note that these pinched counterterms $\delta\alpha$, $\delta\beta$ and $\delta\beta'$ are applied to the counterterms generated via the parameter shifts but not to those generated via the field shifts for off-diagonal components (see Eq. (93) of [18]).

In this section, we introduce the following expression calculated by the R_ξ gauge

$$\mathcal{O}_{\xi_V} = \mathcal{O}|_{\xi_V=1} + \mathcal{O}|_{\text{G.D.}}, \quad (4.4)$$

where the first term on the RHS represents the quantity calculated in the 't Hooft–Feynman gauge, and the second term depends on the gauge parameter ξ_V ($V = W, Z, \gamma$). We also introduce the shorthand notation for the Passarino–Veltman functions [111], defined as

$$C_0(p^2; X, Y) \equiv \frac{1}{m_X^2 - m_Y^2} [B_0(p^2; X, X) - B_0(p^2; Y, Y)], \quad (4.5)$$

$$C_0(p^2; X, Y, Z) \equiv \frac{1}{m_X^2 - m_Y^2} [B_0(p^2; X, Z) - B_0(p^2; Y, Z)], \quad (4.6)$$

which are convenient in the following calculations.

4.1 CP-even sector

We first discuss the calculation of the pinch terms for two-point functions of the CP-even scalar fields h_i ($h_1 = h$, $h_2 = H$). Fig. 1⁹ presents the diagrams for the gauge-dependent

⁹For drawing the Feynman diagrams, we have used **Feynman diagram maker** [112] and **TikZ-FeynHand** [113, 114].

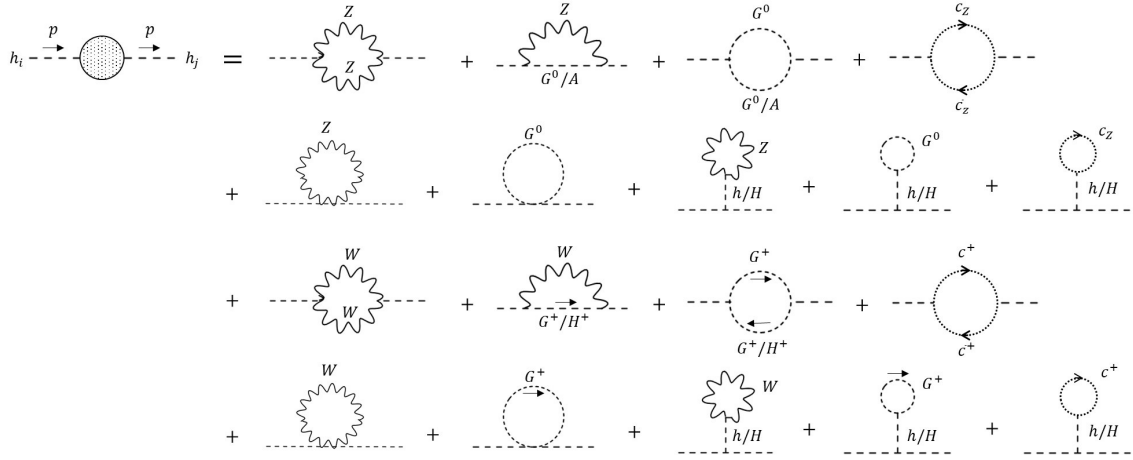


Figure 1: Diagrams dependent on the gauge parameters ξ_V for the self-energy of the CP-even Higgs bosons.

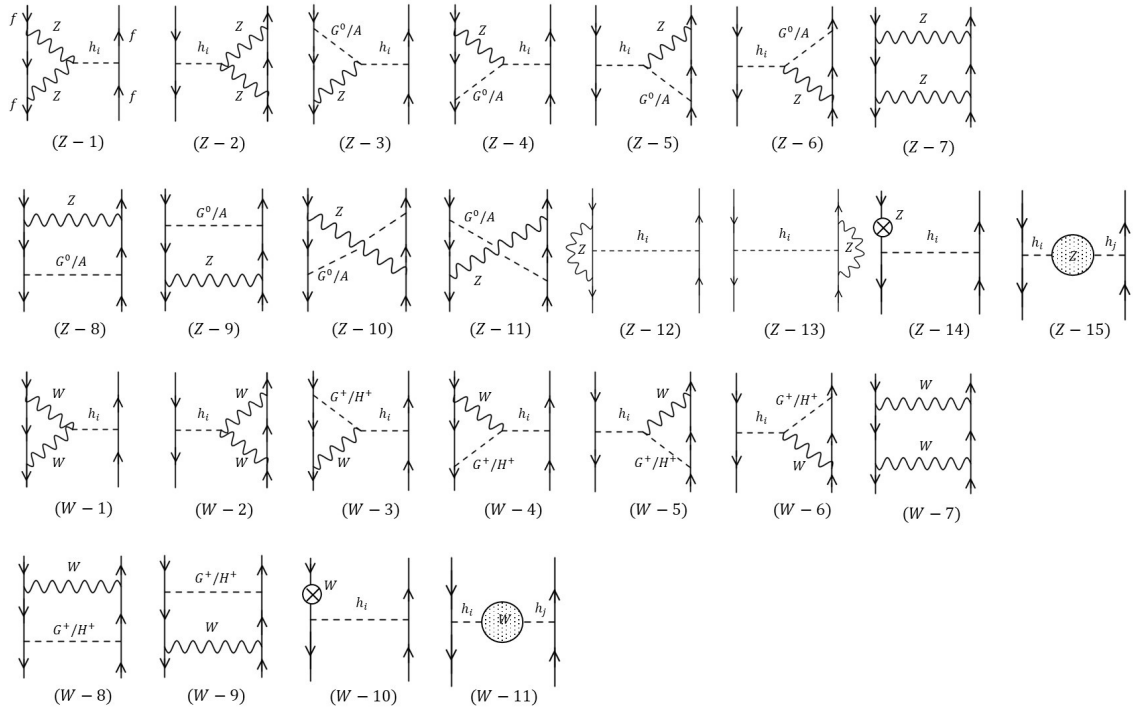


Figure 2: Diagrams dependent on the gauge parameters ξ_V for two-point functions of the CP-even Higgs bosons in the $f\bar{f} \rightarrow f\bar{f}$ scattering.

two-point functions of the CP-even scalar fields. To extract the pinch terms, we consider the $f\bar{f} \rightarrow f\bar{f}$ scattering process and introduce the reduced amplitude $\bar{\mathcal{M}}$, defined as

$$\mathcal{M} = \bar{\mathcal{M}} \left(\frac{m_f}{v} \right)^2 (\bar{f}f) \times (\bar{f}f). \quad (4.7)$$

The diagrams that contain the gauge-dependent contributions to the $f\bar{f} \rightarrow f\bar{f}$ scattering are shown in Fig. 2. The diagrams shown in Fig. 1 also give contributions to the scattering, which are represented by the diagrams (Z-15) and (W-11) in Fig. 2. They can be expressed as

$$\begin{aligned} \bar{\mathcal{M}}_{Z-15}^{hh} \Big|_{\text{G.D.}} + \bar{\mathcal{M}}_{W-11}^{hh} \Big|_{\text{G.D.}} = & \frac{g_Z^2}{128\pi^2} \frac{\zeta_h^2}{p^2 - m_h^2} (1 - \xi_Z) \left[-2c_{hhZZ} B_0(0; Z, G^0) \right. \\ & + c_{G^0hZ}^2 (p^2 + m_h^2) C_0(p^2; Z, G^0) + 2c_{AhZ}^2 (p^2 - 2m_A^2 + m_h^2) C_0(p^2; Z, G^0, A) \left. \right] \\ & + \frac{g^2}{64\pi^2} \frac{\zeta_h^2}{p^2 - m_h^2} (1 - \xi_W) \left[-2c_{hhWW} B_0(0; W, G^\pm) \right. \\ & \left. + 2c_{H^\pm hW^\mp}^2 (p^2 + m_h^2 - 2m_{H^\pm}^2) C_0(p^2; W, G^\pm, H^\pm) + c_{G^\pm hW^\mp}^2 (p^2 + m_h^2) C_0(p^2; W, G^\pm) \right], \end{aligned} \quad (4.8)$$

$$\begin{aligned} \bar{\mathcal{M}}_{Z-15}^{HH} \Big|_{\text{G.D.}} + \bar{\mathcal{M}}_{W-11}^{HH} \Big|_{\text{G.D.}} = & \frac{g_Z^2}{128\pi^2} \frac{\zeta_h^2}{p^2 - m_H^2} (1 - \xi_Z) \left[-2c_{HHZZ} B_0(0; Z, G^0) \right. \\ & + c_{G^0HZ}^2 (p^2 + m_H^2) C_0(p^2; Z, G^0) - 2c_{AHZ}^2 (2m_A^2 - m_H^2 - p^2) C_0(p^2; Z, G^0, A) \left. \right] \\ & + \frac{g^2}{64\pi^2} \frac{\zeta_H^2}{p^2 - m_H^2} (1 - \xi_W) \left[-2c_{HHWW} B_0(0; W, G^\pm) \right. \\ & \left. + 2c_{H^\pm HW^\mp}^2 (p^2 + m_H^2 - 2m_{H^\pm}^2) C_0(p^2; W, G^\pm, H^\pm) + c_{G^\pm HW^\mp}^2 (p^2 + m_H^2) C_0(p^2; W, G^\pm) \right], \end{aligned} \quad (4.9)$$

$$\begin{aligned} \bar{\mathcal{M}}_{Z-15}^{hH} \Big|_{\text{G.D.}} + \bar{\mathcal{M}}_{W-11}^{hH} \Big|_{\text{G.D.}} = & \frac{g_Z^2}{256\pi^2} \frac{\zeta_H \zeta_h}{(p^2 - m_h^2)(p^2 - m_H^2)} (1 - \xi_Z) \\ & \times \left[-c_{hHZZ} (2p^2 - m_h^2 - m_H^2) B_0(0; Z, G^0) + 2c_{G^0hZ} c_{G^0HZ} (p^4 - m_h^2 m_H^2) C_0(p^2; Z, G^0) \right. \\ & + 4c_{AhZ} c_{AHZ} \{p^4 + m_A^2 (m_h^2 + m_H^2 - 2p^2) - m_h^2 m_H^2\} C_0(p^2; Z, G^0, A) \left. \right] \\ & + \frac{g^2}{128\pi^2} \frac{\zeta_h \zeta_H}{(p^2 - m_h^2)(p^2 - m_H^2)} (1 - \xi_W) \left[-c_{hHWW} (2p^2 - m_h^2 - m_H^2) B_0(0; W, G^\pm) \right. \\ & + 4c_{H^\pm hW^\mp} c_{H^\mp HW^\pm} \{p^2 (p^2 - 2m_{H^\pm}^2) - m_h^2 m_H^2 + m_h^2 m_{H^\pm}^2 + m_H^2 m_{H^\pm}^2\} C_0(p^2; W, G^\pm, H^\pm) \\ & \left. + 2c_{G^\pm hW^\mp} c_{G^\mp HW^\pm} (p^4 - m_h^2 m_H^2) C_0(p^2; W, G^\pm) \right], \end{aligned} \quad (4.10)$$

where the mixing factors for the Yukawa couplings, ζ_X , are defined in Eq. (2.23), while those for the gauge couplings, $c_{XYZ(V)}$, are listed in Table 1 in Appendix A.

The reduced amplitudes of the other diagrams shown in Fig. 2 are expressed as

$$\sum_{i=1,2} \bar{\mathcal{M}}_{Z-i} \Big|_{\text{G.D.}} = \frac{c_{\beta'}}{c_\beta} \left(\zeta_h c_{hZZ} \bar{\mathcal{M}}_{\text{ver1}} \left[\frac{g_Z}{\sqrt{2}}, Z, h \right] \Big|_{\text{G.D.}} + \zeta_H c_{HZZ} \bar{\mathcal{M}}_{\text{ver1}} \left[\frac{g_Z}{\sqrt{2}}, Z, H \right] \Big|_{\text{G.D.}} \right), \quad (4.11)$$

$$\begin{aligned}
\sum_{i=3-6} \overline{\mathcal{M}}_{Z-i} \Big|_{\text{G.D.}} &= \zeta_{G^0} \zeta_h c_{G^0 h Z} \overline{\mathcal{M}}_{\text{ver2}} \left[\frac{g_Z}{\sqrt{2}}, Z, h \right] \Big|_{\text{G.D.}} + \zeta_{G^0} \zeta_H c_{G^0 H Z} \overline{\mathcal{M}}_{\text{ver2}} \left[\frac{g_Z}{\sqrt{2}}, Z, H \right] \Big|_{\text{G.D.}} \\
&+ \zeta_A \zeta_h c_{A h Z} \overline{\mathcal{M}}_{\text{ver3}} \left[\frac{g_Z}{\sqrt{2}}, Z, h \right] \Big|_{\text{G.D.}} + \zeta_A \zeta_H c_{A H Z} \overline{\mathcal{M}}_{\text{ver3}} \left[\frac{g_Z}{\sqrt{2}}, Z, H \right] \Big|_{\text{G.D.}}, \tag{4.12}
\end{aligned}$$

$$\overline{\mathcal{M}}_{Z-7} \Big|_{\text{G.D.}} = \frac{c_{\beta'}^2}{c_{\beta}^2} \overline{\mathcal{M}}_{\text{box1}} \left[\frac{g_Z}{\sqrt{2}}, Z \right] \Big|_{\text{G.D.}}, \tag{4.13}$$

$$\sum_{i=8-11} \overline{\mathcal{M}}_{Z-i} \Big|_{\text{G.D.}} = \zeta_{G^0}^2 \overline{\mathcal{M}}_{\text{box2}} \left[\frac{g_Z}{\sqrt{2}}, Z, G^0 \right] \Big|_{\text{G.D.}} + \zeta_A^2 \overline{\mathcal{M}}_{\text{box2}} \left[\frac{g_Z}{\sqrt{2}}, Z, A \right] \Big|_{\text{G.D.}}, \tag{4.14}$$

$$\sum_{i=12-14} \overline{\mathcal{M}}_{Z-i} \Big|_{\text{G.D.}} = \zeta_h^2 \overline{\mathcal{M}}_{\text{ver}+\delta} \left[\frac{g_Z}{\sqrt{2}}, Z, h \right] \Big|_{\text{G.D.}} + \zeta_H^2 \overline{\mathcal{M}}_{\text{ver}+\delta} \left[\frac{g_Z}{\sqrt{2}}, Z, H \right] \Big|_{\text{G.D.}}, \tag{4.15}$$

$$\sum_{i=1,2} \overline{\mathcal{M}}_{W-i} \Big|_{\text{G.D.}} = \zeta_h c_{h W W} \overline{\mathcal{M}}_{\text{ver1}} \left[g, W, h \right] \Big|_{\text{G.D.}} + \zeta_H c_{H W W} \overline{\mathcal{M}}_{\text{ver1}} \left[g, W, H \right] \Big|_{\text{G.D.}}, \tag{4.16}$$

$$\begin{aligned}
\sum_{i=3-6} \overline{\mathcal{M}}_{W-i} \Big|_{\text{G.D.}} &= \zeta_{G^{\pm}} \zeta_h c_{G^{\pm} h W^{\mp}} \overline{\mathcal{M}}_{\text{ver2}} \left[g, W, h \right] \Big|_{\text{G.D.}} + \zeta_{G^{\pm}} \zeta_H c_{G^{\pm} H W^{\mp}} \overline{\mathcal{M}}_{\text{ver2}} \left[g, W, H \right] \Big|_{\text{G.D.}} \\
&+ \zeta_{H^{\pm}} \zeta_h c_{H^{\pm} h W^{\mp}} \overline{\mathcal{M}}_{\text{ver3}} \left[g, W, h \right] \Big|_{\text{G.D.}} + \zeta_{H^{\pm}} \zeta_H c_{H^{\pm} H W^{\mp}} \overline{\mathcal{M}}_{\text{ver3}} \left[g, W, H \right] \Big|_{\text{G.D.}}, \tag{4.17}
\end{aligned}$$

$$\overline{\mathcal{M}}_{W-7} \Big|_{\text{G.D.}} = \overline{\mathcal{M}}_{\text{box1}} \left[g, W \right] \Big|_{\text{G.D.}}, \tag{4.18}$$

$$\sum_{i=8,9} \overline{\mathcal{M}}_{W-i} \Big|_{\text{G.D.}} = \zeta_{G^{\pm}}^2 \overline{\mathcal{M}}_{\text{box2}} \left[g, W, G^{\pm} \right] \Big|_{\text{G.D.}} + \zeta_{H^{\pm}}^2 \overline{\mathcal{M}}_{\text{box2}} \left[g, W, H^{\pm} \right] \Big|_{\text{G.D.}}, \tag{4.19}$$

$$\overline{\mathcal{M}}_{W-10} \Big|_{\text{G.D.}} = \zeta_h^2 \overline{\mathcal{M}}_{\text{ver}+\delta} \left[g, W, h \right] \Big|_{\text{G.D.}} + \zeta_H^2 \overline{\mathcal{M}}_{\text{ver}+\delta} \left[g, W, H \right] \Big|_{\text{G.D.}}, \tag{4.20}$$

where

$$\begin{aligned}
\overline{\mathcal{M}}_{\text{ver1}} \left[g_i, V, \phi \right] \Big|_{\text{G.D.}} &= \frac{g_i^2}{16\pi^2} \frac{1}{p^2 - m_{\phi}^2} \left[- \left(1 + \frac{p^2}{2m_V^2} \right) B_0(p^2; V, V) \right. \\
&+ \left. \left(1 - \xi_V + \frac{p^2}{m_V^2} \right) B_0(p^2; V, G_V) + \left(\xi_V - \frac{p^2}{2m_V^2} \right) B_0(p^2; G_V, G_V) \right], \tag{4.21}
\end{aligned}$$

$$\begin{aligned}
\overline{\mathcal{M}}_{\text{ver2}} \left[g_i, V, \phi \right] \Big|_{\text{G.D.}} &= \frac{g_i^2}{16\pi^2} \frac{1}{p^2 - m_{\phi}^2} \left[B_0(p^2; V, V) - \left(1 - \xi_V + \frac{p^2}{m_V^2} \right) B_0(p^2; V, G_V) \right. \\
&- \left. \left(\xi_V - \frac{p^2}{m_V^2} \right) B_0(p^2; G_V, G_V) + (1 - \xi_V) B_0(0; V, G_V) \right], \tag{4.22}
\end{aligned}$$

$$\overline{\mathcal{M}}_{\text{ver3}} \left[g_i, V, \phi \right] \Big|_{\text{G.D.}} = \frac{g_i^2}{16\pi^2} \frac{1}{p^2 - m_{\phi}^2} (1 - \xi_V) \left[B_0(0; V, G_V) - (p^2 - m_{\phi}^2) C_0(p^2; V, G_V, \phi) \right], \tag{4.23}$$

$$\overline{\mathcal{M}}_{\text{box1}} \left[g_i, V \right] \Big|_{\text{G.D.}} = \frac{g_i^2}{64\pi^2} \frac{1}{m_V^2} \left[B_0(p^2; V, V) - 2B_0(p^2; V, G_V) + B_0(p^2; G_V, G_V) \right], \tag{4.24}$$

$$\overline{\mathcal{M}}_{\text{box2}} \left[g_i, V, \phi \right] \Big|_{\text{G.D.}} = \frac{g_i^2}{32\pi^2} \frac{1}{m_V^2} \left[B_0(p^2; V, \phi) - B_0(p^2; G_V, \phi) \right], \tag{4.25}$$

$$\overline{\mathcal{M}}_{\text{ver}+\delta}[g_i, V, \phi] \Big|_{\text{G.D.}} = -\frac{g_i^2}{32\pi^2} \frac{1}{p^2 - m_\phi^2} (1 - \xi_V) B_0(0; V, G_V), \quad (4.26)$$

where G_V denotes the NG boson associated with the vector boson V . It can be confirmed analytically that the sum of all the contributions $\overline{\mathcal{M}}_{Z-1}|_{\text{G.D.}}$ ($\overline{\mathcal{M}}_{W-1}|_{\text{G.D.}}$) to $\overline{\mathcal{M}}_{Z-15}|_{\text{G.D.}}$ ($\overline{\mathcal{M}}_{W-11}|_{\text{G.D.}}$) completely cancel each other. In particular, in the 't Hooft-Feynman gauge, the gauge-dependent parts $\overline{\mathcal{M}}|_{\text{G.D.}}$ survive only in diagrams (Z-3) to (Z-6), (Z-15), (W-3) to (W-6) and (W-11). Therefore, in the 't Hooft-Feynman gauge, the pinch terms with ξ_V of the two-point functions for CP-even scalar bosons can be extracted from diagrams (Z-3) to (Z-6) and (W-3) to (W-6). Since the pinch terms extracted from the reduced amplitude have the dimension of a scattering amplitude, it is necessary to multiply them by the factor $(p^2 - m_\phi^2)(p^2 - m_{\phi'}^2)/(\zeta_\phi \zeta_{\phi'})$, in order to obtain quantities with the dimension of a self-energy. As a consequence, the pinch terms for the self-energies in the 't Hooft-Feynman gauge are given by

$$\begin{aligned} \Pi_{hh}^{\text{PT}}(p^2) &= -\frac{g^2}{16\pi^2} (p^2 - m_h^2) [c_{G^\pm h W^\mp}^2 B_0(p^2; W, W) + c_{H^\pm h W^\mp}^2 B_0(p^2; W, H^\pm)] \\ &\quad - \frac{g_Z^2}{32\pi^2} (p^2 - m_h^2) [c_{G^0 h Z}^2 B_0(p^2; Z, Z) + c_{A h Z}^2 B_0(p^2; Z, A)], \end{aligned} \quad (4.27)$$

$$\begin{aligned} \Pi_{HH}^{\text{PT}}(p^2) &= -\frac{g^2}{16\pi^2} (p^2 - m_H^2) [c_{G^\pm H W^\mp}^2 B_0(p^2; W, W) + c_{H^\pm H W^\mp}^2 B_0(p^2; W, H^\pm)] \\ &\quad - \frac{g_Z^2}{32\pi^2} (p^2 - m_H^2) [c_{G^0 H Z}^2 B_0(p^2; Z, Z) + c_{A H Z}^2 B_0(p^2; Z, A)], \end{aligned} \quad (4.28)$$

$$\begin{aligned} \Pi_{hH}^{\text{PT}}(p^2) &= -\frac{g^2}{32\pi^2} (2p^2 - m_h^2 - m_H^2) [c_{G^\pm h W^\mp} c_{G^\mp H W^\pm} B_0(p^2; W, W) \\ &\quad + c_{H^\pm h W^\mp} c_{H^\mp H W^\pm} B_0(p^2; W, H^\pm)] \\ &\quad - \frac{g_Z^2}{64\pi^2} (2p^2 - m_h^2 - m_H^2) [c_{G^0 h Z} c_{G^0 H Z} B_0(p^2; Z, Z) + c_{A h Z} c_{A H Z} B_0(p^2; Z, A)]. \end{aligned} \quad (4.29)$$

In order to distribute the contributions of Eqs. (4.11)-(4.20) into the contributions of Eqs. (4.8), (4.9) and (4.10), we use the following relations among the scaling factors:

$$\zeta_h = \zeta_A c_{A h Z} + \zeta_{G^0} c_{G^0 h Z} = \zeta_{G^\pm} c_{G^\pm h W^\mp} + \zeta_{H^\pm} c_{H^\pm h W^\mp}, \quad (4.30)$$

$$\zeta_H = \zeta_A c_{A H Z} + \zeta_{G^0} c_{G^0 H Z} = \zeta_{G^\pm} c_{G^\pm H W^\mp} + \zeta_{H^\pm} c_{H^\pm H W^\mp}, \quad (4.31)$$

$$\zeta_{G^0} = \zeta_h c_{G^0 h Z} + \zeta_H c_{G^0 H Z} = \zeta_{G^\pm} c_{G^\pm G^0 W} + \zeta_{H^\pm} c_{H^\pm G^0 W}, \quad (4.32)$$

$$\zeta_A = \zeta_h c_{A h Z} + \zeta_H c_{A H Z} = \zeta_{G^\pm} c_{G^\pm A W} + \zeta_{H^\pm} c_{H^\pm A W^\mp}, \quad (4.33)$$

$$\zeta_{G^\pm} = \zeta_h c_{G^\pm h W^\mp} + \zeta_H c_{G^\pm H W^\mp}, \quad (4.34)$$

$$\zeta_{H^\pm} = \zeta_h c_{H^\pm h W^\mp} + \zeta_H c_{H^\pm H W^\mp}. \quad (4.35)$$

4.2 CP-odd sector

In this subsection, we derive the pinch terms for the two-point functions of the CP-odd scalar fields, which eliminate the gauge dependence arising from the diagrams shown in

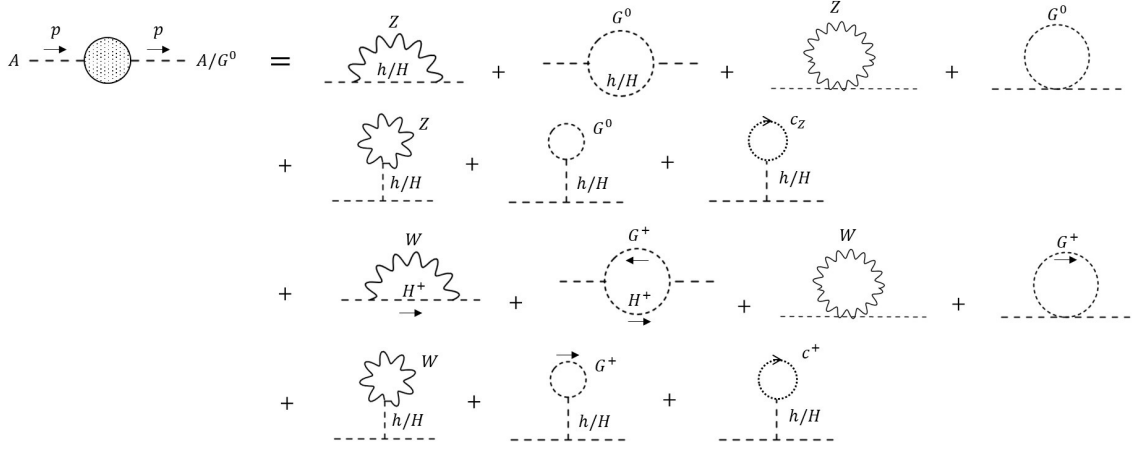


Figure 3: Diagrams dependent on the gauge parameters ξ_V for the self-energy of the CP-odd Higgs bosons.

Fig. 3. The reduced amplitude $\overline{\mathcal{M}}$ for the CP-odd sector is defined as

$$\mathcal{M} = -\overline{\mathcal{M}} \left(\frac{m_f}{v} \right)^2 (\bar{f} \gamma_5 f) \times (\bar{f} \gamma_5 f). \quad (4.36)$$

The contributions of the CP-odd scalar boson two-point functions to the $f\bar{f} \rightarrow f\bar{f}$ scattering amplitude with gauge dependence are shown in Fig. 4. The contributing diagrams for the AA two-point function are the same as those in the 2HDMs. However, for the AG^0 two-point function, the situation differs from the 2HDMs in the sense that there are contributions from the (W, H^\pm) , (G^\pm, H^\pm) and (W) -loop diagrams. Although those diagrams generate an additional ξ_W -dependent part, this contribution is canceled by the diagrams (W-1) to (W-4) in Fig. 4, in which the G^0 propagates. Because of these contributions, the AG^0 two-point function also acquires a pinch term that contains the ξ_W part. As a result, the gauge-dependent contributions of diagrams (Z-12) and (W-8) are derived as

$$\begin{aligned} \overline{\mathcal{M}}_{W-8}^{AA} \Big|_{\text{G.D.}} + \overline{\mathcal{M}}_{Z-12}^{AA} \Big|_{\text{G.D.}} &= \frac{g^2}{16\pi^2} \frac{\zeta_A^2 \zeta_{G^0}^2}{p^2 - m_A^2} (1 - \xi_W) \\ &\times \left[-B_0(0; W, G^\pm) + (p^2 + m_A^2 - 2m_{H^\pm}^2) C_0(p^2; W, G^\pm, H^\pm) \right] \\ &+ \frac{g_Z^2}{64\pi^2} \frac{\zeta_A^2}{p^2 - m_A^2} (1 - \xi_Z) \left[-(c_{AHZ}^2 + c_{AhZ}^2) B_0(0; Z, G^0) \right. \\ &+ c_{AHZ}^2 (p^2 + m_A^2 - 2m_H^2) C_0(p^2; Z, G^0, H) \\ &\left. + c_{AhZ}^2 (p^2 + m_A^2 - 2m_h^2) C_0(p^2; Z, G^0, h) \right], \quad (4.37) \\ \overline{\mathcal{M}}_{W-8}^{AG^0} \Big|_{\text{G.D.}} + \overline{\mathcal{M}}_{Z-12}^{AG^0} \Big|_{\text{G.D.}} &= \frac{g^2}{32\pi^2} \frac{\zeta_A \zeta_{G^0} c_{H^\pm AW^\mp} c_{H^\pm G^0 W^\mp}}{(p^2 - m_A^2)(p^2 - m_{G^0}^2)} (1 - \xi_W) \\ &\times \left[-(2p^2 - m_A^2) B_0(0; W, G^\pm) + 2\{p^2(p^2 - 2m_{H^\pm}^2) + m_A^2 m_{H^\pm}^2\} C_0(p^2; W, G^\pm, H^\pm) \right] \end{aligned}$$

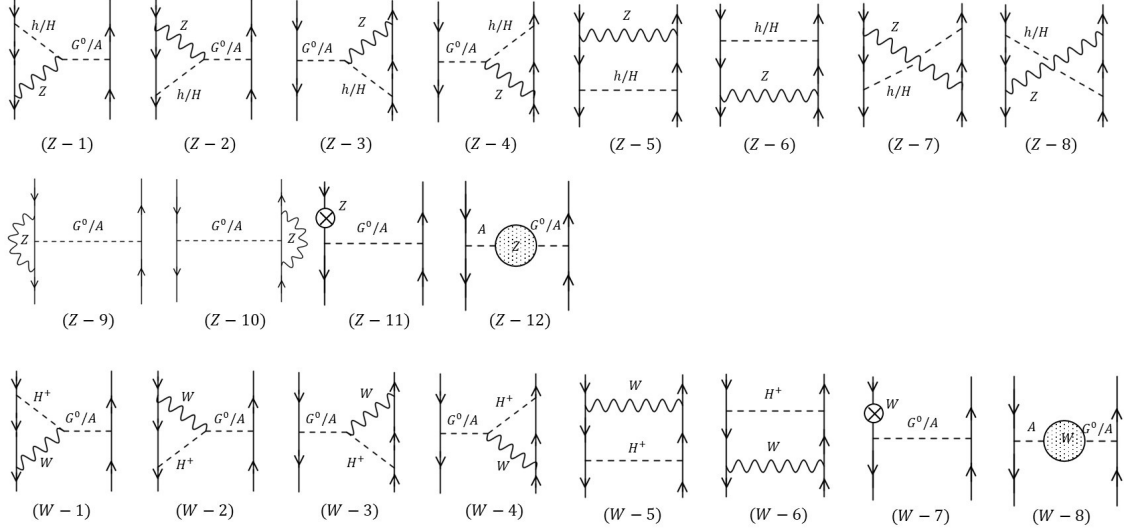


Figure 4: Diagrams dependent on the gauge parameters ξ_V for two-point functions of the CP-odd scalar bosons in the $f\bar{f} \rightarrow f\bar{f}$ scattering.

$$\begin{aligned}
& + \frac{g_Z^2}{128\pi^2} \frac{2\zeta_A \zeta_{G^0}}{(p^2 - m_A^2)(p^2 - m_{G^0}^2)} (1 - \xi_Z) \\
& \times \left[- (c_{AhZ} c_{G^0hZ} + c_{AHZ} c_{G^0HZ}) (2p^2 - m_A^2) B_0(0; Z, G^0) \right. \\
& + 2c_{AhZ} c_{G^0hZ} \{m_A^2 m_h^2 + p^2(p^2 - 2m_h^2)\} C_0(p^2; Z, G^0, h) \\
& \left. + 2c_{AHZ} c_{G^0HZ} \{m_A^2 m_H^2 + p^2(p^2 - 2m_H^2)\} C_0(p^2; Z, G^0, H) \right]. \tag{4.38}
\end{aligned}$$

Contributions from other diagrams are calculated as

$$\begin{aligned}
\sum_{i=1-11} \overline{\mathcal{M}}_{Z-i} \Big|_{\text{G.D.}} & = \frac{g_Z^2}{64\pi^2} (1 - \xi_Z) \left[\frac{\zeta_A}{p^2 - m_A^2} \left\{ \zeta_A B_0(0; Z, G^0) \right. \right. \\
& - 2c_{AHZ} \zeta_H (p^2 - m_H^2) C_0(p^2; Z, G^0, H) - 2(p^2 - m_h^2) c_{AhZ} \zeta_h C_0(p^2; Z, G^0, h) \Big\} \\
& + \frac{\zeta_{G^0}}{p^2 - m_{G^0}^2} \left\{ \zeta_{G^0} B_0(0; Z, G^0) - 2c_{G^0HZ} \zeta_H (p^2 - m_H^2) C_0(p^2; Z, G^0, H) \right. \\
& \left. \left. - 2(p^2 - m_h^2) c_{G^0hZ} \zeta_h C_0(p^2; Z, G^0, h) \right\} \right. \\
& \left. + \zeta_h^2 C_0(p^2; Z, G^0, h) + \zeta_H^2 C_0(p^2; Z, G^0, H) \right], \tag{4.39}
\end{aligned}$$

$$\begin{aligned}
\sum_{i=1-7} \overline{\mathcal{M}}_{W-i} \Big|_{\text{G.D.}} & = \frac{g^2(1 - \xi_W)}{32\pi^2} \left[\frac{\zeta_A \zeta_{H^\pm} c_{H^\pm AW^\mp}}{p^2 - m_A^2} \left\{ B_0(0; W, G^\pm) - 2(p^2 - m_{H^\pm}^2) C_0(p^2; W, G^\pm, H^\pm) \right\} \right. \\
& + \frac{\zeta_{G^0}}{p^2 - m_{G^0}^2} \left\{ - (\zeta_{G^0} - 2\zeta_{H^\pm} c_{H^\pm G^0 W^\mp}) B_0(0; W, G^\pm) \right. \\
& \left. \left. - 2(p^2 - m_{H^\pm}^2) c_{H^\pm G^0 W^\mp} \zeta_{H^\pm} C_0(p^2; W, G^\pm, H^\pm) \right\} \right]
\end{aligned}$$

$$+ \zeta_{H^\pm}^2 C_0(p^2; W, G^\pm, H^\pm) \Big]. \quad (4.40)$$

Part of contributions of Eqs. (4.39) and (4.40) cancels those of (Z-12) and (W-8). However, they also contain contributions that cancel the gauge-dependent part of the AZ^μ mixing. In order to extract only the pinch term of the gauge-dependent parts from the AG^0 mixing diagram, we use the following relation implied by the Ward–Takahashi identity,

$$\Lambda_{G^0} = \frac{p^2}{p^2 - m_{G^0}^2} \Lambda_{G^0} - i m_Z \Lambda_Z^\mu (\Delta_Z)_{\mu\nu} p^\nu, \quad (4.41)$$

where the $\bar{f}fG^0$ and $\bar{f}fZ^\mu$ vertex functions and the Z-boson propagator are expressed by

$$\begin{aligned} \Lambda_{G^0} &= -\frac{m_f}{v} \bar{f} \gamma_5 f, \quad \Lambda_Z^\mu = i g_Z \bar{f} \gamma^\mu (v_f - a_f \gamma_5) f, \\ (\Delta_Z)_{\mu\nu} &= \frac{1}{p^2 - m_Z^2} \left(-g_{\mu\nu} + \frac{(1 - \xi_Z) p_\mu p_\nu}{p^2 - \xi_Z m_Z^2} \right), \end{aligned} \quad (4.42)$$

where the vector and axial-vector couplings are denoted by $v_f = I_f/2 - s_W^2 Q_f$ and $a_f = I_f/2$, respectively. The product of the $\bar{f}fG^0$ vertex function and the propagators in the diagrams shown in Fig. 4, except for (Z-12) and (W-8), can be rewritten as follows:

$$\begin{aligned} \left(\frac{1}{m^2} + \frac{1}{p^2 - m_{G^0}^2} + \frac{1}{p^2 - m_A^2} \right) \Lambda_{G^0} &= \left(\frac{p^2(p^2 - m_A^2)}{m^2(p^2 - m_{G^0}^2)(p^2 - m_A^2)} + \frac{p^2 - m_A^2}{(p^2 - m_{G^0}^2)(p^2 - m_A^2)} \right. \\ &\quad \left. + \frac{p^2}{(p^2 - m_{G^0}^2)(p^2 - m_A^2)} \right) \Lambda_{G^0} + \dots \end{aligned} \quad (4.43)$$

The term enclosed in parentheses can be extracted as the pinch term of the AG^0 mixing.

As in the CP-even sector, in the 't Hooft-Feynman gauge, the pinch terms of the AA and AG^0 two-point functions can be extracted from the diagrams (Z-1) to (Z-4) and (W-1) to (W-4) as

$$\begin{aligned} \Pi_{AA}^{\text{PT}}(p^2) &= -\frac{g^2}{16\pi^2} c_{H^\pm AW^\mp}^2 (p^2 - m_A^2) B_0(p^2; W, H^\pm) \\ &\quad - \frac{g_Z^2}{32\pi^2} (p^2 - m_A^2) [c_{AhZ}^2 B_0(p^2; Z, h) + c_{AHZ}^2 B_0(p^2; Z, H)], \end{aligned} \quad (4.44)$$

$$\begin{aligned} \Pi_{AG^0}^{\text{PT}}(p^2) &= -\frac{g^2}{32\pi^2} c_{H^\pm G^0 W^\mp} c_{H^\pm A W^\mp} (2p^2 - m_A^2) B_0(p^2; W, H^\pm) \\ &\quad - \frac{g_Z^2}{64\pi^2} (2p^2 - m_A^2) [c_{hG^0 Z} c_{AhZ} B_0(p^2; Z, h) + c_{HG^0 Z} c_{AHZ} B_0(p^2; Z, H)]. \end{aligned} \quad (4.45)$$

Although the above pinch term formulae take the same form as those in the 2HDMs, the $H^\pm G^0 W$ coupling does not appear in multi-doublet structures. As a result, the first term in Eq. (4.45) is absent in the 2HDMs.

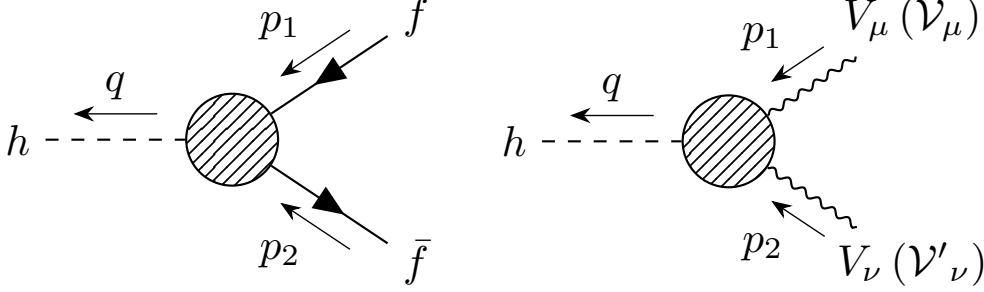


Figure 5: Momentum assignment for the $h f \bar{f}$ vertex (left) and the $h V V$ ($h \mathcal{V} \mathcal{V}'$) vertex (right).

5 Decays of the SM-like Higgs boson

In this section, we discuss the decay of the SM-like Higgs boson including higher-order corrections. In Sec. 5.1, we define the renormalized $h f \bar{f}$, $h V V$ and $h \mathcal{V} \mathcal{V}'$ vertex functions, where $V = Z, W^\pm$ and $(\mathcal{V}, \mathcal{V}') = (g, g), (\gamma, \gamma)$, and (Z, γ) . The renormalized $h h h$ vertex is given in Ref. [18]. In Sec. 5.2, we present the decay rates in terms of the renormalized vertex functions.

5.1 Renormalized vertex functions

5.1.1 $h f \bar{f}$ vertex

The renormalized $h f \bar{f}$ vertex can be decomposed as [45]

$$\begin{aligned} \widehat{\Gamma}_{h f \bar{f}}(p_1, p_2, q) = & \widehat{\Gamma}_{h f \bar{f}}^S + \gamma_5 \widehat{\Gamma}_{h f \bar{f}}^P + \not{p}_1 \widehat{\Gamma}_{h f \bar{f}}^{V_1} + \not{p}_2 \widehat{\Gamma}_{h f \bar{f}}^{V_2} \\ & + \not{p}_1 \gamma_5 \widehat{\Gamma}_{h f \bar{f}}^{A_1} + \not{p}_2 \gamma_5 \widehat{\Gamma}_{h f \bar{f}}^{A_2} + \not{p}_1 \not{p}_2 \widehat{\Gamma}_{h f \bar{f}}^T + \not{p}_1 \not{p}_2 \gamma_5 \widehat{\Gamma}_{h f \bar{f}}^{PT}, \end{aligned} \quad (5.1)$$

where p_1^μ (p_2^μ) is the incoming four-momentum of the fermion (anti-fermion), and q^μ is the outgoing four-momentum of the SM-like Higgs boson (see the left panel of Fig. 5). The following relations hold for the on-shell fermions:

$$\widehat{\Gamma}_{h f \bar{f}}^P = \widehat{\Gamma}_{h f \bar{f}}^{PT} = 0, \quad \widehat{\Gamma}_{h f \bar{f}}^{V_1} = -\widehat{\Gamma}_{h f \bar{f}}^{V_2}, \quad \widehat{\Gamma}_{h f \bar{f}}^{A_1} = -\widehat{\Gamma}_{h f \bar{f}}^{A_2} \quad \text{with} \quad p_1^2 = p_2^2 = m_f^2. \quad (5.2)$$

The renormalized form factors consist of the tree-level and one-loop parts as

$$\widehat{\Gamma}_{h f \bar{f}}^X = \Gamma_{h f \bar{f}}^{X, \text{tree}} + \Gamma_{h f \bar{f}}^{X, \text{loop}}, \quad (X = S, P, V_1, V_2, A_1, A_2, T, PT), \quad (5.3)$$

where the tree-level parts are given by

$$\Gamma_{h f \bar{f}}^{S, \text{tree}} = -\frac{m_f}{v} \zeta_h, \quad \Gamma_{h f \bar{f}}^{X, \text{tree}} = 0 \quad \text{for} \quad X \neq S. \quad (5.4)$$

The one-loop parts are decomposed into the 1PI diagrams and the counterterms.

$$\Gamma_{h f \bar{f}}^{X, \text{loop}} = \Gamma_{h f \bar{f}}^{X, \text{1PI}} + \delta \Gamma_{h f \bar{f}}^X. \quad (5.5)$$

The analytic expressions for $\Gamma_{h\bar{f}\bar{f}}^{X,1\text{PI}}$ are presented in Appendix. B, while $\delta\Gamma_{h\bar{f}\bar{f}}^X$ are given by

$$\delta\Gamma_{h\bar{f}\bar{f}}^S = \Gamma_{h\bar{f}\bar{f}}^{S,\text{tree}} \left(\frac{\delta m_f}{m_f} - \frac{\delta v}{v} + \tan\beta\delta\beta + \delta Z_V^f + \frac{\delta Z_h}{2} \right) + \Gamma_{H\bar{f}\bar{f}}^{S,\text{tree}} \left(\delta\alpha + \frac{\delta Z_{Hh}}{2} \right), \quad (5.6)$$

where $\Gamma_{H\bar{f}\bar{f}}^{S,\text{tree}} = -m_f\zeta_H/v$, and $\delta\Gamma_{h\bar{f}\bar{f}}^X = 0$ for $X \neq S$. The expressions for the counterterms are given in Ref. [18], while we include the tadpole contributions as in Eq. (3.1) and use gauge-independent mixing counterterms given in Eqs. (4.2) and (4.3).

5.1.2 hVV vertex

The renormalized hVV vertex ($V = Z, W^\pm$) can be decomposed as [43, 45]

$$\widehat{\Gamma}_{hVV}^{\mu\nu}(p_1, p_2, q) = g^{\mu\nu} \widehat{\Gamma}_{hVV}^1 + \frac{p_1^\nu p_2^\mu}{m_V^2} \widehat{\Gamma}_{hVV}^2 + i\epsilon^{\mu\nu\rho\sigma} \frac{p_1\rho p_2\sigma}{m_V^2} \widehat{\Gamma}_{hVV}^3, \quad (5.7)$$

where p_1^μ and p_2^μ are the incoming four-momenta of the weak bosons, and q^μ is the outgoing four-momentum of the SM-like Higgs boson (see the right panel of Fig. 5). When we neglect the effects of the CP violation, we have $\widehat{\Gamma}_{hVV}^3(p_1^2, p_2^2, q^2) = 0$. The renormalized form factors are composed of the tree-level and one-loop-level parts as

$$\widehat{\Gamma}_{hVV}^i = \Gamma_{hVV}^{i,\text{tree}} + \Gamma_{hVV}^{i,\text{loop}}, \quad (i = 1, 2, 3). \quad (5.8)$$

The tree-level couplings are given by

$$\Gamma_{hVV}^{1,\text{tree}} = c_V g_{hVV}, \quad \Gamma_{hVV}^{2,\text{tree}} = \Gamma_{hVV}^{3,\text{tree}} = 0, \quad (5.9)$$

where $c_{Z(W)} = 2(1)$, and g_{hVV} is given by

$$g_{hZZ} = \frac{1}{2} c_{hZZ} g_Z m_Z, \quad g_{hWW} = c_{hWW} g_W m_W. \quad (5.10)$$

The one-loop parts are decomposed into the 1PI diagrams, tadpole diagrams, and the counterterms.

$$\Gamma_{hVV}^{i,\text{loop}} = \Gamma_{hVV}^{i,1\text{PI}} + \Gamma_{hVV}^{i,\text{Tad}} + \delta\Gamma_{hVV}^i. \quad (5.11)$$

The analytic expressions for $\Gamma_{hVV}^{i,1\text{PI}}$ and $\delta\Gamma_{hVV}^i$ are presented in Ref. [18]. In the alternative tadpole scheme, the tadpole contributions appear and are given by

$$\Gamma_{hVV}^{1,\text{Tad}} = c_V \left(2g_{hhVV} \frac{\Gamma_h^{1\text{PI}}}{m_h^2} + g_{hHVV} \frac{\Gamma_H^{1\text{PI}}}{m_H^2} \right), \quad \Gamma_{hVV}^{2,\text{Tad}} = \Gamma_{hVV}^{3,\text{Tad}} = 0, \quad (5.12)$$

where g_{hhVV} and g_{hHVV} are given by

$$g_{hhZZ} = \frac{1}{8} c_{hhZZ} g_Z^2, \quad g_{hhWW} = \frac{1}{4} c_{hhWW} g^2, \quad (5.13)$$

$$g_{hHZZ} = \frac{1}{8} c_{hHZZ} g_Z^2, \quad g_{hHWW} = \frac{1}{4} c_{hHWW} g^2. \quad (5.14)$$

The analytic expressions for the 1PI tadpoles, $\Gamma_h^{1\text{PI}}$ and $\Gamma_H^{1\text{PI}}$, are presented in Ref. [18].

5.1.3 $h\mathcal{V}\mathcal{V}'$ vertex

The loop-induced $h\mathcal{V}\mathcal{V}'$ vertex with $(\mathcal{V}, \mathcal{V}') = (g, g), (\gamma, \gamma), (Z, \gamma)$ can be decomposed as [48]

$$\widehat{\Gamma}_{h\mathcal{V}\mathcal{V}'}^{\mu\nu}(p_1, p_2, q) = g^{\mu\nu}\widehat{\Gamma}_{h\mathcal{V}\mathcal{V}'}^1 + p_1^\nu p_2^\mu\widehat{\Gamma}_{h\mathcal{V}\mathcal{V}'}^2 + i\epsilon^{\mu\nu\rho\sigma}p_{1\rho}p_{2\sigma}\widehat{\Gamma}_{h\mathcal{V}\mathcal{V}'}^3, \quad (5.15)$$

where p_1^μ and p_2^μ are the incoming four-momenta of \mathcal{V} and \mathcal{V}' , and q^μ is the outgoing four-momentum of the SM-like Higgs boson (see the right panel of Fig. 5). When we neglect the effects of the CP violation, $\widehat{\Gamma}_{h\mathcal{V}\mathcal{V}'}^3 = 0$. For the on-shell photon and gluon with a four-momentum $p_{2,\nu}$ ($\mathcal{V}' = \gamma$ or g), the Ward-Takahashi identity holds, i.e. $p_{2,\nu}\widehat{\Gamma}_{h\mathcal{V}\mathcal{V}'}^{\mu\nu} = 0$, and we obtain

$$\widehat{\Gamma}_{h\mathcal{V}\mathcal{V}'}^1 = -p_1 \cdot p_2 \widehat{\Gamma}_{h\mathcal{V}\mathcal{V}'}^2. \quad (5.16)$$

The renormalized form factors are composed of the one-loop part as

$$\widehat{\Gamma}_{h\mathcal{V}\mathcal{V}'}^i = \Gamma_{h\mathcal{V}\mathcal{V}'}^{i,\text{loop}}, \quad (i = 1, 2, 3). \quad (5.17)$$

The one-loop contributions are decomposed into the 1PI diagrams and the counterterms.

$$\Gamma_{h\mathcal{V}\mathcal{V}'}^{i,\text{loop}} = \Gamma_{h\mathcal{V}\mathcal{V}'}^{i,\text{1PI}} + \delta\Gamma_{h\mathcal{V}\mathcal{V}'}^i, \quad (i = 1, 2, 3). \quad (5.18)$$

The analytic expressions for $\Gamma_{h\mathcal{V}\mathcal{V}'}^{i,\text{1PI}}$ are presented in Appendix C. For $(\mathcal{V}, \mathcal{V}') = (g, g), (\gamma, \gamma)$, we have no counterterm at the one-loop level, i.e. $\delta\Gamma_{hgg}^i = \delta\Gamma_{h\gamma\gamma}^i = 0$ ($i = 1, 2, 3$). On the other hand, $\delta\Gamma_{hZ\gamma}^i$ are obtained as

$$\delta\Gamma_{hZ\gamma}^1 = g_{hZZ}\left(\delta Z_{Z\gamma} - \frac{\delta s_W^2}{c_W s_W}\right), \quad \delta\Gamma_{hZ\gamma}^2 = \delta\Gamma_{hZ\gamma}^3 = 0, \quad (5.19)$$

where the expressions for the counterterms are given in Ref. [18].

5.2 Decay rates of the SM-like Higgs boson

5.2.1 $h \rightarrow f\bar{f}$

The decay rate for $h \rightarrow f\bar{f}$ ($f \neq t$) is given by

$$\Gamma(h \rightarrow f\bar{f}) = \Gamma_{\text{LO}}(h \rightarrow f\bar{f})(1 - \Delta r) + \Gamma^{\text{EW}}(h \rightarrow f\bar{f}) + \Gamma^{\text{QCD}}(h \rightarrow f\bar{f}), \quad (5.20)$$

where the LO decay rate is given by

$$\Gamma_{\text{LO}}(h \rightarrow f\bar{f}) = N_c^f \frac{m_h}{8\pi} \left| \Gamma_{hff}^{S,\text{tree}} \right|^2 \lambda^{3/2} \left(\frac{m_f^2}{m_h^2}, \frac{m_f^2}{m_h^2} \right), \quad (5.21)$$

with $N_c^f = 3$ (1) for f being quarks (leptons). The kinematical factor is defined by

$$\lambda(x, y) = (1 - x - y)^2 - 4xy. \quad (5.22)$$

The correction Δr appears when one replaces the electroweak VEV into the Fermi constant in $\Gamma_{\text{LO}}(h \rightarrow f\bar{f})$ as discussed in Sec. 3.2.

The electroweak correction is given by [48]

$$\begin{aligned} \Gamma^{\text{EW}}(h \rightarrow f\bar{f}) &= N_c^f \frac{m_h}{8\pi} \lambda^{3/2} \left(\frac{m_f^2}{m_h^2}, \frac{m_f^2}{m_h^2} \right) \\ &\times 2 \text{Re} \left\{ \Gamma_{h\bar{f}\bar{f}}^{S,\text{tree}} \left[\Gamma_{h\bar{f}\bar{f}}^{S,\text{loop}} + 2m_f \Gamma_{h\bar{f}\bar{f}}^{V_1,\text{loop}} + m_h^2 \left(1 - \frac{m_f^2}{m_h^2} \right) \Gamma_{h\bar{f}\bar{f}}^{T,\text{loop}} \right]^* \right\} \\ &+ \Gamma(h \rightarrow f\bar{f}\gamma), \end{aligned} \quad (5.23)$$

where $\Gamma(h \rightarrow f\bar{f}\gamma)$ is the decay rate of the real-photon emission process and is obtained as

$$\Gamma(h \rightarrow f\bar{f}\gamma) = N_c^f \frac{2\alpha_{\text{em}} Q_f^2}{16\pi^2 m_h} \left| \Gamma_{h\bar{f}\bar{f}}^{S,\text{tree}} \right|^2 [\Omega_{11}^{LL} + \Omega_{11}^{LR} + \Omega_{22}^{LL} + \Omega_{22}^{LR} + \Omega_{12}^{LL} + \Omega_{12}^{LR}], \quad (5.24)$$

where Ω_{ij}^{XY} ($X, Y = L, R$; $i, j = 1, 2$) are presented in Ref. [115]. We regulate infrared divergences in 1PI diagrams by introducing the photon mass. The photon mass dependence is canceled by the soft-photon emission part of $\Gamma(h \rightarrow f\bar{f}\gamma)$. We also add the hard-photon emission part so that $\Gamma^{\text{EW}}(h \rightarrow f\bar{f})$ is independent of the detector cutoff. For decays into quarks, we include the QCD correction $\Gamma^{\text{QCD}}(h \rightarrow f\bar{f})$ up to NNLO in the $\overline{\text{MS}}$ scheme [116–119]. For their formulae, for instance, see Refs. [48, 120].

5.2.2 $h \rightarrow ZZ^* \rightarrow Zf\bar{f}$

We assign the momenta of the external particles as

$$h(p_h) \rightarrow Z(k_Z) + f(k_f) + \bar{f}(k_{\bar{f}}), \quad (5.25)$$

where p_i (k_i) is the incoming (outgoing) momentum. In the following, we neglect the masses of final-state fermions. Then, the Mandelstam variables are given by $s = (k_{\bar{f}} + k_f)^2$, $t = (k_Z + k_f)^2$, and $u = (k_Z + k_{\bar{f}})^2$ and satisfy $s + t + u = m_h^2 + m_Z^2$. Instead of t , we use the polar angle θ of f in the rest frame of Z^* , and the t parameter is written as

$$t = \frac{1}{2} \left[m_h^2 + m_Z^2 - s + m_h^2 \lambda^{1/2} \left(\frac{m_Z^2}{m_h^2}, \frac{s}{m_h^2} \right) \cos \theta \right]. \quad (5.26)$$

The decay rate for $h \rightarrow ZZ^*$ can be written as

$$\Gamma(h \rightarrow ZZ^*) = \sum_{f \neq t} \Gamma(h \rightarrow Zf\bar{f}), \quad (5.27)$$

where the partial decay rate for $h \rightarrow Zf\bar{f}$ is given by

$$\Gamma(h \rightarrow Zf\bar{f}) = \Gamma_{\text{LO}}(h \rightarrow Zf\bar{f})(1 - 2\Delta r) + \Gamma^{\text{EW}}(h \rightarrow Zf\bar{f}) + \Gamma^{\text{QCD}}(h \rightarrow Zf\bar{f}). \quad (5.28)$$

The LO decay rate is given by

$$\Gamma_{\text{LO}}(h \rightarrow Zf\bar{f}) = N_c^f \left(\frac{c_{hZZ}}{1 + s_\beta^2} \right)^2 \frac{G_F^2 m_h m_Z^4}{24\pi^3} (v_f^2 + a_f^2) F(\epsilon_Z), \quad (5.29)$$

where the kinematical function $F(x)$ is defined as [121]

$$F(x) = \frac{3(1 - 8x^2 + 20x^4)}{\sqrt{4x^2 - 1}} \arccos\left(\frac{3x^2 - 1}{2x^3}\right) - (1 - x^2)\left(\frac{47}{2}x^2 - \frac{13}{2} + \frac{1}{x^2} - 3(1 - 6x^2 + x^4)\ln x\right) \quad (5.30)$$

with $\epsilon_Z = m_Z/m_h$. We use s_{W,G_F} for $v_f = I_f/2 - Q_f s_W^2$ in the LO decay rate.

The electroweak correction is obtained as [48]

$$\Gamma^{\text{EW}}(h \rightarrow Z f \bar{f}) = \int_0^{(m_h - m_Z)^2} ds \frac{d\Gamma_{hZZ}}{ds} + \int_0^{(m_h - m_Z)^2} ds \int_{-1}^1 d\cos\theta \frac{d\Gamma_{hZZ}}{ds d\cos\theta} + \Gamma^{\text{QED}}(h \rightarrow Z f \bar{f}), \quad (5.31)$$

where we have separated the weak correction and the QED correction. The weak correction is divided into two parts. The first term is obtained as

$$\begin{aligned} \frac{d\Gamma_{hZZ}}{ds} = N_c^f \frac{m_h^3}{96\pi^3} \frac{g_Z^2 \Gamma_{hZZ}^{1,\text{tree}}}{4m_Z^2} (v_f^2 + a_f^2) \frac{c_a^{\text{kin}}}{(s - m_Z^2)^2} \text{Re} \left\{ -\Gamma_{hZZ}^{1,\text{tree}} \frac{\hat{\Pi}'_{ZZ}(m_Z^2)}{2} \right. \\ + \left[\Gamma_{hZZ}^{1,\text{loop}} + \frac{c_b^{\text{kin}}}{c_a^{\text{kin}}} \frac{\Gamma_{hZZ}^{2,\text{loop}}}{m_Z^2} \right] (m_Z^2, s, m_h^2) - \Gamma_{hZZ}^{1,\text{tree}} \frac{\hat{\Pi}_{ZZ}(s)}{s - m_Z^2} \\ + \frac{v_f Q_f c_W s_W}{v_f^2 + a_f^2} \left(\frac{s - m_Z^2}{s} \left[\hat{\Gamma}_{hZ\gamma}^1 + \frac{c_b^{\text{kin}}}{c_a^{\text{kin}}} \hat{\Gamma}_{hZ\gamma}^2 \right] (m_Z^2, s, m_h^2) - \Gamma_{hZZ}^{1,\text{tree}} \frac{\hat{\Pi}_{Z\gamma}(s)}{s} \right) \\ \left. + \Gamma_{hZZ}^{1,\text{tree}} \frac{\left[v_f \Gamma_{Zff}^{V,\text{loop}} + a_f \Gamma_{Zff}^{A,\text{loop}} \right] (0, 0, s)}{v_f^2 + a_f^2} \right\}, \end{aligned} \quad (5.32)$$

where the term $\hat{\Pi}'_{ZZ}(m_Z^2) = d\hat{\Pi}_{ZZ}(p^2)/dp^2|_{p^2=m_Z^2}$ is included since the residue of the renormalized Z -boson propagator is not unity [98, 99]. The kinematical factors are given by

$$c_a^{\text{kin}} = \sqrt{x_1^2 - 4x_Z} [(x_1 - 6x_Z)^2 + 8x_Z(1 - 3x_Z)], \quad (5.33)$$

$$c_b^{\text{kin}} = \frac{m_h^2}{2} (x_1^2 - 4x_Z)^{3/2} (x_1 - 2x_Z), \quad (5.34)$$

with $x_Z = m_Z^2/m_h^2$, $x_s = s/m_h^2$ and $x_1 = 1 + x_Z - x_s$. The second term involves the $h f \bar{f}$ vertex correction and the box contributions and is obtained as

$$\frac{d\Gamma_{hZZ}}{ds d\cos\theta} = N_c^f \frac{1}{512\pi^3 m_h} \sqrt{x_1^2 - 4x_Z} \frac{g_Z \Gamma_{hZZ}^{1,\text{tree}}}{s - m_Z^2} \text{Re} \left[c_1^{\text{kin}} T_{hff}^Z + B_Z \right], \quad (5.35)$$

with $c_1^{\text{kin}} = 4s + 2(tu - m_h^2 m_Z^2)/m_Z^2$. The $h f \bar{f}$ vertex correction is expressed as

$$T_{h f \bar{f}}^Z = \frac{2g_Z}{16\pi^2} \left\{ 4g_Z^3 m_Z c_{hZZ} (v_f^4 + 6v_f^2 a_f^2 + a_f^4) \right. \\ \times \left[\left(\frac{C_0 + C_{11}}{-2} \right) (t, 0, m_h^2; Z, 0, Z) + \left(\frac{C_{12}}{2} \right) (0, u, m_h^2; Z, 0, Z) \right] \\ + g^3 m_W c_{hWW} (v_f + a_f)^2 \\ \times \left[\left(\frac{C_0 + C_{11}}{-2} \right) (t, 0, m_h^2; W, 0, W) + \left(\frac{C_{12}}{2} \right) (0, u, m_h^2; W, 0, W) \right] \left. \right\}. \quad (5.36)$$

The box contribution can be written as

$$B_Z = \frac{1}{16\pi^2} \left[4(v_f + a_f) \sum_{i \neq 6} C^{BZi} B^{BZi} + 8(v_f^4 + 6v_f^2 a_f^2 + a_f^4) C^{BZ6} B^{BZ6} \right], \quad (5.37)$$

where the coefficients C^{BZi} and the box functions B^{BZi} are presented in Appendix. D.1.

For the implementation of QED and QCD corrections, we follow Ref. [48]. In the massless limit of the external fermions, they only appear in the $Z f \bar{f}$ vertex. Then, QED and QCD corrections are given by [122]

$$\Gamma^{\text{QED}}(h \rightarrow Z f \bar{f}) = \left(Q_f^2 \frac{3\alpha_{\text{em}}}{4\pi} \right) \Gamma_{\text{LO}}(h \rightarrow Z f \bar{f}), \quad (5.38)$$

$$\Gamma^{\text{QCD}}(h \rightarrow Z f \bar{f}) = \left(\frac{\alpha_s}{\pi} \right) \Gamma_{\text{LO}}(h \rightarrow Z f \bar{f}) \quad \text{for } f = q. \quad (5.39)$$

5.2.3 $h \rightarrow WW^* \rightarrow W f' \bar{f}$

We assign the momenta of the external particles as

$$h(p_h) \rightarrow W^-(k_W) + f'(k_{f'}) + \bar{f}(k_{\bar{f}}), \quad (5.40)$$

where $p_i(k_i)$ is the incoming (outgoing) momentum, and f' (f) denotes a fermion with $I_f = +1/2$ ($-1/2$). Similarly to the $h \rightarrow ZZ^*$ decay, we neglect the masses of the final-state fermions. The Mandelstam variables are given by $s = (k_{\bar{f}} + k_{f'})^2$, $t = (k_W + k_{\bar{f}})^2$, and $u = (k_W + k_{f'})^2$ and satisfy $s + t + u = m_h^2 + m_W^2$. Instead of t , we use the polar angle θ of f' in the rest frame of W^{+*} . The t parameter is obtained by replacing $m_Z \rightarrow m_W$ in Eq. (5.26).

The decay rate for $h \rightarrow WW^*$ can be written as

$$\Gamma(h \rightarrow WW^*) = 2 \sum_{f, f'} \Gamma(h \rightarrow W^- f' \bar{f}). \quad (5.41)$$

The factor of two accounts for the charge-conjugate process $h \rightarrow W^+ f \bar{f}'$. The partial decay rate for $h \rightarrow W^- f' \bar{f}$ is given by

$$\Gamma(h \rightarrow W^- f' \bar{f}) = \Gamma_{\text{LO}}(h \rightarrow W^- f' \bar{f}) (1 - 2\Delta r) + \Gamma^{\text{EW}}(h \rightarrow W^- f' \bar{f}) \\ + \Gamma^{\text{QCD}}(h \rightarrow W^- f' \bar{f}). \quad (5.42)$$

In the following, we neglect the effects of quark mixing and assume that the CKM matrix is the identity matrix. Then, the LO decay rate is given by

$$\Gamma_{\text{LO}}(h \rightarrow W^- f' \bar{f}) = N_c^f c_{hWW}^2 \frac{G_F^2 m_h m_W^4}{96\pi^3} F(\epsilon_W), \quad (5.43)$$

with $\epsilon_W = m_W/m_h$. We use m_{W,G_F} for m_W in the LO decay rate instead of \bar{m}_W (See Sec. 3.2). We note that Δr shifts the W -mass with $\mathcal{O}(100)$ MeV [18], and there are artificially large corrections if one uses \bar{m}_W in Eq. (5.43).

The electroweak correction is given by [48]

$$\begin{aligned} \Gamma^{\text{EW}}(h \rightarrow W^- f' \bar{f}) = R_{f' \bar{f}} & \left[\int_0^{(m_h - m_W)^2} ds \frac{d\Gamma_{hWW}}{ds} + \int_0^{(m_h - m_W)^2} ds \int_{-1}^1 d\cos\theta \frac{d\Gamma_{hWW}}{ds d\cos\theta} \right. \\ & \left. + \Gamma(h \rightarrow W^- f' \bar{f} \gamma) \right], \end{aligned} \quad (5.44)$$

where we have multiplied $R_{f' \bar{f}} = \Gamma_{\text{LO}}(h \rightarrow W^- f' \bar{f})|_{m_W=m_{W,G_F}}/\Gamma_{\text{LO}}(h \rightarrow W^- f' \bar{f})|_{m_W=\bar{m}_W}$ to replace \bar{m}_W in the kinematical factor with m_{W,G_F} . We note that, different from $h \rightarrow Z f \bar{f}$, the weak and QED corrections cannot be separated for $h \rightarrow W^- f' \bar{f}$ since virtual photons appear together with virtual W bosons in vertex corrections. Therefore, we add the real-photon emission $\Gamma(h \rightarrow W^- f' \bar{f} \gamma)$ and cancel IR divergences [48]. The first term on the right-hand side of Eq. (5.44) is obtained as

$$\begin{aligned} \frac{d\Gamma_{hWW}}{ds} = N_c^f \frac{m_h^3}{384\pi^3} \frac{g^2 \Gamma_{hWW}^{\text{1,tree}}}{4m_W^2} \frac{c_a^{\text{kin}}}{(s - m_W^2)^2} \text{Re} \left\{ -\Gamma_{hWW}^{\text{1,tree}} \frac{\hat{\Pi}'_{WW}(m_W^2)}{2} \right. \\ + \left[\Gamma_{hWW}^{\text{1,loop}} + \frac{c_b^{\text{kin}}}{c_a^{\text{kin}}} \frac{\Gamma_{hWW}^{\text{2,loop}}}{m_W^2} \right] (m_W^2, s, m_h^2) - \Gamma_{hWW}^{\text{1,tree}} \frac{\hat{\Pi}_{WW}(s)}{s - m_W^2} \\ \left. + \Gamma_{hWW}^{\text{1,tree}} \left[\Gamma_{Wff}^{V,\text{loop}} + \Gamma_{Wff}^{A,\text{loop}} \right] (0, 0, s) \right\}, \end{aligned} \quad (5.45)$$

where the term $\hat{\Pi}'_{WW}(m_W^2) = d\hat{\Pi}_{WW}(p^2)/dp^2|_{p^2=m_W^2}$ is included since the residue of the renormalized W -boson propagator is not unity [98, 99]. The expressions for the loop-corrected Wff vertices, $\Gamma_{Wff}^{V/A,\text{loop}}(0, 0, p^2)$, are the same as those in the SM in the massless limit of the external fermions, and their explicit formulae can be found, for instance, in Ref. [48]. The second term is given by

$$\frac{d\Gamma_{hWW}}{ds d\cos\theta} = N_c^f \frac{1}{512\pi^3 m_h} \sqrt{x_1^2 - 4x_W} \frac{g_W \Gamma_{hWW}^{\text{1,tree}}}{s - m_W^2} \text{Re} \left[c_1^{\text{kin}} T_{hff}^W + B_W \right], \quad (5.46)$$

where $g_W = g/\sqrt{2}$. The kinematical factors c_a^{kin} , c_b^{kin} , x_1 , and c_1^{kin} are obtained from those for $h \rightarrow ZZ^*$ by the replacements $m_Z \rightarrow m_W$ and $x_Z \rightarrow x_W$. The hff contribution is

expressed as

$$\begin{aligned}
T_{h\bar{f}\bar{f}}^W = & \frac{g_W}{16\pi^2} \left\{ 4g_Z^3 m_Z c_{hZZ} \left[(v_{f'} + a_{f'})^2 \left(\frac{C_0 + C_{11}}{-2} \right) (t, 0, m_h^2; Z, 0, Z) \right. \right. \\
& + (v_f + a_f)^2 \left(\frac{C_{12}}{2} \right) (0, u, m_h^2; Z, 0, Z) \left. \right] \\
& + 2g^3 m_W c_{hWW} \left[\left(\frac{C_0 + C_{11}}{-2} \right) (t, 0, m_h^2; W, 0, W) + \left(\frac{C_{12}}{2} \right) (0, u, m_h^2; W, 0, W) \right] \right\}. \tag{5.47}
\end{aligned}$$

The box contribution can be written as

$$B_W = \frac{4}{16\pi^2} \sum C^{BW_i} B^{BW_i}, \tag{5.48}$$

where the coefficients C^{BW_i} and the box functions B^{BW_i} are given in Appendix. D.1.

In the massless limit of the external fermions, the QCD correction only appears in the $Wf\bar{f}$ vertex and is given by [122]

$$\Gamma^{\text{QCD}}(h \rightarrow W^- f' \bar{f}) = \left(\frac{\alpha_s}{\pi} \right) \Gamma_{\text{LO}}(h \rightarrow W^- f' \bar{f}) \quad \text{for } f = q. \tag{5.49}$$

5.2.4 $h \rightarrow gg, \gamma\gamma, Z\gamma$

The LO decay rates for the loop-induced processes $h \rightarrow gg, \gamma\gamma$ and $Z\gamma$ can be expressed as [48]

$$\Gamma_{\text{LO}}(h \rightarrow \mathcal{V}\mathcal{V}') = \frac{1}{8\pi(1 + \delta_{\mathcal{V}\mathcal{V}'})m_h} \left| \widehat{\Gamma}_{h\mathcal{V}\mathcal{V}'}^1(m_{\mathcal{V}}^2, m_{\mathcal{V}'}^2, m_h^2) \right|^2 \lambda^{1/2} \left(\frac{m_{\mathcal{V}}^2}{m_h^2}, \frac{m_{\mathcal{V}'}^2}{m_h^2} \right). \tag{5.50}$$

The quark-loop contributions receive QCD corrections. For $h \rightarrow gg$ and $\gamma\gamma$, we include them up to NNLO following Refs. [123–125]. For $h \rightarrow Z\gamma$, we replace a quark mass in the Yukawa coupling with a running mass. For their explicit formulae, see Ref. [120] for instance.

The LO decay rate for $h \rightarrow \gamma\gamma$ can be simplified as follows [18, 126–129].

$$\begin{aligned}
\Gamma_{\text{LO}}(h \rightarrow \gamma\gamma) = & \frac{\sqrt{2}G_F \alpha_{\text{em}}^2 m_h^3}{256\pi^3} \left| \zeta_h \sum_f N_c^f Q_f^2 I_F^h(f) + c_{hWW} I_V^h(W) \right. \\
& \left. - \frac{\lambda_{H^+ H^- h}}{v} I_S^h(H^\pm) - \frac{4\lambda_{H^{++} H^{--} h}}{v} I_S^h(H^{\pm\pm}) \right|^2, \tag{5.51}
\end{aligned}$$

where the loop functions are defined as [45]

$$I_F^h(f) = -\frac{8m_f^2}{m_h^2} \left[1 + \left(2m_f^2 - \frac{m_h^2}{2} \right) C_0(0, 0, h; f, f, f) \right], \tag{5.52}$$

$$I_V^h(W) = \frac{2m_W^2}{m_h^2} \left[6 + \frac{m_h^2}{m_W^2} + (12m_W^2 - 6m_h^2) C_0(0, 0, h; W, W, W) \right], \tag{5.53}$$

$$I_S^h(H^\pm) = \frac{2v^2}{m_h^2} [1 + 2m_{H^\pm}^2 C_0(0, 0, h; H^\pm, H^\pm, H^\pm)]. \tag{5.54}$$

The $H^{\pm\pm}$ contribution can be obtained by replacing H^\pm with $H^{\pm\pm}$.

Similarly to $h \rightarrow \gamma\gamma$, we write the decay rate for $h \rightarrow Z\gamma$ as [126, 127, 129–131]

$$\Gamma_{\text{LO}}(h \rightarrow Z\gamma) = \frac{\sqrt{2}G_F\alpha_{\text{em}}^2 m_h^3}{128\pi^3} \left(1 - \frac{m_Z^2}{m_h^2}\right)^3 \left| \zeta_h \sum_f N_c^f Q_f v_f J_F^h(f) + J_B^h \right|^2, \quad (5.55)$$

where the fermionic loop function is given by [45]

$$\begin{aligned} J_F^h(f) = & -\frac{4m_f^2}{s_W c_W (m_h^2 - m_Z^2)} \left[2 + (4m_f^2 - m_h^2 + m_Z^2) C_0(Z, 0, h; f, f, f) \right. \\ & \left. + \frac{2m_Z^2}{m_h^2 - m_Z^2} [B_0(h; f, f) - B_0(Z; f, f)] \right], \end{aligned} \quad (5.56)$$

and we have defined the bosonic loop function as follows.

$$J_B^h = \frac{16\pi^2 v}{e^2(m_h^2 - m_Z^2)} \hat{\Gamma}_{hZ\gamma}^1(m_Z^2, 0, m_h^2)_B. \quad (5.57)$$

When $\beta' = 0$, J_B^h is consistent with that in Ref. [131].

5.3 Theoretical behaviors of radiative corrections

We here study the behavior of one-loop contributions, especially focusing on the decoupling of the additional Higgs bosons. To study the decoupling behavior, we assume that all the additional Higgs bosons are degenerate in their mass: $m_\Phi \equiv m_A = m_H = m_{H^\pm} = m_{H^{\pm\pm}}$. We take μ as an input parameter instead of \bar{v}_Δ and take $\bar{v}_\Delta = \mu\bar{v}^2/(\sqrt{2}m_A^2)$ according to the decoupling relation (see the discussion of the decoupling limit in Sec. 2.3). When $m_A \gg \mu$, \bar{v}_Δ is negligible and the Higgs quartic couplings are obtained as

$$\lambda_1 = \frac{m_h^2}{2v^2}, \quad \lambda_2 = -\frac{v^2}{2(m_\Phi^2 - m_h^2)} \left(\lambda_4^2 - \frac{4m_\Phi^2}{v^2} \lambda_4 + \frac{4m_\Phi^2 m_h^2}{v^4} \right), \quad \lambda_3 = \lambda_5 = 0. \quad (5.58)$$

In Fig. 6, we show the allowed region in the λ_4 – λ_2 plane with $\lambda_1 = m_h^2/(2v^2)$ and $\lambda_3 = \lambda_5 = 0$ under the vacuum stability and the tree-level unitarity conditions as well as the perturbativity criterion. The blue, orange and green curves correspond to λ_2 given in Eq. (5.58) for $m_\Phi = 400, 450$, and 500 GeV, respectively. From the vacuum stability conditions in Eq. (2.24), λ_2 must be positive for $\lambda_3 = 0$. In addition, for $m_\Phi > m_h$, λ_2 is a convex function of λ_4 . For $m_\Phi \gg m_h$, the solutions of $\lambda_2 = 0$ are given by

$$\lambda_4^- = \frac{m_h^2}{v^2}, \quad \lambda_4^+ = \frac{4m_\Phi^2}{v^2} \left(1 - \frac{m_h^2}{4m_\Phi^2} \right). \quad (5.59)$$

Therefore, since $\lambda_2 > 0$ and $\lambda_4^\pm > 0$, λ_4 must be positive in the decoupling limit.

The maximal value of λ_4 depends on m_Φ , and there are three distinct cases. The first case corresponds to small m_Φ , which is represented by the blue line with $m_\Phi = 400$ GeV in Fig. 6. In this case, the whole parabola lies in the allowed region, and λ_4 takes its maximal value at $\lambda_4^{\max} \simeq \lambda_4^+$ with $\lambda_2 \simeq 0$, while λ_2 becomes maximal at the top of the parabola

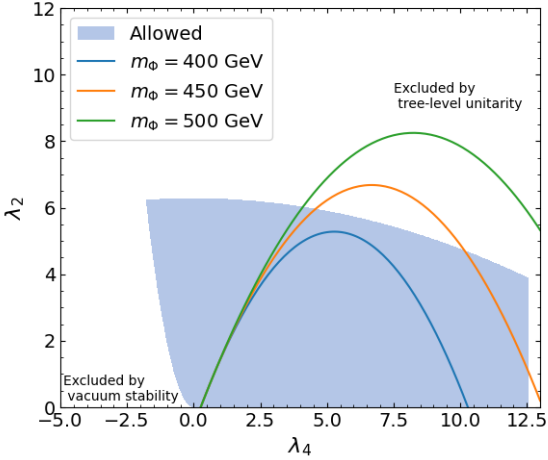


Figure 6: Allowed region in the λ_4 – λ_2 plane for the decoupling scenario under the vacuum stability and the tree-level unitarity conditions as well as the perturbativity criterion.

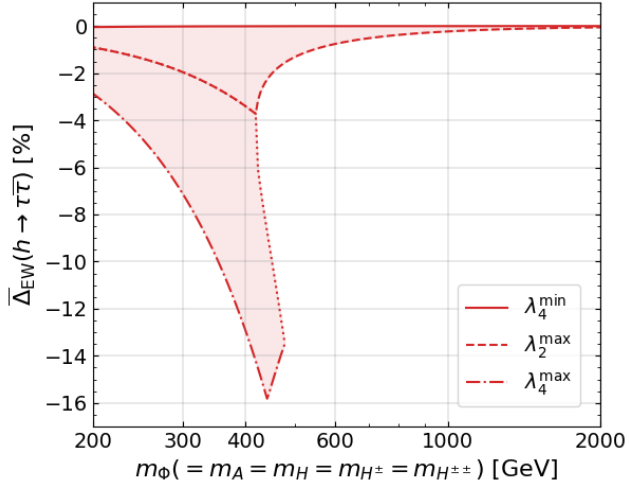


Figure 7: Decoupling behavior in the NLO EW corrections to the $h \rightarrow \tau\bar{\tau}$ decay.

with $\lambda_2^{\max} = 2m_\Phi^2/v^2$. The second case corresponds to an intermediate value of m_Φ , e.g. $m_\Phi = 450$ GeV, where a part of the parabola is outside the allowed region as shown by the orange line, and the intermediate range of λ_4 is not allowed. In this case, $\lambda_4^{\max} = 4\pi < \lambda_4^+$ due to the perturbativity criterion. We note that $\lambda_4 \lesssim 20$ is allowed only by perturbative unitarity with $\zeta_{\text{LQT}} = 1$. The third case corresponds to large m_Φ . In this case, as shown by the green line with $m_\Phi = 500$ GeV, there is no solution on the right-hand side of the parabola, and λ_4 and λ_2 take their maximal values at the same time.

We define $\overline{\Delta}_{\text{EW}}(h \rightarrow XY)$ as [48]

$$\overline{\Delta}_{\text{EW}}(h \rightarrow XY) = \left. \frac{\Gamma(h \rightarrow XY)}{\Gamma_{\text{LO}}(h \rightarrow XY)} \right|_{\text{CHTM}} - \left. \frac{\Gamma(h \rightarrow XY)}{\Gamma_{\text{LO}}(h \rightarrow XY)} \right|_{\text{SM}}, \quad (5.60)$$

where $\Gamma(h \rightarrow XY)$ and $\Gamma_{\text{LO}}(h \rightarrow XY)$ are given in Sec. 5.2. We note that $\overline{\Delta}_{\text{EW}}(h \rightarrow XY)$ represents scalar mixing and additional scalar loop contributions. Therefore, it vanishes in the decoupling limit.

In Fig. 7, we show the allowed range of $\overline{\Delta}_{\text{EW}}(h \rightarrow \tau\bar{\tau})$ as a function of m_Φ . We take $\mu = 1$ GeV and scan λ_4 under the vacuum stability, tree-level unitarity and perturbativity constraints. The solid line corresponds to the prediction with $\lambda_4^{\min} \sim 0$. In this case, all Higgs quartic couplings take small values, so that $\overline{\Delta}_{\text{EW}}(h \rightarrow \tau\bar{\tau})$ is almost zero. The dashed and dot-dashed lines correspond to the predictions with λ_2^{\max} and λ_4^{\max} , respectively. For $m_\Phi \lesssim 450$ GeV, λ_2 becomes maximal at the top of the parabola in Fig. 6, $\lambda_2^{\max} = 2m_\Phi^2/v^2$, while $\lambda_4^{\max} \simeq \lambda_4^+$ with $\lambda_2 \simeq 0$. Since both increase as m_Φ becomes larger, the magnitude of $\overline{\Delta}_{\text{EW}}(h \rightarrow \tau\bar{\tau})$ also increases. For $450 \text{ GeV} \lesssim m_\Phi \lesssim 470$ GeV, there exist two distinct ranges of $\overline{\Delta}_{\text{EW}}(h \rightarrow \tau\bar{\tau})$. This corresponds to the second case discussed in Fig. 6, where a part of the parabola lies outside the allowed region. For example, for $m_\Phi = 450$ GeV, $-2\% \lesssim \overline{\Delta}_{\text{EW}}(h \rightarrow \tau\bar{\tau}) \leq 0\%$ and $-15\% \lesssim \overline{\Delta}_{\text{EW}}(h \rightarrow \tau\bar{\tau}) \lesssim -11.5\%$ are allowed. For $m_\Phi \gtrsim 470$ GeV, $\overline{\Delta}_{\text{EW}}(h \rightarrow \tau\bar{\tau})$ exhibits decoupling behavior as m_Φ increases.

The results for the other decay modes are almost identical except for $h \rightarrow WW^*$. Since $\overline{\Delta}_{\text{EW}}(h \rightarrow WW^*)$ is sensitive to corrections to m_W as discussed in Sec. 5.2.3, it exhibits nontrivial behavior for small m_Φ , but shows decoupling behavior as m_Φ increases.

We briefly discuss the case with $\bar{v}_\Delta \neq 0$. For $\bar{v}_\Delta \ll \bar{v}$, we have $\mu \simeq \sqrt{2}m_\Phi^2\bar{v}_\Delta/\bar{v}^2$, and μ becomes large as m_Φ increases. As a result, the Higgs quartic couplings become large, and the new physics contributions do not decouple. Since the size of the Higgs quartic couplings is constrained by the theoretical requirements, there is an upper bound on m_Φ for $\bar{v}_\Delta \neq 0$. For example, m_Φ should be smaller than 7.5 TeV for $\bar{v}_\Delta = 10$ GeV.

6 Deviations from the SM predictions in the Higgs boson decays

6.1 Constraints on the parameter space

From the tree-level analysis of ρ_0 in Sec. 2, we find that $v_\Delta \ll v$. Then, the following mass relations are approximately satisfied.

$$m_A^2 = m_H^2, \quad m_{H^\pm}^2 - m_A^2 = m_{H^{\pm\pm}}^2 - m_{H^\pm}^2. \quad (6.1)$$

There are three scenarios depending on the value of $\xi = m_{H^\pm}^2 - m_A^2$. The first is the degenerate scenario with $\xi = 0$, where all of the additional Higgs bosons are degenerate in their mass. The second is the lightest $H^{\pm\pm}$ scenario (LS) with $\xi < 0$ and $m_{H^{\pm\pm}} < m_{H^\pm} < m_A$. The third is the heaviest $H^{\pm\pm}$ scenario (HS) with $\xi > 0$ and $m_A < m_{H^\pm} < m_{H^{\pm\pm}}$.

Constraints from direct searches for the additional Higgs bosons have been studied in Ref. [132]. In the degenerate scenario, $m_{H^{\pm\pm}} < 950$ GeV is excluded for $v_\Delta < \mathcal{O}(10^{-4})$ GeV by multi-lepton searches. On the other hand, for $v_\Delta > \mathcal{O}(10^{-4})$ GeV, multi-boson searches exclude $m_{H^{\pm\pm}} < 400$ GeV. In the HS, $m_{H^{\pm\pm}} \lesssim 900$ GeV is excluded for $v_\Delta < \mathcal{O}(10^{-6})$ GeV and $m_{H^{\pm\pm}} - m_{H^\pm} = 10$ GeV, similarly to the degenerate scenario. By contrast, for $v_\Delta > \mathcal{O}(10^{-6})$ GeV, the constraints weaken, and $m_{H^{\pm\pm}} \lesssim 400$ GeV is excluded for $v_\Delta > \mathcal{O}(10^{-1})$ GeV with $m_{H^{\pm\pm}} - m_{H^\pm} = 10$ GeV. In the LS, $m_{H^{\pm\pm}} \lesssim 1000$ GeV is excluded

for $v_\Delta < \mathcal{O}(10^{-4})$ GeV by multi-lepton searches, while $m_{H^\pm} \lesssim 600$ GeV is excluded for $v_\Delta > \mathcal{O}(10^{-4})$ GeV.

The CHTM parameters, especially v_Δ , are constrained by the electroweak precision observables [18, 22, 26]. We calculate m_{W,G_F} , ρ , s_e^2 and $\Gamma(Z \rightarrow \ell\bar{\ell})$ at the one-loop level and require that the differences between the CHTM and the SM predictions are within the experimental uncertainties. The 2σ errors of these quantities are given by¹⁰ [91]

$$\begin{aligned} |\Delta m_W| &\leq 2.66 \text{ MeV}, \quad |\rho - 1| \leq 1.8 \times 10^{-3}, \quad |\Delta s_e^2| \leq 6.6 \times 10^{-4}, \\ |\Delta\Gamma(Z \rightarrow \ell\bar{\ell})| &\leq 0.17 \text{ MeV}. \end{aligned} \quad (6.2)$$

In addition, measurements of the signal strength of $h \rightarrow \gamma\gamma$, $\mu_{\gamma\gamma} = \sigma(gg \rightarrow h)\text{Br}(h \rightarrow \gamma\gamma)$, constrain the CHTM parameters. We define $\Delta\mu_{\gamma\gamma}$ as

$$\Delta\mu_{\gamma\gamma} = \frac{\mu_{\gamma\gamma}^{\text{CHTM}} - \mu_{\gamma\gamma}^{\text{SM}}}{\mu_{\gamma\gamma}^{\text{SM}}} = \zeta_h^2 \frac{\text{Br}(h \rightarrow \gamma\gamma)_{\text{CHTM}}}{\text{Br}(h \rightarrow \gamma\gamma)_{\text{SM}}} - 1, \quad (6.3)$$

where we have used $\sigma(gg \rightarrow h)_{\text{CHTM}} = \zeta_h^2 \sigma(gg \rightarrow h)_{\text{SM}}$ at LO. The current bound is $|\Delta\mu_{\gamma\gamma}| < 0.18$ at 2σ , which is taken in light of the experimental uncertainties, rather than the central values, reported by ATLAS [133] and CMS [134].

We first discuss the allowed parameter region in the HS. In the upper left panel of Fig. 8, we show the prediction for $\Delta m_{W,G_F}$ as a function of $\Delta m = m_{H^\pm} - m_A$. The color indicates the value of \bar{v}_Δ . We scan the ranges $300 \text{ GeV} \leq m_A \leq 1000 \text{ GeV}$ and $-5 \leq \lambda_4 \leq 4\pi$. At the tree level, m_{W,G_F} becomes smaller than the SM value as \bar{v}_Δ increases. On the other hand, one-loop effects induced by the mass-squared difference ξ increase the value of m_W . Thus, a larger Δm is preferred for a larger \bar{v}_Δ .

In the upper right (lower left) panel of Fig. 8, we show the prediction for $\Delta\mu_{\gamma\gamma}$ at LO as a function of λ_4 , where the color indicates the value of m_{H^\pm} (Δm) and the solid line represents the current bound. In the HS, the $H^{\pm\pm}$ contribution (the fourth term in the right-hand side of Eq. (5.51)), which is proportional to $\lambda_{hH^{++}H^{--}} \simeq -\lambda_4 v$, decreases $\mu_{\gamma\gamma}$ as λ_4 increases. This loop effect is suppressed by $1/m_{H^\pm}^2$, and thus a heavier $H^{\pm\pm}$ is preferred for larger λ_4 . On the other hand, a large Δm requires a sizable λ_4 . This is because a large Δm leads to a large negative value of λ_5 ($\simeq -4(m_{H^\pm}^2 - m_A^2)/v^2$). From vacuum stability, we require $\lambda_4 + \lambda_5 \gtrsim 0$, so a larger λ_4 is favored for more negative λ_5 .

In the lower right panel of Fig. 8, we show the allowed parameter points in the HS under the constraints from the electroweak precision observables and $\Delta\mu_{\gamma\gamma}$. The gray points are consistent with the electroweak precision observables but are excluded by $\Delta\mu_{\gamma\gamma}$, while the colored points satisfy both constraints. If $m_A \lesssim 650$ GeV, the points with large \bar{v}_Δ are excluded by $\Delta\mu_{\gamma\gamma}$. As a result of the combined constraints, an upper bound on \bar{v}_Δ is obtained as $v_\Delta \lesssim 17.5$ GeV in the HS.

Next, we discuss the allowed parameter region in the LS. In the upper left panel of Fig. 9, we show the prediction for $\Delta m_{W,G_F}$ as a function of $\Delta m = m_{H^\pm} - m_{H^{\pm\pm}}$. The color indicates the value of \bar{v}_Δ . We scan the ranges $400 \text{ GeV} \leq m_{H^{\pm\pm}} \leq 1000 \text{ GeV}$ and

¹⁰We take the value of $|\rho - 1|$ from a result corresponding to a three-parameter fit including the T parameter.

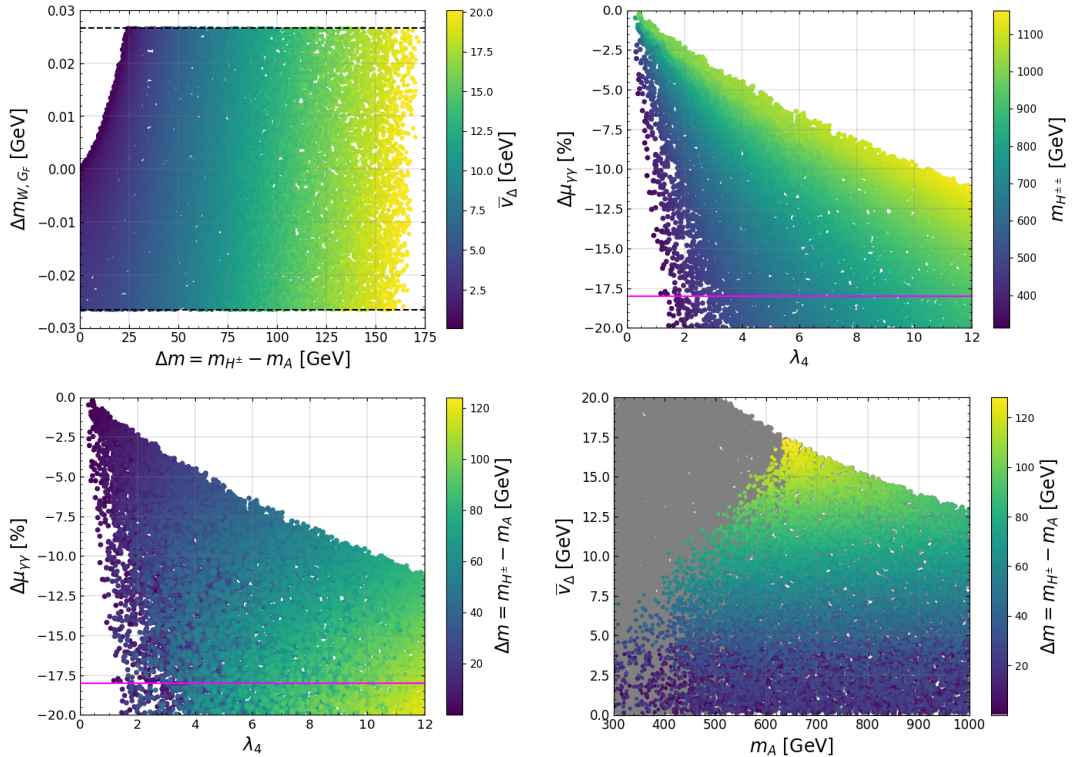


Figure 8: Predictions for $\Delta m_{W,G_F}$ (upper left) and $\Delta\mu_{\gamma\gamma}$ (upper right and lower left), together with the allowed parameter points (lower right) in the HS.

$-5 \leq \lambda_4 \leq 4\pi$. As in the HS, loop effects compensate for the tree-level reduction of m_W , and thus a larger Δm is preferred for a larger \bar{v}_Δ .

In the upper right (lower left) panel of Fig. 9, we show the allowed parameter points in the LS in the λ_4 – Δm plane, where the color indicates the value of \bar{v}_Δ ($m_{H^\pm\pm}$). The gray points are excluded by the constraint from $\Delta\mu_{\gamma\gamma}$. For $m_{H^\pm\pm} \lesssim 450$ GeV, values of λ_4 as large as 4π are allowed, whereas we find $\lambda_4 \lesssim 5$ for $m_{H^\pm\pm} \gtrsim 450$ GeV. These limits on λ_4 are obtained from perturbativity and tree-level unitarity, in particular from $a_{5,+}$, and parameter points with large λ_4 and light $m_{H^\pm\pm}$ satisfy the theoretical constraints and are consistent with the electroweak precision observables. However, such points are excluded by the constraint from $\Delta\mu_{\gamma\gamma}$. As a result of the combined constraints, an upper bound $\lambda_4^{\max} \simeq 3$ is obtained for small \bar{v}_Δ .

We now turn to the region with large \bar{v}_Δ , where the constraint from $\Delta\mu_{\gamma\gamma}$ becomes less effective, and the allowed parameter region is instead determined by the electroweak precision observables, vacuum stability, and tree-level unitarity. Since a larger Δm is preferred for a larger \bar{v}_Δ , λ_3 ($\simeq \lambda_5 \simeq 4(m_{H^\pm}^2 - m_{H^\pm\pm}^2)/v^2$) becomes sizable and positive. As a consequence, negative values of λ_4 are allowed under the vacuum stability condition, $\lambda_4 + 2\sqrt{\lambda_1(\lambda_2 + \lambda_3/2)} > 0$. As λ_3 increases, or equivalently as Δm and \bar{v}_Δ increase, the upper bound on λ_4 imposed by tree-level unitarity ($a_{5,+}$) becomes negative. Since the lower bound on λ_4 is determined by vacuum stability, this interplay leads to an upper bound on

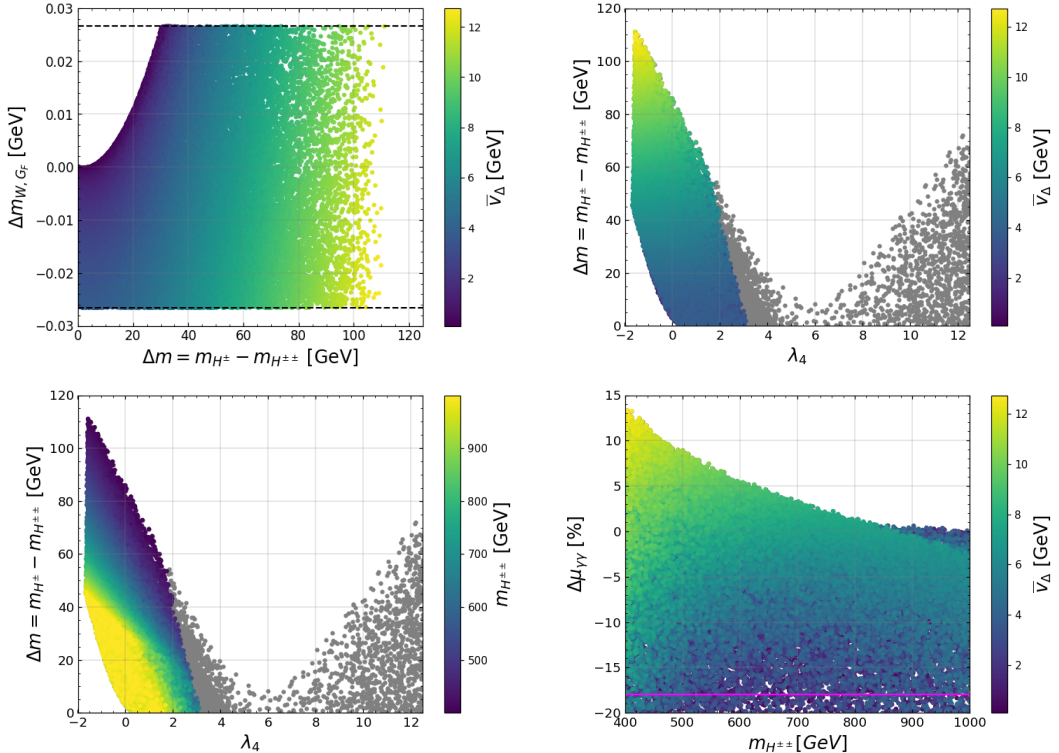


Figure 9: Predictions for $\Delta m_{W,G_F}$ (upper left) and $\Delta\mu_{\gamma\gamma}$ (upper right and lower left), together with the allowed parameter points (lower right) in the LS.

λ_3 . Consequently, the maximal allowed value of Δm , which depends on $m_{H\pm\pm}$, is about 110 GeV for $m_{H\pm\pm} \simeq 400$ GeV in the LS.

In the lower right panel of Fig. 9, we show the prediction for $\Delta\mu_{\gamma\gamma}$ at LO as a function of $m_{H\pm\pm}$, where the color indicates the value of \bar{v}_Δ and the solid line represents the current bound. Since the $H^{\pm\pm}$ contribution is proportional to λ_4 , $\Delta\mu_{\gamma\gamma}$ is sensitive to the sign of λ_4 , and a positive $\Delta\mu_{\gamma\gamma}$ is a clear signature of the LS with a large \bar{v}_Δ .

6.2 Numerical results in the heaviest $H^{\pm\pm}$ scenario

6.2.1 Correlations in the decay rates of h

In this section, we discuss deviations from the SM predictions in the Higgs boson decay rates and the branching ratios. For convenience, we quantify the deviations by

$$\Delta R(h \rightarrow XX) = \frac{\Gamma(h \rightarrow XX)^{\text{NP}}}{\Gamma(h \rightarrow XX)^{\text{SM}}} - 1, \quad (6.4)$$

where $\Gamma(h \rightarrow XX)^{\text{NP(SM)}}$ is the decay rate for a new physics model (the SM).

To demonstrate how one can distinguish CHTM from other extended Higgs models, we perform a scan analysis, calculating the deviations in the decay rates and the branching ratios with higher-order corrections. We impose the theoretical constraints discussed in Sec. 2 and the experimental constraints presented above (direct searches, electroweak

precision observables, and measurements of $h \rightarrow \gamma\gamma$ at the LHC). As discussed above, the upper limit of \bar{v}_Δ is $\bar{v}_\Delta \lesssim 17.5$ GeV in the HS. Thus, we fix $\bar{v}_\Delta = 1, 10$ and 15 GeV in the analysis of the HS. Other parameters are in the following ranges,

$$\text{HS: } 300 \text{ GeV} \leq m_A \leq 1000 \text{ GeV}, \quad 0 \leq \lambda_4 \leq 4\pi, \quad 0 \leq \Delta m \leq 150 \text{ GeV}, \quad (6.5)$$

where Δm gives the mass difference among the heavy Higgs bosons; $\Delta m = m_{H^\pm} - m_A$ for the HS.¹¹

To discuss the distinguishability of the CHTM, we not only display the results for the CHTM, but also present the results of four types of 2HDMs, the inert doublet model (IDM), and the HSM. The predictions for the decays of h for all of these models are calculated by `H-COUP` [72–74]. For these models, the input parameters, which are defined in Ref. [74], are set as¹²

$$\begin{aligned} \text{2HDM Type-I: } & 400 \text{ GeV} < m_H < 1 \text{ TeV}, \quad 0.99 < \sin(\beta - \alpha) < 1, \\ & 1.5 < \tan \beta < 10, \quad 0 < M < m_H + 500 \text{ GeV}, \end{aligned} \quad (6.6)$$

$$\begin{aligned} \text{2HDM Type-II: } & 800 \text{ GeV} < m_H < 1 \text{ TeV}, \quad 0.995 < \sin(\beta - \alpha) < 1, \\ & 1 < \tan \beta < 10, \quad 0 < M < m_H + 500 \text{ GeV}, \end{aligned} \quad (6.7)$$

$$\begin{aligned} \text{HSM: } & 400 \text{ GeV} < m_H < 1000 \text{ GeV}, \quad \lambda_S = 0.1, \quad \mu_s = 0, \\ & 0.95 < \cos \alpha < 1, \quad 0 < m_s < m_H + 500 \text{ GeV}, \end{aligned} \quad (6.8)$$

$$\begin{aligned} \text{IDM: } & 100 \text{ GeV} < m_{H^\pm} < 1000 \text{ GeV}, \quad m_H = 60 \text{ GeV}, \quad m_A = m_{H^\pm} \\ & 0 < \lambda_2 < 4\pi, \quad \mu_2^2 = 3581 \text{ GeV}^2. \end{aligned} \quad (6.9)$$

We assume the degenerate mass scenario for the 2HDMs, i.e., $m_A = m_{H^\pm} = m_H$. For Type-I, the lower bounds of m_H and $\tan \beta$ are taken under the consideration of constraints from $b \rightarrow s\gamma$ [135, 136]. The same is true for the lower bounds of m_H for Type-II 2HDM. For IDM, we consider the scenario where H is dark matter with a mass of 60 GeV. We note that, in this scenario, μ_2^2 is fixed, so that loop corrections by additional Higgs bosons do not decouple in the decay rates of h as can be seen in the following numerical results [47, 68]. In this scan region, particularly in the 2HDMs, the predicted Higgs decay rates can deviate significantly from the SM. Hence, we conservatively impose the current LHC constraints on 2σ allowed ranges of the Higgs coupling modifiers κ_i without their central values under the assumption that the branching ratio to beyond-the-Standard-Model (BSM) final states is zero [137]. We apply the bounds on $\kappa_\tau, \kappa_b, \kappa_\gamma, \kappa_g, \kappa_\lambda$. Including higher-order corrections,

¹¹In the degenerate scenario $m_{H^{\pm\pm}} = m_{H^\pm} = m_A = m_H$, the upper bound on \bar{v}_Δ becomes more stringent, reaching approximately 1 GeV. Consequently, the predictions for the Higgs decay rates are close to those obtained in the HS with $\bar{v}_\Delta = 1$ GeV. Note that the deviations from the SM in the decay rate are relatively smaller than the HS with $\bar{v}_\Delta = 1$ GeV since the lower bound of $m_{H^{\pm\pm}}$ is 400 GeV in the degenerate case [132].

¹²Although, in `H-COUP 3.0`, $\lambda_{\Phi S}$ in the HSM is taken as an input parameter instead of m_s , we here scan m_s with a relation written in Ref. [60].

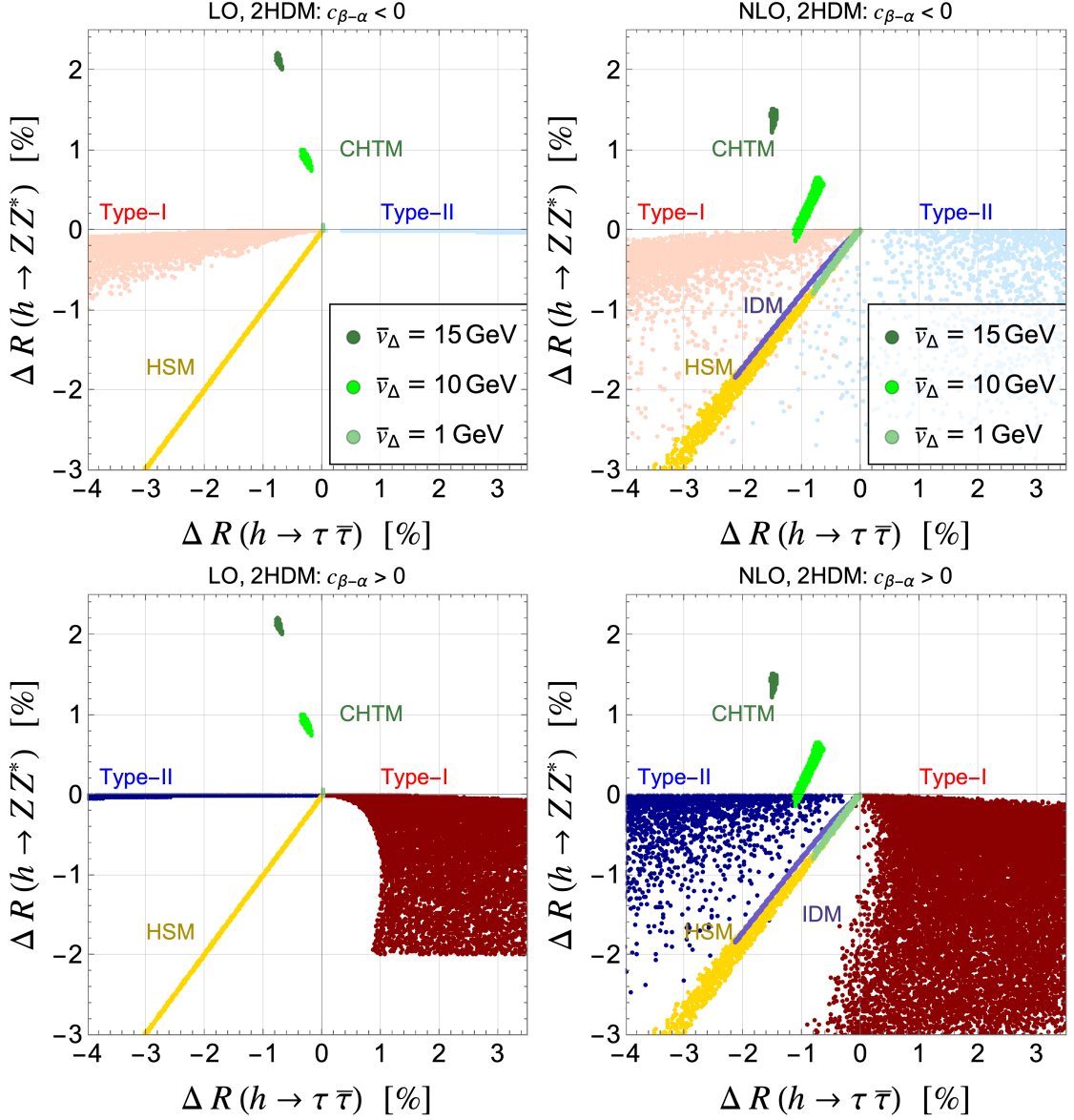


Figure 10: Correlations for $h \rightarrow ZZ^*$ and $h \rightarrow \tau\bar{\tau}$ in the HS. The left (right) panels show the results at the LO (NLO). Upper (lower) panels show 2HDM predictions with $c_{\beta-\alpha} < 0$ ($c_{\beta-\alpha} > 0$).

they are theoretically evaluated by $\kappa_X^2 = \Gamma^{\text{2HDM}}(h \rightarrow XX)/\Gamma^{\text{SM}}(h \rightarrow XX)$ ($X = \tau, b, g, \gamma$) and $\kappa_\lambda = \lambda_{hhh}^{\text{2HDM}}/\lambda_{hhh}^{\text{SM}}$ ^{13 14}.

In this section, we present the numerical results for each model, distinguished by different colors in the figures. The results of the CHTM are shown in several shades of

¹³We confirmed that for the CHTM, IDM and HSM there are no excluded points by the constraint of the Higgs coupling in the chosen scan region.

¹⁴The one-loop corrections to λ_{hhh} depend on the external incoming momenta p_1 and p_2 and the outgoing momentum $q = p_1 + p_2$. We set them as $p_1^2 = p_2^2 = m_h^2$ and $q^2 = (2m_h + 10 \text{ GeV})^2$.

green, where each shade represents a different value of \bar{v}_Δ , i.e., dark green, green, and light green correspond to the results for $\bar{v}_\Delta = 15, 10$, and 1 GeV, respectively. The results for the Type-I (Type-II) 2HDM with $c_{\beta-\alpha} < 0$ and those with $c_{\beta-\alpha} > 0$ are shown by the light magenta (light blue) and dark red (dark blue) regions, respectively. In Fig. 10, the results for the two signs of $c_{\beta-\alpha}$ are plotted in separate panels. In the other figures, however, the results are shown in the same panel without separation. We also plot the results of the HSM and the IDM using yellow and purplish blue points, respectively. This color scheme is used consistently in the following numerical figures.

While we will discuss numerical results with NLO EW and N(N)LO QCD corrections below, let us first discuss the behavior of the deviations in the LO decay rate. At the tree-level, $\Delta R(h \rightarrow XX)$ is governed by the square of coupling modifiers, i.e., ζ_h^2 for $h \rightarrow f\bar{f}$, c_{hVV}^2 for $h \rightarrow VV^*$. The shift of the gauge boson masses is also relevant for the latter process, i.e., Eqs. (2.19) and (3.7). The coupling modifiers are controlled by the scalar mixing parameters. Larger mixing leads to larger deviations from unity in them. Due to the larger \bar{v}_Δ , decays into weak gauge bosons deviate in the positive direction as shown in the left panels of Fig. 10, which are characteristic predictions for the exotic Higgs sector [30, 138–140]. Thus, the CHTM can be separated from the simple extended Higgs models with $\rho_0 = 1$ by looking at the correlation between the $\Delta R(h \rightarrow ZZ^*)$ and $\Delta R(h \rightarrow \tau\bar{\tau})$.

The NLO EW corrections significantly alter the quantitative results. As a concrete example illustrating this point, we show the correlation between $\Delta R(h \rightarrow \tau\bar{\tau})$ and $\Delta R(h \rightarrow ZZ^*)$ obtained from the LO and NLO analyses in the left and right panels of Fig. 10, respectively. As can be seen from a comparison of these figures, the theoretical predictions of the CHTM are shifted by almost -1% in the negative direction relative to the LO results for both $h \rightarrow ZZ^*$ and $h \rightarrow \tau\bar{\tau}$, independently of the value of \bar{v}_Δ . This behavior originates from the loop corrections involving the scalar couplings $\lambda_{h\phi\phi}$ of the charged and doubly charged Higgs bosons (for instance, the counterterm δZ_h contains a term proportional to $\lambda_{h\phi\phi}^2$). Assuming a small mixing angle α , it scales as $\alpha \sim \bar{v}_\Delta$. Because of this, the three scenarios with different values of \bar{v}_Δ correspond to different possible values of α . In addition, the mass splitting Δm increases with \bar{v}_Δ . For example, after imposing the theoretical and experimental constraints discussed above, we find that for $\bar{v}_\Delta = 15$ (1) GeV, one typically obtains $\sin \alpha \sim 0.1$ (0) and $\Delta m_{\max} \sim 120$ (30) GeV. When $\sin \alpha \neq 0$, the contributions proportional to $\sin \alpha$ become sizable. (As shown in Appendix A of Ref. [18], the coupling $\lambda_{h\phi\phi}$ can be expressed as $\lambda_{h\phi\phi} \sim A \cos \alpha + B \sin \alpha$, where A and B are coefficients with mass dimension one.) This enhances the loop contributions from both the doubly and singly charged Higgs bosons. As a result, $\Delta R(h \rightarrow ZZ^*)$ and $\Delta R(h \rightarrow \tau\bar{\tau})$ deviate from their tree-level predictions by $\mathcal{O}(1)\%$. In the case of $\bar{v}_\Delta = 1$ GeV, since $\sin \alpha$ takes a value close to zero, there exists a parameter region where the loop contributions from the additional Higgs bosons almost decouple, namely reproducing the LO results. A similar behavior can also be observed in the 2HDMs. Namely, the NLO predictions deviate from the tree-level results at the level of a few percent by loop corrections. While the LO predictions are well separated among the 2HDMs, HSM, and IDM, these predictions overlap with each other at the NLO level.

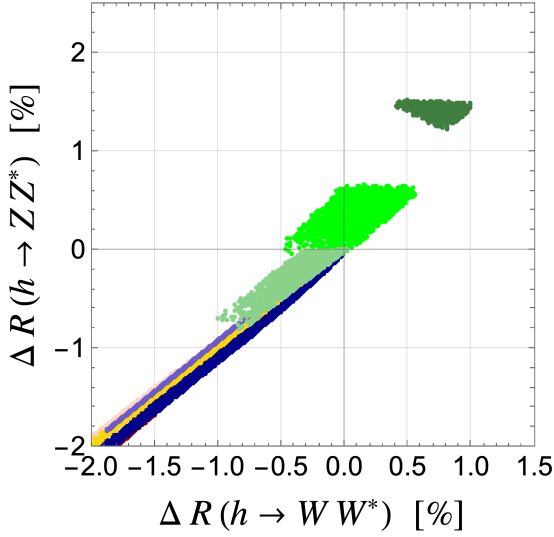


Figure 11: Correlations for the $h \rightarrow ZZ^*$ and $h \rightarrow WW^*$ in the HS.

We also show the correlation between $\Delta R(h \rightarrow ZZ^*)$ and $\Delta R(h \rightarrow WW^*)$ in Fig. 11. A point worth emphasizing is that, in the CHTM, the deviation of $h \rightarrow ZZ^*$ tends to be relatively larger than that of $h \rightarrow WW^*$ in the case of $\Delta R(h \rightarrow ZZ^*) > 0$. In contrast, $\Delta R(h \rightarrow ZZ^*)$ and $\Delta R(h \rightarrow WW^*)$ are approximately equal in other models. This characteristic difference between the $h \rightarrow ZZ^*$ and $h \rightarrow WW^*$ decay modes in the CHTM originates from the difference in the coupling modifiers. In addition, it also comes from the fact that $h \rightarrow WW^*$ is affected by corrections of Δr associated with the W -boson mass as discussed in Sec. 5.2.

Let us discuss whether one can distinguish the CHTM from the other models¹⁵. Although the inclusion of NLO corrections shifts the predictions in the negative direction regardless of the decay mode, the tendency that $h \rightarrow ZZ^*$ and $h \rightarrow WW^*$ can have positive deviations remains unchanged. Therefore, if such a positive deviation is observed in future collider experiments, one could identify the CHTM. The result of $h \rightarrow ZZ^*$ for $\bar{v}_\Delta = 15$ GeV is indeed comparable with the precision of the future Higgs factory, e.g. the ILC with 250 GeV, 0.58%, referring to the accuracy of κ_Z [142] (although $h \rightarrow \tau\bar{\tau}$ is challenging due to around the 4% measurement accuracy).

When $h \rightarrow ZZ^*$ and $h \rightarrow WW^*$ have positive deviations, other observables also show characteristic predictions. In particular, both $h \rightarrow \gamma\gamma$ and the Higgs self-coupling receive significant corrections originating from the charged and doubly charged Higgs bosons through the $\lambda_{h\phi\phi}$ coupling. As shown in Fig. 12, for $\bar{v}_\Delta = 15$ GeV, $\Delta R(h \rightarrow \gamma\gamma)$ can be as large as -18% , while the deviation of λ_{hhh} from the SM prediction can reach about 130%.¹⁶ The projected sensitivity for the measurement of the triple Higgs coupling at the

¹⁵Discrimination of the 2HDMs, HSM and IDM by the Higgs precision measurement is discussed in Refs. [48, 49, 139, 141] in detail.

¹⁶In the 2HDMs, we see that λ_{hhh} can deviate in a negative direction in certain regions of parameter space. The main sources of the negative shift arise from the tree-level contribution of order $c_{\beta-\alpha}^2$ and the

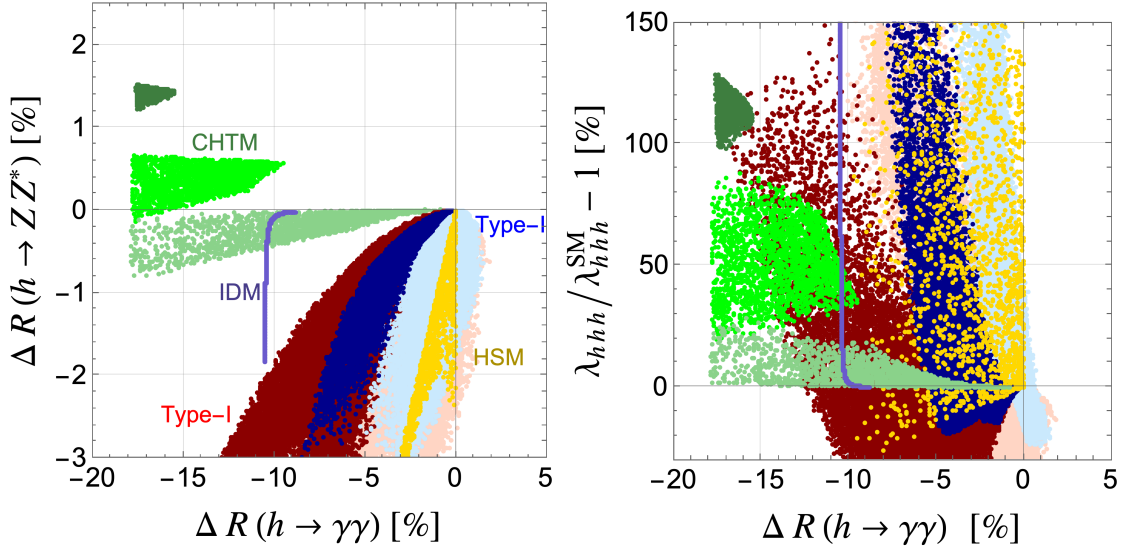


Figure 12: Correlations for the deviations in the decay rates and the Higgs self-coupling in the HS.

HL-LHC is below 30% at the 68% confidence level [32], whereas that for the $h\gamma\gamma$ coupling is around 1.8% [32]. Therefore, if the characteristic positive deviations in $h \rightarrow ZZ^*$ and $h \rightarrow WW^*$ predicted by the CHTM are realized, their indications should become visible already at the HL-LHC stage.

6.2.2 Correlations of the branching ratios of h

We then discuss the deviations from the SM predictions in the branching ratio of h , which are parameterized by

$$\Delta\mu(h \rightarrow XX) = \frac{\text{BR}(h \rightarrow XX)^{\text{NP}}}{\text{BR}(h \rightarrow XX)^{\text{SM}}} - 1, \quad (6.10)$$

where $\text{BR}(h \rightarrow XX)^{\text{NP(SM)}}$ is the branching ratio for a new physics model (SM). This quantity is approximated by

$$\Delta\mu(h \rightarrow XX) \simeq \Delta R(h \rightarrow XX) - \Delta R^{\text{tot}}, \quad (6.11)$$

where ΔR^{tot} denotes the deviation in the total decay width. It is defined by $\Delta R^{\text{tot}} = \Gamma_h^{\text{tot,NP}} / \Gamma_h^{\text{tot,SM}} - 1$. In the derivation of this equation, we have assumed that ΔR^{tot} , $\Delta R(h \rightarrow XX) \ll 1$.

In Fig. 13, to understand the behavior of $\Delta\mu(h \rightarrow XX)$, we display the deviations of the total decay width of h as a function of $\sin\alpha$. Since the dominant contribution to the total width comes from $h \rightarrow b\bar{b}$, ΔR^{tot} mainly reflects the effects of new physics on this decay mode. In $h \rightarrow b\bar{b}$, the loop contributions of the additional Higgs bosons induced

one-loop correction of order $c_{\beta-\alpha}$. These negative contributions appear in the case where $c_{\beta-\alpha}$ is not too small and $M \sim m_H$ [43].

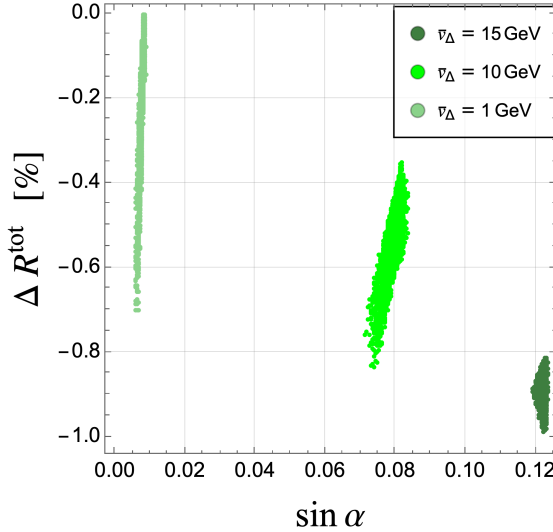


Figure 13: Deviations from the SM predictions in the total decay width defined of h are shown in the CHTM by $\Delta R^{\text{tot}} = \Gamma_h^{\text{tot, NP}} / \Gamma_h^{\text{tot, SM}} - 1$ with $\Gamma_h^{\text{tot, NP(SM)}}$ being the total decay width for new physics models (SM).

by the $\lambda_{h\phi\phi}$ coupling also become significant, especially in the regime of large \bar{v}_Δ . As a consequence, the deviation in the total width increases as the size of \bar{v}_Δ grows.

The behavior of the deviations in the Higgs boson branching ratios from the SM predictions can be understood from Eq. (6.11). As an example, let us focus on the deviation in the branching ratio of $h \rightarrow ZZ^*$. As shown in Fig. 14, $\Delta\mu(h \rightarrow ZZ^*)$ is approximately 0% for $\bar{v}_\Delta = 0$ and about 2.4% for $\bar{v}_\Delta = 15$ GeV. For $\bar{v}_\Delta = 0$, since $\Delta R(h \rightarrow ZZ^*) \simeq \Delta R^{\text{tot}} \simeq [0, -0.8\%]$, these two deviations largely cancel each other, leading to a small deviation in $\Delta\mu(h \rightarrow ZZ^*)$. On the other hand, for $\bar{v}_\Delta = 15$ GeV, since $\Delta R(h \rightarrow ZZ^*) \simeq [1.2\%, 1.5\%]$ and $\Delta R^{\text{tot}} \simeq [-0.8\%, -1\%]$, the contributions of $\Delta R(h \rightarrow ZZ^*)$ and ΔR^{tot} add up to enhance $\Delta\mu(h \rightarrow ZZ^*)$. A similar behavior can be understood for $h \rightarrow \tau\bar{\tau}$, $h \rightarrow WW^*$, and $h \rightarrow \gamma\gamma$ modes as well, based on Eq. (6.11). As a result, the deviation of $h \rightarrow ZZ^*$ reaches a maximum of 2.5%; however, this would be challenging to detect compared to the measurement accuracy currently estimated for future collider experiments, e.g., 6.7% at the ILC at 250 GeV [34]. When looking at the deviations in the branching ratios, the characteristic positive shift in the $h \rightarrow VV^*$ modes overlaps with the theoretical predictions of the Type-I 2HDM in the plane of $\Delta\mu(h \rightarrow \tau\bar{\tau})$ and $\Delta\mu(h \rightarrow ZZ^*)$. As can be seen in Ref. [48], when $\cos(\beta - \alpha) < 0$, the total width in the Type-I 2HDM tends to shift in the negative direction, resulting in a positive deviation in $\Delta\mu(h \rightarrow VV^*)$. However, the discrimination between the CHTM and the Type-I 2HDM is possible in the $h \rightarrow \gamma\gamma$ mode. In the CHTM, $\Delta\mu(h \rightarrow \gamma\gamma)$ shows a negative deviation exceeding 10%, which is not observed in the 2HDMs. Therefore, similar to the discussion on the deviations in decay rates from the SM predictions, the $h \rightarrow \gamma\gamma$ mode plays a crucial role in identifying the CHTM.

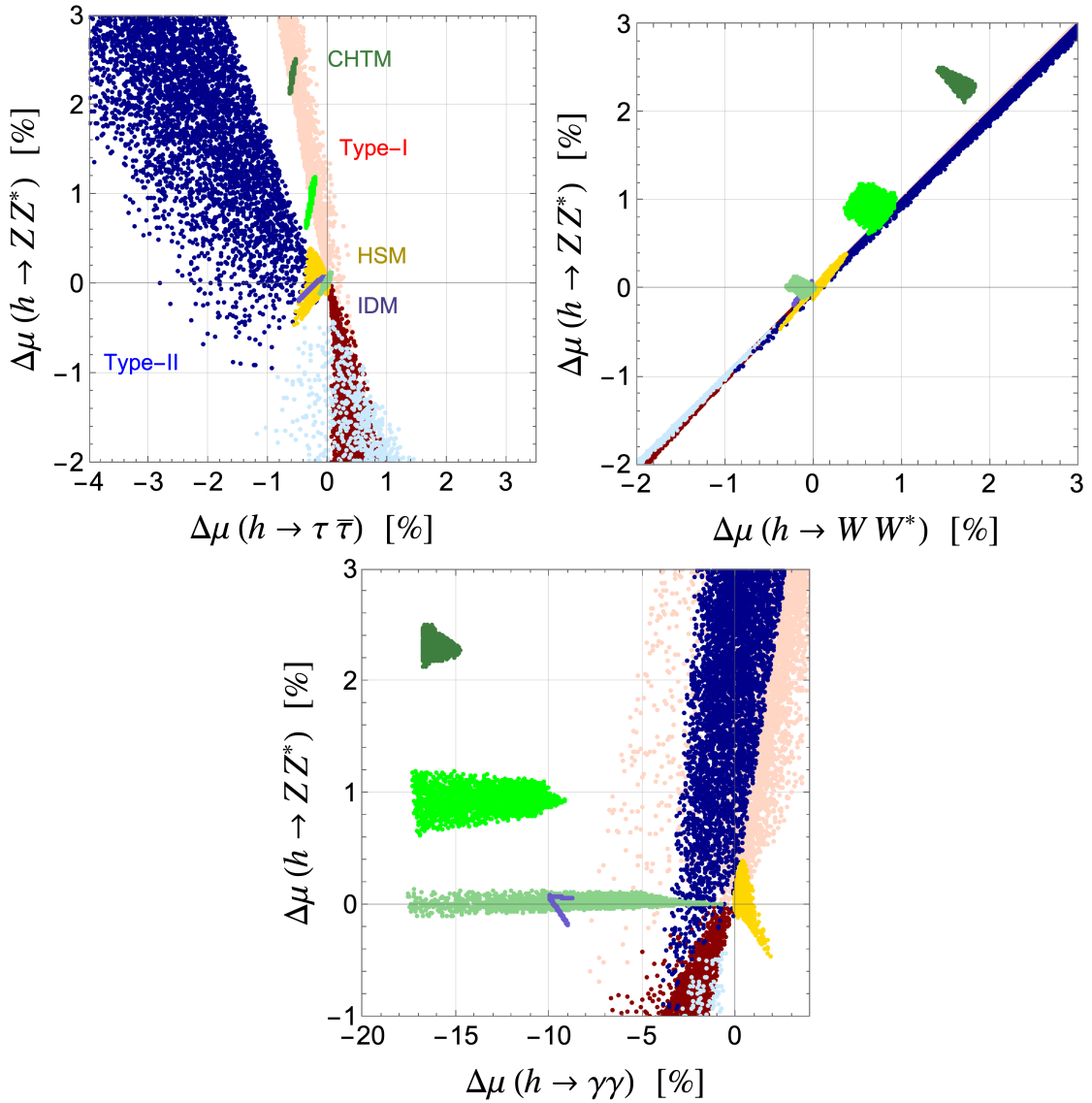


Figure 14: Correlations for the deviations in the branching ratios for the HS.

6.3 Numerical results in the lightest $H^{\pm\pm}$ scenario

We discuss the deviations in the decay rates and branching ratios in the LS ($m_{H^{\pm\pm}} < m_{H^\pm}$). In the following analysis, we take $\bar{v}_\Delta = 1$ and 10 GeV. As discussed in Sec. 6.1, $\bar{v}_\Delta = 15$ GeV is excluded by the theoretical and experimental constraints. Other parameters are in the following ranges,

$$\text{LS: } 400 \text{ GeV} \leq m_{H^{\pm\pm}} \leq 1000 \text{ GeV}, \quad -5 \leq \lambda_4 \leq 4\pi, \quad 0 \leq \Delta m \leq 150 \text{ GeV}, \quad (6.12)$$

where $\Delta m = m_{H^\pm} - m_{H^{\pm\pm}}$.

In Fig. 15, we show the correlation between $\Delta R(h \rightarrow \tau\bar{\tau})$ and $\Delta R(h \rightarrow ZZ^*)$ (left panel) and $\Delta R(h \rightarrow WW^*)$ and $\Delta R(h \rightarrow ZZ^*)$ (right panel), where all the predictions

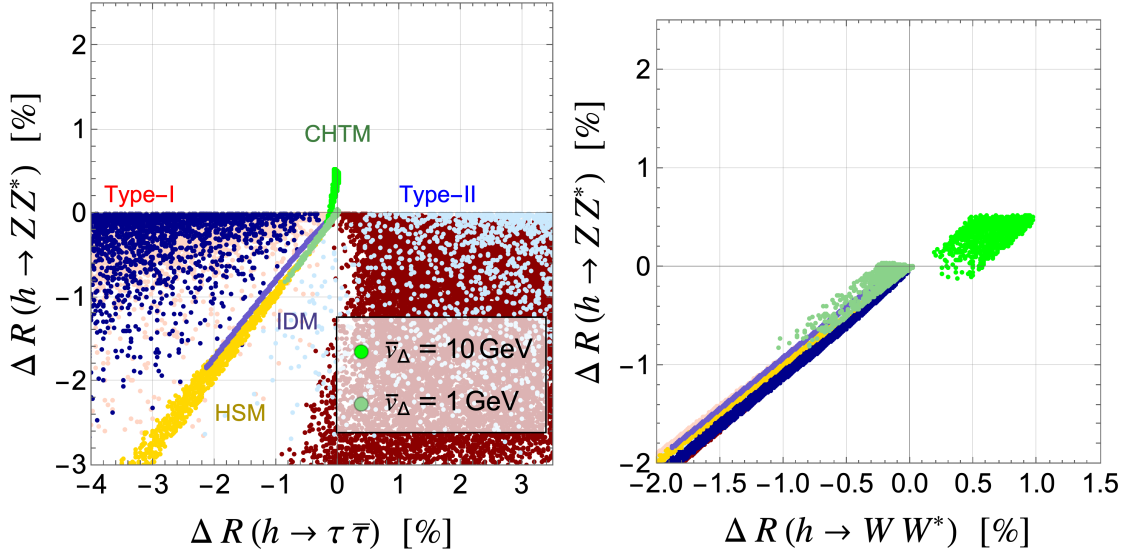


Figure 15: Correlations for the deviations in the decay rates in the LS. The color code is the same as that in the HS.

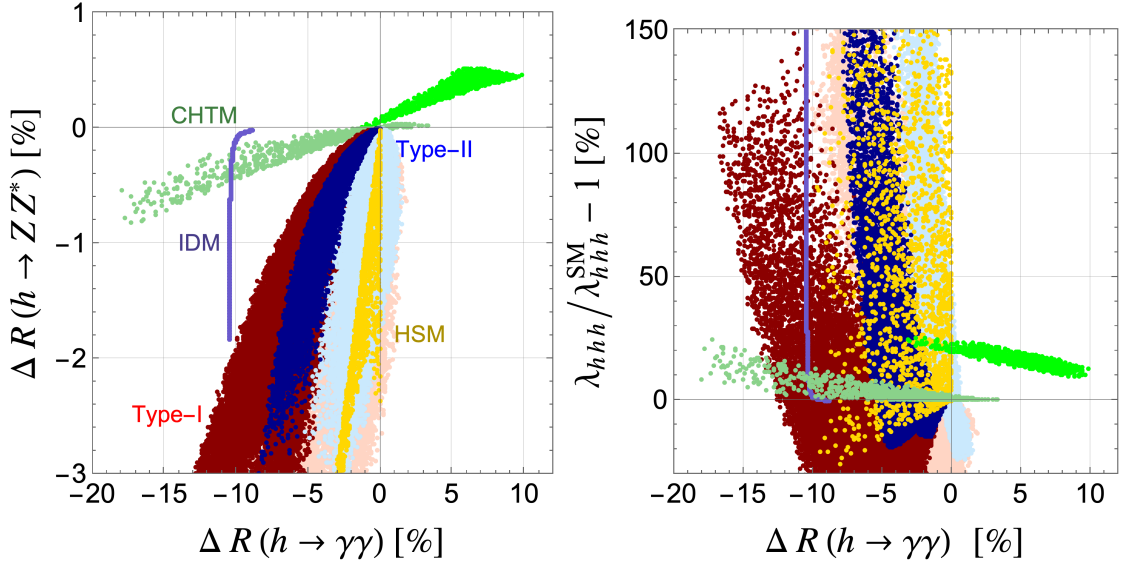


Figure 16: Correlations for the deviations in the decay rates in the LS.

except for the CHTM are the same as those shown in Fig. 10 and Fig. 11, respectively. Since a smaller λ_4 leads to a smaller s_α , the deviations in the Higgs decays are suppressed compared to the HS. The clear signal in the CHTM is a positive deviation in $h \rightarrow VV^*$ with large \bar{v}_Δ , and the maximal values are $\Delta R(h \rightarrow ZZ^*) \simeq 0.5\%$ and $\Delta R(h \rightarrow WW^*) \simeq 1.0\%$.

In Fig. 16, we show the correlation between $\Delta R(h \rightarrow \gamma\gamma)$ and $\Delta R(h \rightarrow ZZ^*)$ (left panel) and $\Delta R(h \rightarrow \gamma\gamma)$ and $\lambda_{hh}/\lambda_{hh}^{\text{SM}} - 1$ similar to the plots shown in Fig. 12. Unlike

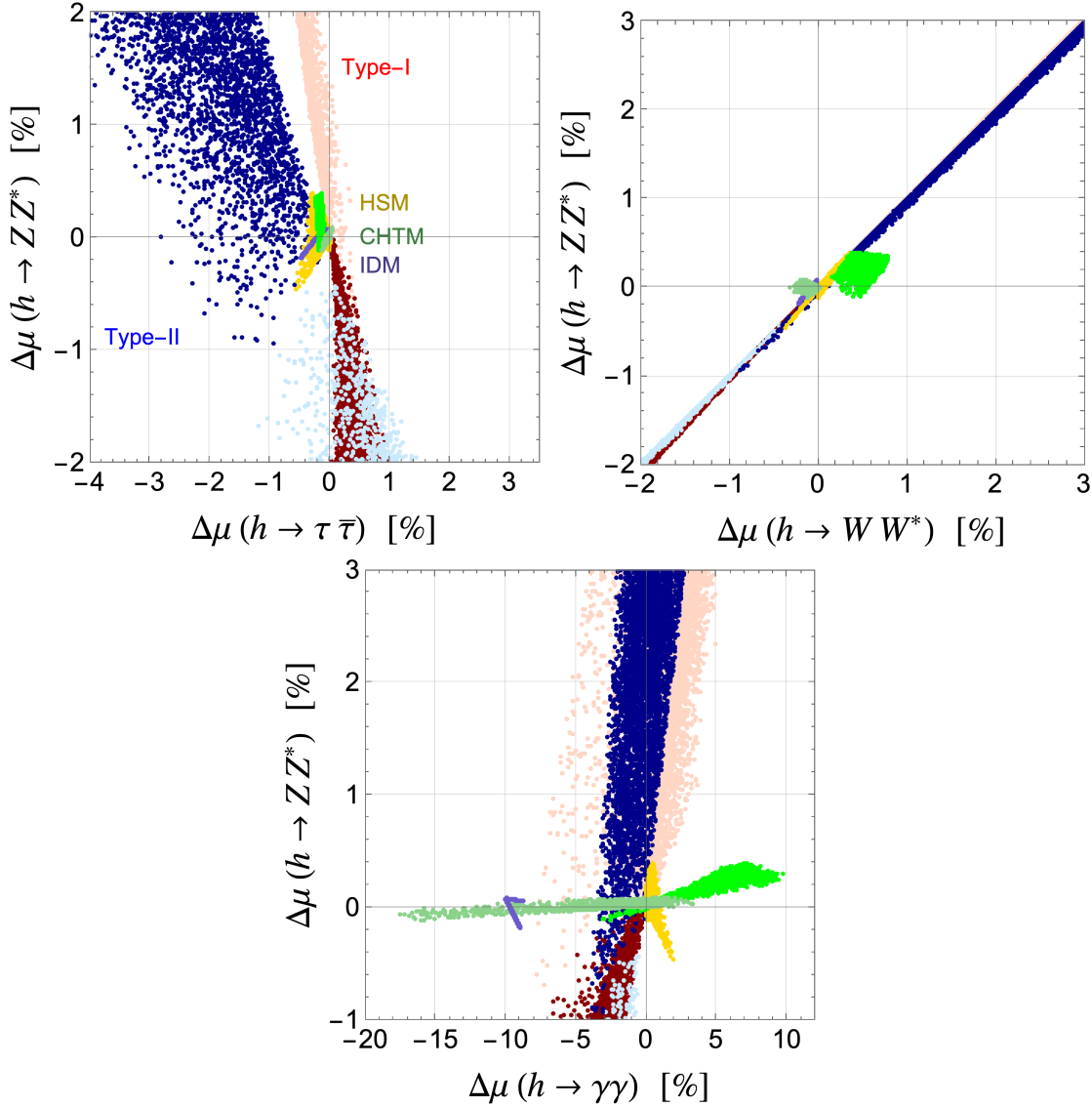


Figure 17: Correlations for the deviations in the branching ratios in the LS.

the HS, the deviation in the decay rate of $h \rightarrow \gamma\gamma$ tends to be predicted in the positive direction for large \bar{v}_Δ as discussed in Sec. 6.1. Such a positive deviation in $h \rightarrow \gamma\gamma$ is rarely seen in the other models, so that this can be a smoking-gun signature in the LS. Regarding the right panel, we see that the amount of the deviation in the λ_{hhh} coupling is maximally given to be about 20% due to the smallness of λ_4 compared to the HS.

Finally, we show the correlation between the deviations in the branching ratios in Fig. 17. Similar to Fig. 14, we display three correlations: $\Delta\mu(h \rightarrow \tau\bar{\tau}) - \Delta\mu(h \rightarrow ZZ^*)$ (upper left), $\Delta\mu(h \rightarrow WW^*) - \Delta\mu(h \rightarrow ZZ^*)$ (upper right) and $\Delta\mu(h \rightarrow \gamma\gamma) - \Delta\mu(h \rightarrow ZZ^*)$ (lower). We see that the correlation $\Delta\mu(h \rightarrow \gamma\gamma) - \Delta\mu(h \rightarrow ZZ^*)$ shows a different pattern from that in the other models as we expect from the behavior of $\Delta R(h \rightarrow \gamma\gamma)$.

Therefore, we can indirectly explore the LS by measuring the deviation in the branching ratio of $h \rightarrow \gamma\gamma$ and other modes such as $h \rightarrow ZZ^*$.

7 Conclusions

In this paper, we present a full set of radiative corrections to decays of the 125 GeV Higgs boson in the CHTM, which is one of the representative examples of an exotic Higgs sector. We have analytically evaluated NLO EW corrections to the Higgs boson two-body decays ($h \rightarrow f\bar{f}$) and three-body decays ($h \rightarrow VV^*$). For the loop-induced processes $h \rightarrow \gamma\gamma$, $Z\gamma$, and gg , we included the higher-order QCD corrections, while the EW corrections are at LO. To perform numerical evaluations of the 125 GeV Higgs boson decays, we have implemented these analytical results into the existing `H-COUP v3` [74] with appropriate extensions. The program for computing the theoretical predictions of the CHTM will be released as the next version of `H-COUP`.

To perform this calculation, we have employed a gauge-invariant on-shell renormalization scheme based on Ref. [74]. In the original work [18], a residual gauge dependence arising from the scalar mixing angle remained. In this paper, we have eliminated this gauge dependence by applying the pinch technique. As discussed in detail in Sec. 4, by focusing on the $f\bar{f} \rightarrow f\bar{f}$ scattering process, we have demonstrated that the relevant pinch terms can be extracted from the vertex, box, and external leg corrections. These pinch terms exactly cancel the gauge-dependent contributions in the Higgs boson self-energy diagrams.

Taking into account various theoretical and experimental constraints, we analyzed the correlations of the deviations in the Higgs boson decay rates and the branching ratios. In the numerical analysis, we focused on the case with $v_\Delta = \mathcal{O}(1\text{--}10)$ GeV, where a characteristic prediction emerges as seen already at LO: the $h \rightarrow VV^*$ modes deviate from the SM in a positive direction in the case where $H^{\pm\pm}$ is the heaviest among the extra Higgs bosons. When NLO corrections are included, the deviations generally shift in the negative direction irrespective of the decay mode ($\sim -1\%$ for $h \rightarrow VV^*$ and $h \rightarrow f\bar{f}$, and $\sim -10\%$ for $h \rightarrow \gamma\gamma$). We demonstrated that even after including NLO corrections, the characteristic predictions of the CHTM are retained. In particular, at the level of decay rates, we have shown that the CHTM can be distinguished from other simple extended Higgs models, such as the 2HDMs, HSM and IDM, through this distinctive feature. Moreover, when such a characteristic positive deviation appears in $h \rightarrow VV^*$, one expects corresponding deviations of $\sim -20\%$ in $h \rightarrow \gamma\gamma$ and $\sim 100\%$ in the hh coupling. Even in the case where $H^{\pm\pm}$ is lightest among the extra Higgs bosons, the CHTM can be identified by detecting $\mathcal{O}(10)\%$ positive deviations in $h \rightarrow \gamma\gamma$. Future precision measurements of the Higgs boson at collider experiments will therefore provide crucial tests for exotic Higgs sectors such as the one investigated in this study.

Finally, although we mainly concentrated on the parameter region with $v_\Delta \sim \mathcal{O}(1\text{--}10)$ GeV where diboson decay is the dominant decay mode of $H^{\pm\pm}$, our calculation can be applied into wider parameter regions, including the case with a smaller v_Δ where $H^{\pm\pm}$ mainly decays into di-leptons.

Acknowledgments

MA was supported by the JSPS Grant-in-Aid for JSPS Fellows No. 22KJ3126. SK was supported, in part, by Grants-in-Aid for Scientific Research(KAKENHI) Nos. 20H00160, 24KF0060, and 24KF0238. KS was supported by the JSPS KAKENHI Grant Numbers 25K17379 and 21K20363. ST was supported by JST SPRING, Grant Number JP-MJSP2138.

A Tree level scalar–vector couplings

In this appendix, we list the coupling modifiers for the Higgs–Higgs–gauge–gauge, Higgs–gauge–gauge, and Higgs–Higgs–gauge interactions, which are expressed as

$$\begin{aligned}
\mathcal{L}_{\text{kin}} \ni & \sum_{\substack{\phi\phi'=hh, hH, HH, \\ AA, G^0A, G^0G^0}} \left[\frac{g^2}{4} c_{\phi\phi'WW} \phi\phi' W^{\pm\mu} W_\mu^\mp + \frac{g_Z^2}{8} c_{\phi\phi'ZZ} \phi\phi' Z^\mu Z_\mu \right] \\
& + \sum_{\phi=h,H} \left[gm_W c_{\phi WW} \phi W^{\pm\mu} W_\mu^\mp + \frac{g_Z}{2} m_Z c_{\phi ZZ} \phi Z^\mu Z_\mu \right. \\
& \pm \frac{g}{2} c_{H^\pm\phi W^\mp} (p_1 - p_2)^\mu H^\pm \phi W_\mu^\mp \pm \frac{g}{2} c_{G^\pm\phi W^\mp} (p_1 - p_2)^\mu G^\pm \phi W_\mu^\mp \\
& \left. - i \frac{g_Z}{2} c_{G^0\phi Z} (p_1 - p_2)^\mu G^0 \phi Z_\mu - i \frac{g_Z}{2} c_{A\phi Z} (p_1 - p_2)^\mu A \phi Z_\mu \right] \\
& - \sum_{\phi=G^0,A} \left[i \frac{g}{2} c_{H^\pm\phi W^\mp} (p_1 - p_2)^\mu H^\pm \phi W_\mu^\mp + i \frac{g}{2} c_{G^\pm\phi W^\mp} (p_1 - p_2)^\mu G^\pm \phi W_\mu^\mp \right], \quad (\text{A.1})
\end{aligned}$$

with p_1 and p_2 being the incoming momenta of X and Y in each XYZ -coupling, respectively. The explicit formula of the mixing factors $c_{XYZ(V)}$ are given in Tab. 1.

B 1PI diagrams for $h f \bar{f}$ vertex

We present the form factors of the 1PI $h f \bar{f}$ vertex at the one-loop level in terms of the Passarino–Veltman functions [111]. We follow the convention of Ref. [45]. The momentum assignment is shown in the left panel of Fig. 5.

$$\begin{aligned}
& \left(\frac{m_f}{v} \right)^{-1} 16\pi^2 \Gamma_{h f \bar{f}}^{S,1\text{PI}} \\
& = -4\zeta_h e^2 Q_f^2 C_{h f \bar{f}}^{FVF}(f, \gamma, f) - 4\zeta_h g_Z^2 (v_f^2 - a_f^2) C_{h f \bar{f}}^{FVF}(f, Z, f) \\
& + \frac{m_f^2}{v^2} \zeta_h [\zeta_h^2 C_{h f \bar{f}}^{FSF}(f, h, f) + \zeta_H^2 C_{h f \bar{f}}^{FSF}(f, H, f) - \zeta_{G^0}^2 C_{h f \bar{f}}^{FSF}(f, G^0, f) - \zeta_A^2 C_{h f \bar{f}}^{FSF}(f, A, f)] \\
& - \frac{2m_f^2}{v^2} \zeta_h [\zeta_{G^\pm}^2 C_{h f \bar{f}}^{FSF}(f', G^\pm, f') + \zeta_{H^\pm}^2 C_{h f \bar{f}}^{FSF}(f', H^\pm, f')] \\
& - 2g_Z^4 v^2 (v_f^2 - a_f^2) \sqrt{1 + s_\beta^2} (c_{\beta'} c_\alpha + 2s_{\beta'} s_\alpha) C_0(Z, f, Z)
\end{aligned}$$

Mixing factors	Expression	Mixing factors	Expression
c_{hhWW}	$\frac{1}{2}(3 - c_{2\alpha})$	c_{hhZZ}	$\frac{1}{2}(5 - 3c_{2\alpha})$
c_{hHWW}	$s_{2\alpha}$	c_{hHZZ}	$3s_{2\alpha}$
c_{HHWW}	$\frac{1}{2}(3 + c_{2\alpha})$	c_{HHZZ}	$\frac{1}{2}(5 + 3c_{2\alpha})$
c_{AAWW}	$\frac{1}{2}(3 + c_{2\beta'})$	c_{AAZZ}	$\frac{1}{2}(5 + 3c_{2\beta'})$
c_{AG^0WW}	$s_{2\beta'}$	c_{AG^0ZZ}	$3s_{2\beta'}$
$c_{G^0G^0WW}$	$\frac{1}{2}(3 - c_{2\beta'})$	$c_{G^0G^0ZZ}$	$\frac{1}{2}(5 - 3c_{2\beta'})$
c_{hWW}	$c_\beta c_\alpha + \sqrt{2} s_\beta s_\alpha$	c_{hZZ}	$c_{\beta'} c_\alpha + 2s_{\beta'} s_\alpha$
c_{HWW}	$-c_\beta s_\alpha + \sqrt{2} s_\beta c_\alpha$	c_{HZZ}	$-c_{\beta'} s_\alpha + 2s_{\beta'} c_\alpha$
$c_{G^\pm G^0W^\mp}$	$c_\beta' c_\beta + \sqrt{2} s_{\beta'} s_\beta$	$c_{G^\pm AW^\mp}$	0
$c_{H^\pm G^0W^\mp}$	$-c_{\beta'} s_\beta + \sqrt{2} s_{\beta'} c_\beta$	$c_{H^\pm AW^\mp}$	$s_{\beta'} s_\beta + \sqrt{2} c_{\beta'} c_\beta$
$c_{G^\pm hW^\mp}$	$c_\beta c_\alpha + \sqrt{2} s_\beta s_\alpha$	c_{G^0hZ}	$c_\alpha c_{\beta'} + 2s_\alpha s_{\beta'}$
$c_{H^\pm hW^\mp}$	$-s_\beta c_\alpha + \sqrt{2} c_\beta s_\alpha$	c_{G^0HZ}	$-c_{\beta'} s_\alpha + 2c_\alpha s_{\beta'}$
$c_{G^\pm HW^\mp}$	$-s_\alpha c_\beta + \sqrt{2} c_\alpha s_\beta$	c_{AhZ}	$-c_\alpha s_{\beta'} + 2s_\alpha c_{\beta'}$
$c_{H^\pm HW^\mp}$	$s_\alpha s_\beta + \sqrt{2} c_\alpha c_\beta$	c_{AHZ}	$2c_\alpha c_{\beta'} + s_\alpha s_{\beta'}$

Table 1: Mixing factors of Scalar–vector interaction.

$$\begin{aligned}
& - \frac{m_f^2}{v} \left\{ 6\lambda_{hh} \zeta_h^2 C_0(h, f, h) + 2\lambda_{HH} \zeta_H^2 C_0(H, f, H) + 2\lambda_{hh} \zeta_h \zeta_H [C_0(h, f, H) + C_0(H, f, h)] \right. \\
& \quad \left. - 2\lambda_{G^0G^0h} \zeta_{G^0}^2 C_0(G^0, f, G^0) - 2\lambda_{AAh} \zeta_A^2 C_0(A, f, A) - \lambda_{AG^0h} \zeta_{G^0} \zeta_A [C_0(A, f, G^0) + C_0(G^0, f, A)] \right\} \\
& + \frac{2m_f^2}{v} \left\{ \lambda_{G^+G^-h} \zeta_{G^\pm}^2 C_0(G^\pm, f', G^\pm) + \lambda_{H^+H^-h} \zeta_{H^\pm}^2 C_0(H^\pm, f', H^\pm) \right. \\
& \quad \left. + \lambda_{H^+G^-h} \zeta_{G^\pm} \zeta_{H^\pm} [C_0(G^\pm, f', H^\pm) + C_0(H^\pm, f', G^\pm)] \right\} \\
& - \frac{g^2}{4} \zeta_{G^\pm} (c_\beta c_\alpha + \sqrt{2} s_\beta s_\alpha) [C_{hff}^{VFS}(W, f', G^\pm) + C_{hff}^{SFV}(G^\pm, f', W)] \\
& - \frac{g^2}{4} \zeta_{H^\pm} (-s_\beta c_\alpha + \sqrt{2} c_\beta s_\alpha) [C_{hff}^{VFS}(W, f', H^\pm) + C_{hff}^{SFV}(H^\pm, f', W)] \\
& - \frac{g_Z^2}{8} \zeta_{G^0} (c_{\beta'} c_\alpha + 2s_{\beta'} s_\alpha) [C_{hff}^{VFS}(Z, f, G^0) + C_{hff}^{SFV}(G^0, f, Z)] \\
& - \frac{g_Z^2}{8} \zeta_A (-s_{\beta'} c_\alpha + 2c_{\beta'} s_\alpha) [C_{hff}^{VFS}(Z, f, A) + C_{hff}^{SFV}(A, f, Z)], \tag{B.1} \\
& \left(\frac{m_f}{v} \right)^{-1} 16\pi^2 \Gamma_{h\bar{f}}^{P,1\text{PI}} \\
& = \frac{g^2}{4} \zeta_{G^\pm} (c_\beta c_\alpha + \sqrt{2} s_\beta s_\alpha) [C_{hff}^{VFS}(W, f', G^\pm) - C_{hff}^{SFV}(G^\pm, f', W)] \\
& + \frac{g^2}{4} \zeta_{H^\pm} (-s_\beta c_\alpha + \sqrt{2} c_\beta s_\alpha) [C_{hff}^{VFS}(W, f', H^\pm) - C_{hff}^{SFV}(H^\pm, f', W)]
\end{aligned}$$

$$\begin{aligned}
& + 2g_Z^2 v_f a_f \zeta_{G^0} (c_{\beta'} c_\alpha + 2s_{\beta'} s_\alpha) [C_{hff}^{VFS}(Z, f, G^0) - C_{hff}^{SFV}(G^0, f, Z)] \\
& + 2g_Z^2 v_f a_f \zeta_A (-s_{\beta'} c_\alpha + 2c_{\beta'} s_\alpha) [C_{hff}^{VFS}(Z, f, A) - C_{hff}^{SFV}(A, f, Z)], \tag{B.2}
\end{aligned}$$

$$\begin{aligned}
& 16\pi^2 \Gamma_{h\bar{f}}^{V_1,1\text{PI}} \\
& = -\frac{2m_f^2}{v} \zeta_h [e^2 Q_f^2 (C_0 + 2C_{11})(f, \gamma, f) + g_Z^2 (v_f^2 + a_f^2) (C_0 + 2C_{11})(f, Z, f)] \\
& - \frac{g^2 m_{f'}^2}{2v} \zeta_h (C_0 + 2C_{11})(f', W, f') \\
& - \frac{m_f^4}{v^3} \zeta_h [\zeta_h^2 (C_0 + 2C_{11})(f, h, f) + \zeta_H^2 (C_0 + 2C_{11})(f, H, f) \\
& + \zeta_{G^0}^2 (C_0 + 2C_{11})(f, G^0, f) + \zeta_A^2 (C_0 + 2C_{11})(f, A, f)] \\
& - \frac{m_{f'}^2}{v^3} (m_f^2 + m_{f'}^2) \zeta_h [\zeta_{G^\pm}^2 (C_0 + 2C_{11})(f', G^\pm, f') + \zeta_{H^\pm}^2 (C_0 + 2C_{11})(f', H^\pm, f')] \\
& + \sqrt{1 + s_\beta^2} (c_{\beta'} c_\alpha + 2s_{\beta'} s_\alpha) g_Z^4 v (v_f^2 + a_f^2) (C_0 + C_{11})(Z, f, Z) \\
& + (c_\beta c_\alpha + \sqrt{2} s_\beta s_\alpha) \frac{g^4}{4} v (C_0 + C_{11})(W, f', W) \\
& - \frac{m_f^2}{v^2} \left\{ 6\lambda_{hh} \zeta_h^2 (C_0 + C_{11})(h, f, h) + 2\lambda_{HH} \zeta_H^2 (C_0 + C_{11})(H, f, H) \right. \\
& + 2\lambda_{Hhh} \zeta_h \zeta_H [(C_0 + C_{11})(H, f, h) + (C_0 + C_{11})(h, f, H)] \\
& + 2\lambda_{G^0 G^0 h} \zeta_{G^0}^2 (C_0 + C_{11})(G^0, f, G^0) + 2\lambda_{AAh} \zeta_A^2 (C_0 + C_{11})(A, f, A) \\
& \left. + \lambda_{AG^0 h} \zeta_{G^0} \zeta_A [(C_0 + C_{11})(A, f, G^0) + (C_0 + C_{11})(G^0, f, A)] \right\} \\
& - \frac{m_f^2 + m_{f'}^2}{v^2} \left\{ \lambda_{G^+ G^- h} \zeta_{G^\pm}^2 (C_0 + C_{11})(G^\pm, f', G^\pm) + \lambda_{H^+ H^- h} \zeta_{H^\pm}^2 (C_0 + C_{11})(H^\pm, f', H^\pm) \right. \\
& + \lambda_{H^+ G^- h} \zeta_{G^\pm} \zeta_{H^\pm} [(C_0 + C_{11})(G^\pm, f', H^\pm) + (C_0 + C_{11})(H^\pm, f', G^\pm)] \left. \right\} \\
& + \frac{g^2 m_{f'}^2}{4v} [\zeta_{G^\pm} (c_\beta c_\alpha + \sqrt{2} s_\beta s_\alpha) [(2C_0 + C_{11})(W, f', G^\pm) + (-C_0 + C_{11})(G^\pm, f', W)] \\
& + \zeta_{H^\pm} (-s_\beta c_\alpha + \sqrt{2} c_\beta s_\alpha) [(2C_0 + C_{11})(W, f', H^\pm) + (-C_0 + C_{11})(H^\pm, f', W)]] \\
& + \frac{g_Z^2 m_f^2}{8v} [\zeta_{G^0} (c_{\beta'} c_\alpha + 2s_{\beta'} s_\alpha) [(2C_0 + C_{11})(Z, f, G^0) + (-C_0 + C_{11})(G^0, f, Z)] \\
& + \zeta_A (-s_{\beta'} c_\alpha + 2c_{\beta'} s_\alpha) [(2C_0 + C_{11})(Z, f, A) + (-C_0 + C_{11})(A, f, Z)]], \tag{B.3}
\end{aligned}$$

$$\begin{aligned}
& 16\pi^2 \Gamma_{h\bar{f}}^{V_2,1\text{PI}} \\
& = -\frac{2m_f^2}{v} \zeta_h [e^2 Q_f^2 (C_0 + 2C_{12})(f, \gamma, f) + g_Z^2 (v_f^2 + a_f^2) (C_0 + 2C_{12})(f, Z, f)] \\
& - \frac{g^2 m_{f'}^2}{2v} \zeta_h (C_0 + 2C_{12})(f', W, f') \\
& - \frac{m_f^4}{v^3} \zeta_h [\zeta_h^2 (C_0 + 2C_{12})(f, h, f) + \zeta_H^2 (C_0 + 2C_{12})(f, H, f) \\
& + \zeta_{G^0}^2 (C_0 + 2C_{12})(f, G^0, f) + \zeta_A^2 (C_0 + 2C_{12})(f, A, f)] \\
\end{aligned}$$

$$\begin{aligned}
& -\frac{m_{f'}^2}{v^3}(m_f^2 + m_{f'}^2)\zeta_h[\zeta_{G^\pm}^2(C_0 + 2C_{12})(f', G^\pm, f') + \zeta_{H^\pm}^2(C_0 + 2C_{12})(f', H^\pm, f')] \\
& + \sqrt{1 + s_\beta^2}(c_{\beta'}c_\alpha + 2s_{\beta'}s_\alpha)g_Z^4v(v_f^2 + a_f^2)C_{12}(Z, f, Z) \\
& + (c_\beta c_\alpha + \sqrt{2}s_\beta s_\alpha)\frac{g^4}{4}vC_{12}(W, f', W) \\
& - \frac{m_f^2}{v^2}\left\{6\lambda_{hh}\zeta_h^2C_{12}(h, f, h) + 2\lambda_{HHh}\zeta_H^2C_{12}(H, f, H)\right. \\
& \quad + 2\lambda_{Hhh}\zeta_h\zeta_H[C_{12}(H, f, h) + C_{12}(h, f, H)] \\
& \quad + 2\lambda_{G^0G^0h}\zeta_{G^0}^2C_{12}(G^0, f, G^0) + 2\lambda_{AAh}\zeta_A^2C_{12}(A, f, A) \\
& \quad \left.+ \lambda_{AG^0h}\zeta_{G^0}\zeta_A[C_{12}(A, f, G^0) + C_{12}(G^0, f, A)]\right\} \\
& - \frac{m_f^2 + m_{f'}^2}{v^2}\left\{\lambda_{G^+G^-h}\zeta_{G^\pm}^2C_{12}(G^\pm, f', G^\pm) + \lambda_{H^+H^-h}\zeta_{H^\pm}^2C_{12}(H^\pm, f', H^\pm)\right. \\
& \quad \left.+ \lambda_{H^+G^-h}\zeta_{G^\pm}\zeta_{H^\pm}[C_{12}(G^\pm, f', H^\pm) + C_{12}(H^\pm, f', G^\pm)]\right\} \\
& + \frac{g^2}{4}\frac{m_{f'}^2}{v}\left[\zeta_{G^\pm}(c_\beta c_\alpha + \sqrt{2}s_\beta s_\alpha)[(2C_0 + C_{12})(W, f', G^\pm) + (-C_0 + C_{12})(G^\pm, f', W)]\right. \\
& \quad \left. + \zeta_{H^\pm}(-s_\beta c_\alpha + \sqrt{2}c_\beta s_\alpha)[(2C_0 + C_{12})(W, f', H^\pm) + (-C_0 + C_{12})(H^\pm, f', W)]\right] \\
& + \frac{g_Z^2}{8}\frac{m_f^2}{v}\left[\zeta_{G^0}(c_{\beta'}c_\alpha + 2s_{\beta'}s_\alpha)[(2C_0 + C_{12})(Z, f, G^0) + (-C_0 + C_{12})(G^0, f, Z)]\right. \\
& \quad \left. + \zeta_A(-s_{\beta'}c_\alpha + 2c_{\beta'}s_\alpha)[(2C_0 + C_{12})(Z, f, A) + (-C_0 + C_{12})(A, f, Z)]\right], \tag{B.4}
\end{aligned}$$

$$\begin{aligned}
& 16\pi^2\Gamma_{h\bar{f}}^{A_1, 1\text{PI}} \\
& = 4g_Z^2v_f a_f \frac{m_f^2}{v}\zeta_h(C_0 + 2C_{11})(f, Z, f) + \frac{g^2}{2}\frac{m_{f'}^2}{v}\zeta_h(C_0 + 2C_{11})(f', W, f') \\
& - \frac{m_{f'}^2}{v^3}(m_f^2 - m_{f'}^2)\zeta_h[\zeta_{G^\pm}^2(C_0 + 2C_{11})(f', G^\pm, f') + \zeta_{H^\pm}^2(C_0 + 2C_{11})(f', H^\pm, f')] \\
& - \sqrt{1 + s_\beta^2}(c_{\beta'}c_\alpha + 2s_{\beta'}s_\alpha)2g_Z^4v_f a_f v(C_0 + C_{11})(Z, f, Z) \\
& - (c_\beta c_\alpha + \sqrt{2}s_\beta s_\alpha)\frac{g^4}{4}v(C_0 + C_{11})(W, f', W) \\
& - \frac{m_f^2 - m_{f'}^2}{v^2}\left[\zeta_{G^\pm}^2\lambda_{G^+G^-h}(C_0 + C_{11})(G^\pm, f', G^\pm) + \zeta_{H^\pm}^2\lambda_{H^+H^-h}(C_0 + C_{11})(H^\pm, f', H^\pm)\right. \\
& \quad \left.+ \zeta_{G^\pm}\zeta_{H^\pm}\lambda_{H^+G^-h}[(C_0 + C_{11})(G^\pm, f', H^\pm) + (C_0 + C_{11})(H^\pm, f', G^\pm)]\right] \\
& - \frac{g^2}{4}\frac{m_{f'}^2}{v}\left[\zeta_{G^\pm}(c_\beta c_\alpha + \sqrt{2}s_\beta s_\alpha)[(2C_0 + C_{11})(W, f', G^\pm) + (-C_0 + C_{11})(G^\pm, f', W)]\right. \\
& \quad \left. + \zeta_{H^\pm}(-s_\beta c_\alpha + \sqrt{2}c_\beta s_\alpha)[(2C_0 + C_{11})(W, f', H^\pm) + (-C_0 + C_{11})(H^\pm, f', W)]\right] \\
& - 2g_Z^2v_f a_f \frac{m_f^2}{v}\left[\zeta_{G^0}(c_{\beta'}c_\alpha + 2s_{\beta'}s_\alpha)[(2C_0 + C_{11})(Z, f, G^0) + (-C_0 + C_{11})(G^0, f, Z)]\right. \\
& \quad \left. + \zeta_A(-s_{\beta'}c_\alpha + 2c_{\beta'}s_\alpha)[(2C_0 + C_{11})(Z, f, A) + (-C_0 + C_{11})(A, f, Z)]\right], \tag{B.5}
\end{aligned}$$

$$16\pi^2\Gamma_{h\bar{f}}^{A_2, 1\text{PI}}$$

$$\begin{aligned}
&= 4g_Z^2 v_f a_f \frac{m_f^2}{v} \zeta_h (C_0 + 2C_{12})(f, Z, f) + \frac{g^2}{2} \frac{m_{f'}^2}{v} \zeta_h (C_0 + 2C_{12})(f', W, f') \\
&\quad - \frac{m_{f'}^2}{v^3} (m_f^2 - m_{f'}^2) \zeta_h [\zeta_{G^\pm}^2 (C_0 + 2C_{12})(f', G^\pm, f') + \zeta_{H^\pm}^2 (C_0 + 2C_{12})(f', H^\pm, f')] \\
&\quad - \sqrt{1 + s_\beta^2} (c_{\beta'} c_\alpha + 2s_{\beta'} s_\alpha) 2g_Z^4 v_f a_f v C_{12}(Z, f, Z) \\
&\quad - (c_\beta c_\alpha + \sqrt{2} s_\beta s_\alpha) \frac{g^4}{4} v C_{12}(W, f', W) \\
&\quad - \frac{m_f^2 - m_{f'}^2}{v^2} [\zeta_{G^\pm}^2 \lambda_{G^+ G^- h} C_{12}(G^\pm, f', G^\pm) + \zeta_{H^\pm}^2 \lambda_{H^+ H^- h} C_{12}(H^\pm, f', H^\pm) \\
&\quad + \zeta_{G^\pm} \zeta_{H^\pm} \lambda_{H^+ G^- h} [C_{12}(G^\pm, f', H^\pm) + C_{12}(H^\pm, f', G^\pm)]] \\
&\quad - \frac{g^2}{4} \frac{m_{f'}^2}{v} [\zeta_{G^\pm} (c_\beta c_\alpha + \sqrt{2} s_\beta s_\alpha) [(2C_0 + C_{12})(W, f', G^\pm) + (-C_0 + C_{12})(G^\pm, f', W)] \\
&\quad + \zeta_{H^\pm} (-s_\beta c_\alpha + \sqrt{2} c_\beta s_\alpha) [(2C_0 + C_{12})(W, f', H^\pm) + (-C_0 + C_{12})(H^\pm, f', W)]] \\
&\quad - 2g_Z^2 v_f a_f \frac{m_f^2}{v} [\zeta_{G^0} (c_{\beta'} c_\alpha + 2s_{\beta'} s_\alpha) [(2C_0 + C_{12})(Z, f, G^0) + (-C_0 + C_{12})(G^0, f, Z)] \\
&\quad + \zeta_A (-s_{\beta'} c_\alpha + 2c_{\beta'} s_\alpha) [(2C_0 + C_{12})(Z, f, A) + (-C_0 + C_{12})(A, f, Z)]], \tag{B.6}
\end{aligned}$$

$$\begin{aligned}
&\left(\frac{m_f}{v}\right)^{-1} 16\pi^2 \Gamma_{h\bar{f}}^{T,1\text{PI}} \\
&= -\frac{m_f^2}{v^2} \zeta_h [\zeta_h^2 (C_{11} - C_{12})(f, h, f) + \zeta_H^2 (C_{11} - C_{12})(f, H, f) \\
&\quad - \zeta_{G^0}^2 (C_{11} - C_{12})(f, G^0, f) - \zeta_A^2 (C_{11} - C_{12})(f, A, f)] \\
&\quad + \frac{2m_{f'}^2}{v^2} \zeta_h [\zeta_{G^\pm}^2 (C_{11} - C_{12})(f', G^\pm, f') + \zeta_{H^\pm}^2 (C_{11} - C_{12})(f', H^\pm, f')] \\
&\quad - \frac{g^2}{4} [\zeta_{G^\pm} (c_\beta c_\alpha + \sqrt{2} s_\beta s_\alpha) [(2C_0 + 2C_{11} - C_{12})(W, f', G^\pm) + (C_0 + C_{11} - 2C_{12})(G^\pm, f', W)] \\
&\quad + \zeta_{H^\pm} (-s_\beta c_\alpha + \sqrt{2} c_\beta s_\alpha) [(2C_0 + 2C_{11} - C_{12})(W, f', H^\pm) + (C_0 + C_{11} - 2C_{12})(H^\pm, f', W)]] \\
&\quad - \frac{g_Z^2}{8} [\zeta_{G^0} (c_{\beta'} c_\alpha + 2s_{\beta'} s_\alpha) [(2C_0 + 2C_{11} - C_{12})(Z, f, G^0) + (C_0 + C_{11} - 2C_{12})(G^0, f, Z)] \\
&\quad + \zeta_A (-s_{\beta'} c_\alpha + 2c_{\beta'} s_\alpha) [(2C_0 + 2C_{11} - C_{12})(Z, f, A) + (C_0 + C_{11} - 2C_{12})(A, f, Z)]], \tag{B.7}
\end{aligned}$$

$$\begin{aligned}
&\left(\frac{m_f}{v}\right)^{-1} 16\pi^2 \Gamma_{h\bar{f}}^{PT,1\text{PI}} \\
&= \frac{g^2}{4} [\zeta_{G^\pm} (c_\beta c_\alpha + \sqrt{2} s_\beta s_\alpha) [(2C_0 + 2C_{11} - C_{12})(W, f', G^\pm) - (C_0 + C_{11} - 2C_{12})(G^\pm, f', W)] \\
&\quad + \zeta_{H^\pm} (-s_\beta c_\alpha + \sqrt{2} c_\beta s_\alpha) [(2C_0 + 2C_{11} - C_{12})(W, f', H^\pm) - (C_0 + C_{11} - 2C_{12})(H^\pm, f', W)]] \\
&\quad + 2g_Z^2 v_f a_f [\zeta_{G^0} (c_{\beta'} c_\alpha + 2s_{\beta'} s_\alpha) [(2C_0 + 2C_{11} - C_{12})(Z, f, G^0) - (C_0 + C_{11} - 2C_{12})(G^0, f, Z)] \\
&\quad + \zeta_A (-s_{\beta'} c_\alpha + 2c_{\beta'} s_\alpha) [(2C_0 + 2C_{11} - C_{12})(Z, f, A) - (C_0 + C_{11} - 2C_{12})(A, f, Z)]], \tag{B.8}
\end{aligned}$$

where the loop functions are defined as [45]

$$\begin{aligned} C_{hff}^{FVF}(X, Y, Z) \\ = [m_f^2 C_0 + p_1^2(C_{11} + C_{21}) + p_2^2(C_{12} + C_{22}) + p_1 \cdot p_2(2C_{23} - C_0) + 4C_{24}](X, Y, Z) - 1, \end{aligned} \quad (\text{B.9})$$

$$\begin{aligned} C_{hff}^{FSF}(X, Y, Z) \\ = [m_f^2 C_0 + p_1^2(C_{11} + C_{21}) + p_2^2(C_{12} + C_{22}) + 2p_1 \cdot p_2(C_{11} + C_{23}) + 4C_{24}](X, Y, Z) - \frac{1}{2}, \end{aligned} \quad (\text{B.10})$$

$$\begin{aligned} C_{hff}^{VFS}(X, Y, Z) \\ = [p_1^2(2C_0 + 3C_{11} + C_{21}) + p_2^2(2C_{12} + C_{22}) + 2p_1 \cdot p_2(2C_{12} + C_{23}) + 4C_{24}](X, Y, Z) - \frac{1}{2}, \end{aligned} \quad (\text{B.11})$$

$$\begin{aligned} C_{hff}^{SFV}(X, Y, Z) \\ = [p_1^2(-C_0 + C_{21}) + p_2^2(-C_{12} + C_{22}) + 2p_1 \cdot p_2(C_{23} + C_{12} - C_0 - C_{11}) + 4C_{24}](X, Y, Z) \\ - \frac{1}{2}. \end{aligned} \quad (\text{B.12})$$

C 1PI diagrams for $h\mathcal{V}\mathcal{V}'$ vertex

The form factors of the 1PI hgg vertex are obtained as

$$\begin{aligned} 16\pi^2 \Gamma_{hg^a g^b}^{1,1\text{PI}}(p_1^2, p_2^2, q^2) \\ = -\zeta_h \sum_q \frac{4g_s^2 m_q^2}{v} [8C_{24}(q, q, q) - 2B_0(q^2; q, q) + (p_1^2 + p_2^2 - q^2)C_0(q, q, q)] \delta^{ab}, \end{aligned} \quad (\text{C.1})$$

$$16\pi^2 \Gamma_{hg^a g^b}^{2,1\text{PI}}(p_1^2, p_2^2, q^2) = -\zeta_h \sum_q \frac{8g_s^2 m_q^2}{v} q^2 [C_0 + 4C_{1223}](q, q, q) \delta^{ab}, \quad (\text{C.2})$$

where $C_{1223} = C_{12} + C_{23}$.

The $h\gamma\gamma$ and $hZ\gamma$ vertices are decomposed into fermionic and bosonic loop contributions. The form factors of the 1PI $h\gamma\gamma$ vertex are obtained as

$$\begin{aligned} 16\pi^2 \Gamma_{h\gamma\gamma}^{1,1\text{PI}}(p_1^2, p_2^2, q^2)_F \\ = -\zeta_h \sum_f N_c^f \frac{4e^2 Q_f^2 m_f^2}{v} [8C_{24}(f, f, f) - 2B_0(q^2; f, f) + (p_1^2 + p_2^2 - q^2)C_0(f, f, f)], \end{aligned} \quad (\text{C.3})$$

$$16\pi^2 \Gamma_{h\gamma\gamma}^{2,1\text{PI}}(p_1^2, p_2^2, q^2)_F = -\zeta_h \sum_f N_c^f \frac{8e^2 Q_f^2 m_f^2}{v} [C_0 + 4C_{1223}](f, f, f), \quad (\text{C.4})$$

$$\begin{aligned} 16\pi^2 \Gamma_{h\gamma\gamma}^{1,1\text{PI}}(p_1^2, p_2^2, q^2)_B \\ = \frac{2e^2 m_W^2}{v} (c_\beta c_\alpha + \sqrt{2} s_\beta s_\alpha) \\ \times \left\{ (5p_1^2 + 5p_2^2 - 7q^2)C_0(W, W, W) - 6[B_0(q^2; W, W) - 4C_{24}(W, W, W)] \right\} \end{aligned}$$

$$\begin{aligned}
& - \frac{m_h^2}{m_W^2} [B_0(q^2; W, W) - 4C_{24}(W, W, W)] - m_h^2 C_0(W, W, W) \Big\} \\
& - 8e^2 \lambda_{hH^{++}H^{--}} [4C_{24}(H^{\pm\pm}, H^{\pm\pm}, H^{\pm\pm}) - B_0(q^2; H^{\pm\pm}, H^{\pm\pm})] \\
& - 2e^2 \lambda_{hH^{+}H^{-}} [4C_{24}(H^{\pm}, H^{\pm}, H^{\pm}) - B_0(q^2; H^{\pm}, H^{\pm})], \tag{C.5}
\end{aligned}$$

$$\begin{aligned}
& 16\pi^2 \Gamma_{h\gamma\gamma}^{2,1\text{PI}}(p_1^2, p_2^2, q^2)_B \\
& = \frac{8e^2 m_W^2}{v} (c_\beta c_\alpha + \sqrt{2} s_\beta s_\alpha) q^2 \left[4C_0 + 6C_{1223} + \frac{m_h^2}{m_W^2} C_{1223} \right] (W, W, W) \\
& - 32e^2 \lambda_{hH^{++}H^{--}} q^2 C_{1223}(H^{\pm\pm}, H^{\pm\pm}, H^{\pm\pm}) - 8e^2 \lambda_{hH^{+}H^{-}} q^2 C_{1223}(H^{\pm}, H^{\pm}, H^{\pm}). \tag{C.6}
\end{aligned}$$

The form factors of the 1PI $hZ\gamma$ vertex are obtained as

$$\begin{aligned}
& 16\pi^2 \Gamma_{hZ\gamma}^{1,1\text{PI}}(p_1^2, p_2^2, q^2)_F \\
& = -\zeta_h \sum_f N_c^f v_f Q_f \frac{4eg_Z m_f^2}{v} [8C_{24}(f, f, f) - 2B_0(q^2; f, f) + (p_1^2 + p_2^2 - q^2) C_0(f, f, f)], \tag{C.7}
\end{aligned}$$

$$16\pi^2 \Gamma_{hZ\gamma}^{2,1\text{PI}}(p_1^2, p_2^2, q^2)_F = -\zeta_h \sum_f N_c^f v_f Q_f \frac{8eg_Z m_f^2}{v} [C_0 + 4C_{1223}] (f, f, f), \tag{C.8}$$

$$\begin{aligned}
& 16\pi^2 \Gamma_{hZ\gamma}^{1,1\text{PI}}(p_1^2, p_2^2, q^2)_B \\
& = eg^2 m_W c_W (c_\alpha c_\beta + \sqrt{2} s_\alpha s_\beta) [2C_{hVV1}^{VV}(W, W, W) - 6B_0(q^2; W, W) + 4 - 2C_{24}(c^\pm, c^\pm, c^\pm)] \\
& + egg_Z m_W (s_W^2 + s_\beta^2) (c_\alpha c_\beta + \sqrt{2} s_\alpha s_\beta) \\
& \times [C_{hVV1}^{SVV}(G^\pm, W, W) + 2m_W^2 C_0(W, G^\pm, W) - 2C_{24}(W, G^\pm, G^\pm) + B_0(p_1^2; G^\pm, W)] \\
& + egg_Z m_W (c_{2W} - s_\beta^2) (c_\alpha c_\beta + \sqrt{2} s_\alpha s_\beta) C_{24}(G^\pm, G^\pm, W) \\
& - eg^2 m_W c_W (c_\alpha c_\beta + \sqrt{2} s_\alpha s_\beta) C_{hVV1}^{VVS}(W, W, G^\pm) \\
& - 2eg_Z m_W^2 (s_W^2 + s_\beta^2) \lambda_{G^+G^-h} C_0(G^\pm, W, G^\pm) \\
& - egg_Z m_W [-c_\alpha c_\beta s_W^2 + \sqrt{2} s_\alpha s_\beta (c_W^2 - 2)] B_0(p_2^2; G^\pm, W) \\
& - 4eg_Z (c_{2W} - s_\beta^2) \lambda_{G^+G^-h} \left[C_{24}(G^\pm, G^\pm, G^\pm) - \frac{1}{4} B_0(q^2; G^\pm, G^\pm) \right] \\
& + egg_Z m_W s_\beta c_\beta (-c_\alpha s_\beta + \sqrt{2} s_\alpha c_\beta) [C_{hVV1}^{SVV}(H^\pm, W, W) - 2C_{24}(W, H^\pm, H^\pm)] \\
& - 2eg_Z m_W^2 s_\beta c_\beta \lambda_{H^+G^-h} C_0(H^\pm, W, G^\pm) \\
& - egg_Z m_W s_\beta c_\beta (-c_\alpha s_\beta + \sqrt{2} s_\alpha c_\beta) [C_{24}(H^\pm, G^\pm, W) - B_0(p_1^2; H^\pm, W)] \\
& - 4eg_Z (c_{2W} - c_\beta^2) \lambda_{H^+H^-h} \left[C_{24}(H^\pm, H^\pm, H^\pm) - \frac{1}{4} B_0(q^2; H^\pm, H^\pm) \right] \\
& - 16eg_Z c_{2W} \lambda_{H^{++}H^{--}h} \left[C_{24}(H^{\pm\pm}, H^{\pm\pm}, H^{\pm\pm}) - \frac{1}{4} B_0(q^2; H^{\pm\pm}, H^{\pm\pm}) \right] \\
& + 4eg_Z s_\beta c_\beta \lambda_{H^+G^-h} \left[C_{24}(H^\pm, G^\pm, G^\pm) + C_{24}(G^\pm, H^\pm, H^\pm) - \frac{1}{2} B_0(q^2; H^\pm, G^\pm) \right], \tag{C.9}
\end{aligned}$$

$$\begin{aligned}
& 16\pi^2 \Gamma_{hZ\gamma}^{2,1\text{PI}}(p_1^2, p_2^2, q^2)_B \\
&= eg^2 m_W c_W (c_\alpha c_\beta + \sqrt{2} s_\alpha s_\beta) [2C_{hVV2}^{VVV}(W, W, W) - 2C_{1223}(c^\pm, c^\pm, c^\pm) - C_{hVV2}^{VVS}(W, W, G^\pm)] \\
&\quad + egg_Z m_W (s_W^2 + s_\beta^2) (c_\alpha c_\beta + \sqrt{2} s_\alpha s_\beta) [C_{hVV2}^{SVV}(G^\pm, W, W) - 2C_{hVV2}^{VSS}(W, G^\pm, G^\pm)] \\
&\quad + egg_Z m_W (c_{2W} - s_\beta^2) (c_\alpha c_\beta + \sqrt{2} s_\alpha s_\beta) C_{hVV2}^{SSV}(G^\pm, G^\pm, W) \\
&\quad - 4eg_Z (c_{2W} - s_\beta^2) \lambda_{G+G-h} C_{1223}(G^\pm, G^\pm, G^\pm) \\
&\quad + egg_Z m_W s_\beta c_\beta (-c_\alpha s_\beta + \sqrt{2} s_\alpha c_\beta) \\
&\quad \times [C_{hVV2}^{SVV}(H^\pm, W, W) - C_{hVV2}^{SSV}(H^\pm, G^\pm, W) - 2C_{hVV2}^{VSS}(W, H^\pm, H^\pm)] \\
&\quad - 4eg_Z (c_{2W} - c_\beta^2) \lambda_{H+H-h} C_{1223}(H^\pm, H^\pm, H^\pm) \\
&\quad - 16eg_Z c_{2W} \lambda_{H++H--h} C_{1223}(H^{\pm\pm}, H^{\pm\pm}, H^{\pm\pm}) \\
&\quad + 4eg_Z s_\beta c_\beta \lambda_{H+G-h} [C_{1223}(H^\pm, G^\pm, G^\pm) + C_{1223}(G^\pm, H^\pm, H^\pm)], \tag{C.10}
\end{aligned}$$

where the loop functions are defined as [45]

$$\begin{aligned}
C_{hVV1}^{VVV}(X, Y, Z) &= \left[18C_{24} + p_1^2(2C_{21} + 3C_{11} + C_0) + p_2^2(2C_{22} + C_{12}) \right. \\
&\quad \left. + p_1 \cdot p_2(4C_{23} + 3C_{12} + C_{11} - 4C_0) \right] (X, Y, Z) - 3, \tag{C.11}
\end{aligned}$$

$$C_{hVV2}^{VVV}(X, Y, Z) = (10C_{23} + 9C_{12} + C_{11} + 5C_0) (X, Y, Z), \tag{C.12}$$

$$\begin{aligned}
C_{hVV1}^{SVV}(X, Y, Z) &= \left[3C_{24} + p_1^2(C_{21} - C_0) + p_2^2(C_{22} - 2C_{12} + C_0) \right. \\
&\quad \left. + 2p_1 \cdot p_2(C_{23} - C_{11}) \right] (X, Y, Z) - \frac{1}{2}, \tag{C.13}
\end{aligned}$$

$$C_{hVV2}^{SVV}(X, Y, Z) = (4C_{11} - 3C_{12} - C_{23}) (X, Y, Z), \tag{C.14}$$

$$\begin{aligned}
C_{hVV1}^{VVS}(X, Y, Z) &= \left[3C_{24} + p_1^2(C_{21} + 4C_{11} + 4C_0) + p_2^2(C_{22} + 2C_{12}) \right. \\
&\quad \left. + 2p_1 \cdot p_2(C_{23} + 2C_{12} + C_{11} + 2C_0) \right] (X, Y, Z) - \frac{1}{2}, \tag{C.15}
\end{aligned}$$

$$C_{hVV2}^{VVS}(X, Y, Z) = (2C_{11} - 5C_{12} - 2C_0 - C_{23}) (X, Y, Z), \tag{C.16}$$

$$C_{hVV2}^{SSV}(X, Y, Z) = (C_{23} - C_{12})(X, Y, Z), \tag{C.17}$$

$$C_{hVV2}^{VSS}(X, Y, Z) = (C_{23} + C_{12} + 2C_{11} + 2C_0)(X, Y, Z). \tag{C.18}$$

D Box diagrams for the $h \rightarrow VV^*$

D.1 Box diagrams for $h \rightarrow Z f \bar{f}$

We here give the analytic expressions for the box diagrams for $h \rightarrow Z f \bar{f}$. For the calculation of box diagrams, we assign all momenta in the incoming way (see Diagram (1) in Fig. 18). These incoming momenta are related to the outgoing momenta, such as $k_Z = -p_Z$, $k_{\bar{f}} = -p_f$ and $k_f = -p_{\bar{f}}$. Then, the Mandelstam variables are obtained as $s = (p_f + p_{\bar{f}})^2$, $t = (p_Z + p_f)^2$, and $u = (p_Z + p_{\bar{f}})^2$. The LO amplitude is obtained as

$$\mathcal{M}_{\text{LO}} = C_{\text{tree}}^Z \bar{v}(p_{\bar{f}}) \gamma^\mu (v_f - a_f \gamma_5) u(p_f) \epsilon_\mu^*(p_Z), \tag{D.1}$$

where $C_{\text{tree}}^Z = g_Z \Gamma_{hZZ}^{1,\text{tree}} / (s - m_Z^2)$.

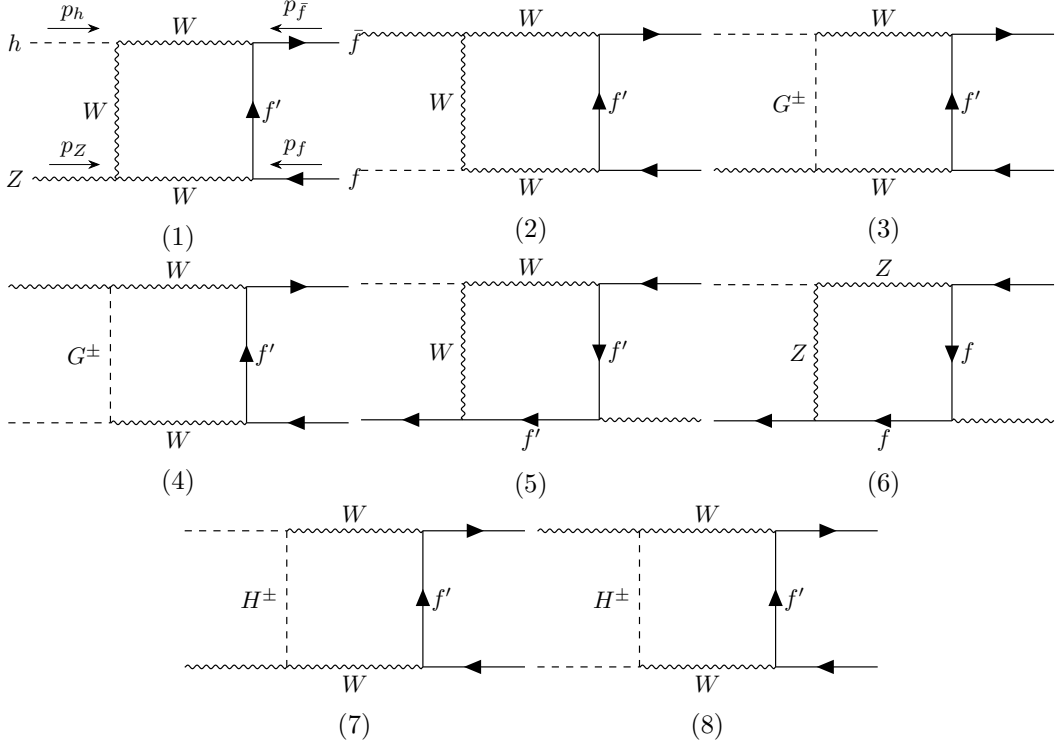


Figure 18: Box diagrams for $h \rightarrow Z f \bar{f}$.

At the one-loop level, there are six SM-like diagrams and two diagrams with new particles as shown in Fig. 18. The box amplitude can be parameterized as

$$\mathcal{M}_{BZi} = \frac{1}{16\pi^2} \bar{v}(p_{\bar{f}}) \mathcal{M}_{BZi}^\mu u(p_f) \epsilon_\mu^*(p_Z), \quad (\text{D.2})$$

where

$$\mathcal{M}_{BZi}^\mu = C^{BZi} \left[\not{p}_h (F_{1,3}^{BZi} p_f^\mu + F_{1,4}^{BZi} p_{\bar{f}}^\mu) + \gamma^\mu F_\gamma^{BZi} \right] P_L \quad (i \neq 6), \quad (\text{D.3})$$

$$\mathcal{M}_{BZ6}^\mu = C^{BZ6} \left[\not{p}_h (F_{1,3}^{BZ6} p_f^\mu + F_{1,4}^{BZ6} p_{\bar{f}}^\mu) + \gamma^\mu F_\gamma^{BZ6} \right] (v_f - a_f \gamma_5)^3. \quad (\text{D.4})$$

Then, the NLO contribution is obtained as

$$(16\pi^2) 2 \text{Re} \left[\sum \mathcal{M}_{\text{tree}}^* \mathcal{M}_{BZi} \right] = 4(v_f + a_f) C_{\text{tree}}^Z C^{BZi} B^{BZi} \quad (i \neq 6), \quad (\text{D.5})$$

$$(16\pi^2) 2 \text{Re} \left[\sum \mathcal{M}_{\text{tree}}^* \mathcal{M}_{BZ6} \right] = 8(v_f^4 + 6v_f^2 a_f^2 + a_f^4) C_{\text{tree}}^Z C^{BZ6} B^{BZ6}, \quad (\text{D.6})$$

where

$$B^{BZi} = s F_\gamma^{BZi} + \frac{tu - m_Z^2 m_h^2}{4m_Z^2} [2F_\gamma^{BZi} - (t - m_Z^2) F_{1,3}^{BZi} - (u - m_Z^2) F_{1,4}^{BZi}]. \quad (\text{D.7})$$

In the following, we use the shorthand notation for D functions.

$$\begin{aligned} & D_{i,ij}(p_1^2, p_2^2, p_3^2, p_4^2, p_{12}^2, p_{23}^2; X, Y, Z, W) \\ &= D_{i,ij}(p_1^2, p_2^2, p_3^2, p_{123}^2, p_{12}^2, p_{23}^2; m_X^2, m_Y^2, m_Z^2, m_W^2), \end{aligned} \quad (\text{D.8})$$

with $p_{123}^2 = (p_1 + p_2 + p_3)^2$, $p_{12}^2 = (p_1 + p_2)^2$, $p_{23}^2 = (p_2 + p_3)^2$. The coefficients and the form factors of each diagram are obtained as follows.

[Diagram (1)]

$$\begin{aligned} C^{BZ1} &= -2a_f g^4 m_W c_W (c_\beta c_\alpha + \sqrt{2} s_\beta s_\alpha), \\ F_{1,3}^{BZ1} &= F_{p\cdot\gamma 1}^{VFFV}(0, 0, m_Z^2, m_h^2, s, t; W, 0, W, W), \\ F_{1,4}^{BZ1} &= F_{p\cdot\gamma 2}^{VFFV}(0, 0, m_Z^2, m_h^2, s, t; W, 0, W, W), \\ F_\gamma^{BZ1} &= F_\gamma^{VFFV}(0, 0, m_Z^2, m_h^2, s, t; W, 0, W, W), \end{aligned} \quad (\text{D.9})$$

where the loop functions are defined as

$$F_{p\cdot\gamma 1}^{VFFV} = 2(D_{13} - D_{12} + 2D_{26}), \quad (\text{D.10})$$

$$F_{p\cdot\gamma 2}^{VFFV} = 4(D_0 + D_{11} + D_{13} + D_{25}), \quad (\text{D.11})$$

$$\begin{aligned} F_\gamma^{VFFV} &= -2C_0(p_{12}^2, p_3^2, p_{123}^2; m_{V_1}^2, m_{V_3}^2, m_{V_4}^2) - [4D_{27} + (2p_{12}^2 + p_{23}^2 - p_{123}^2)(D_0 + D_{11}) \\ &\quad + 2(p_{23}^2 - p_3^2)D_{12} + p_{23}^2 D_{13}], \end{aligned} \quad (\text{D.12})$$

The coefficient of Diagram (2) is the same as that of Diagram (1). Its form factors are obtained by interchanging $F_{1,3}^{BZ1}$ and $F_{1,4}^{BZ1}$ and replacing $t \rightarrow u$.

[Diagram (3)]

$$\begin{aligned} C^{BZ3} &= a_f g^3 g_Z m_W (s_W^2 + s_\beta^2) (c_\beta c_\alpha + \sqrt{2} s_\beta s_\alpha), \\ F_{1,3}^{BZ3} &= F_{p\cdot\gamma}^{VFFS}(0, 0, m_Z^2, m_h^2, s, t; W, 0, W, G^\pm), \\ F_{1,4}^{BZ3} &= 0, \\ F_\gamma^{BZ3} &= F_\gamma^{VFFS}(0, 0, m_Z^2, m_h^2, s, t; W, 0, W, G^\pm), \end{aligned} \quad (\text{D.13})$$

where the loop functions are defined as

$$F_{p\cdot\gamma}^{VFFS} = -4(D_{12} - D_{13}), \quad (\text{D.14})$$

$$\begin{aligned} F_\gamma^{VFFS} &= C_0(p_{12}^2, p_3^2, p_{123}^2; m_{V_1}^2, m_{V_3}^2, m_{S_4}^2) \\ &\quad + 2[-(p_{23}^2 - p_{123}^2)(D_0 + D_{11}) + p_{23}^2 D_{13}]. \end{aligned} \quad (\text{D.15})$$

The coefficient of Diagram (4) is the same as that of Diagram (3). Its form factors are obtained by interchanging $F_{1,3}^{BZ3}$ and $F_{1,4}^{BZ3}$ and replacing $t \rightarrow u$.

[Diagram (5)]

$$\begin{aligned} C^{BZ5} &= -(v_{f'} + a_{f'}) g^3 g_Z m_W (c_\beta c_\alpha + \sqrt{2} s_\beta s_\alpha), \\ F_{1,3}^{BZ5} &= F_{p\cdot\gamma 1}^{VFFV}(0, m_Z^2, 0, m_h^2, t, u; W, 0, 0, W), \\ F_{1,4}^{BZ5} &= F_{p\cdot\gamma 2}^{VFFV}(0, m_Z^2, 0, m_h^2, t, u; W, 0, 0, W), \\ F_\gamma^{BZ5} &= F_\gamma^{VFFV}(0, m_Z^2, 0, m_h^2, t, u; W, 0, 0, W). \end{aligned} \quad (\text{D.16})$$

where the loop functions are defined as

$$F_{p\cdot\gamma 1}^{VFFV} = -2(D_0 + D_{11} + D_{12} + D_{24}), \quad (\text{D.17})$$

$$F_{p\cdot\gamma 2}^{VFFV} = -2D_{26}, \quad (\text{D.18})$$

$$\begin{aligned} F_{\gamma}^{VFFV} = & -C_0(p_{12}^2, p_3^2, p_{123}^2; m_{V_1}^2, m_{F_3}^2, m_{V_4}^2) \\ & - [-2D_{27} + (p_{12}^2 - p_2^2)(D_0 + D_{11}) + p_2^2 D_{12}]. \end{aligned} \quad (\text{D.19})$$

The coefficient of Diagram (6) is obtained as

$$C^{BZ6} = -2g_Z^4 m_Z (c_{\beta'} c_{\alpha} + 2s_{\beta'} s_{\alpha}). \quad (\text{D.20})$$

Its form factors are obtained from those of Diagram (5) by replacing $W \rightarrow Z$.

[Diagram (7)]

$$\begin{aligned} C^{BZ7} &= a_f g^3 g_Z m_W s_{\beta} c_{\beta} (-s_{\beta} c_{\alpha} + \sqrt{2} c_{\beta} s_{\alpha}), \\ F_{1,3}^{BZ7} &= F_{p\cdot\gamma}^{VFVS}(0, 0, m_Z^2, m_h^2, s, t; W, 0, W, H^{\pm}) \\ F_{1,4}^{BZ7} &= 0, \\ F_{\gamma}^{BZ7} &= F_{\gamma}^{VFVS}(0, 0, m_Z^2, m_h^2, s, t; W, 0, W, H^{\pm}). \end{aligned} \quad (\text{D.21})$$

The coefficient of Diagram (8) is the same as that of Diagram (7). Its form factors are obtained by interchanging $F_{1,3}^{BZ7}$ and $F_{1,4}^{BZ7}$ and replacing $t \rightarrow u$.

D.2 Box diagrams for $h \rightarrow W^- f' \bar{f}$

We here give the analytic expressions for the box diagrams for $h \rightarrow W^- f' \bar{f}$. Similarly to $h \rightarrow Z f \bar{f}$, we assign all momenta in the incoming way (see Diagram (1) in Fig. 19). These incoming momenta are related to the out-going momenta, such as $k_W = -p_W$, $k_{\bar{f}} = -p_f$ and $k_{f'} = -p_{\bar{f}'}$. Then, the Mandelstam variables are obtained as $s = (p_f + p_{\bar{f}'})^2$, $t = (p_W + p_f)^2$, and $u = (p_W + p_{\bar{f}'})^2$. The LO amplitude is obtained as

$$\mathcal{M}_{\text{tree}} = C_{\text{tree}}^W \bar{v}(p_{\bar{f}'}) \gamma^{\mu} P_L u(p_f) \epsilon_{\mu}^*(p_W), \quad (\text{D.22})$$

where $C_{\text{tree}}^W = g_W \Gamma_{hWW}^{1,\text{tree}} / (s - m_W^2)$.

At the one-loop level, there are eleven SM-like diagrams and two diagrams with new particles as shown in Fig. 19. The box amplitude can be parameterized as

$$\mathcal{M}_{BWi} = \frac{1}{16\pi^2} \bar{v}(p_{\bar{f}'}) \mathcal{M}_{BWi}^{\mu} u(p_f) \epsilon_{\mu}^*(p_W), \quad (\text{D.23})$$

where

$$\mathcal{M}_{BWi}^{\mu} = C^{BWi} \left[\not{p}_h (F_{1,3}^{BWi} p_f^{\mu} + F_{1,4}^{BWi} p_{\bar{f}'}^{\mu}) + \gamma^{\mu} F_{\gamma}^{BWi} \right] P_L. \quad (\text{D.24})$$

Then, the NLO contribution is obtained as

$$(16\pi^2) 2 \text{Re} \left[\sum \mathcal{M}_{\text{tree}}^* \mathcal{M}_{BWi} \right] = 4C_{\text{tree}}^W C^{BWi} \text{Re} [B^{BWi}], \quad (\text{D.25})$$

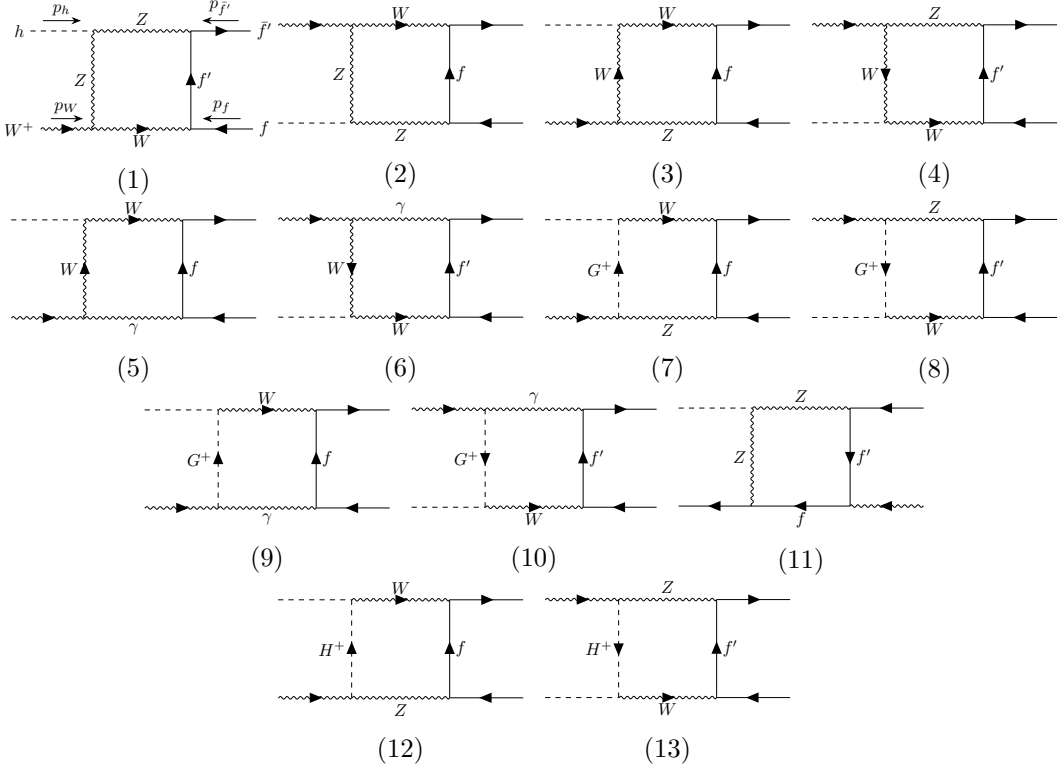


Figure 19: Box diagrams for $h \rightarrow W^- f' \bar{f}$.

where

$$B^{BWi} = s F_\gamma^{BWi} + \frac{tu - m_W^2 m_h^2}{4m_W^2} [2F_\gamma^{BWi} - (t - m_W^2) F_{1,3}^{BWi} - (u - m_W^2) F_{1,4}^{BWi}]. \quad (\text{D.26})$$

The coefficients and the form factors of each diagram are obtained as follows.

[Diagram (1)]

$$\begin{aligned} C^{BW1} &= -4a_{f'}(v_{f'} + a_{f'}) \frac{g^2 g_Z^2}{\sqrt{2}} c_W m_Z c_{hZZ}, \\ F_{1,3}^{BW1} &= F_{p\gamma 1}^{V F V V}(m_{f'}^2, m_f^2, m_W^2, m_h^2, s, t; Z, f', W, Z), \\ F_{1,4}^{BW1} &= F_{p\gamma 2}^{V F V V}(m_{f'}^2, m_f^2, m_W^2, m_h^2, s, t; Z, f', W, Z), \\ F_\gamma^{BW1} &= F_\gamma^{V F V V}(m_{f'}^2, m_f^2, m_W^2, m_h^2, s, t; Z, f', W, Z). \end{aligned} \quad (\text{D.27})$$

The coefficient of Diagram (2) is obtained by replacing $f' \rightarrow f$. Its form factors are obtained by interchanging $F_{1,3}^{BW1}$ and $F_{1,4}^{BW1}$, exchanging f' and f , and replacing $t \rightarrow u$.

[Diagram (3)]

$$\begin{aligned}
C^{BW3} &= -4a_f(v_f + a_f) \frac{g^3 g_Z}{\sqrt{2}} c_W m_W c_h W W, \\
F_{1,3}^{BW3} &= F_{p\gamma 1}^{V F V V}(m_{f'}^2, m_f^2, m_W^2, m_h^2, s, t; W, f, Z, W), \\
F_{1,4}^{BW3} &= F_{p\gamma 2}^{V F V V}(m_{f'}^2, m_f^2, m_W^2, m_h^2, s, t; W, f, Z, W), \\
F_\gamma^{BW3} &= F_\gamma^{V F V V}(m_{f'}^2, m_f^2, m_W^2, m_h^2, s, t; W, f, Z, W).
\end{aligned} \tag{D.28}$$

The coefficient of Diagram (4) is obtained by replacing $f' \rightarrow f$. Its form factors are obtained by interchanging $F_{1,3}^{BW3}$ and $F_{1,4}^{BW3}$, exchanging f' and f , and replacing $t \rightarrow u$.

[Diagram (5)]

$$\begin{aligned}
C^{BW5} &= -4a_f e Q_f \frac{g^3}{\sqrt{2}} s_W m_W c_h W W, \\
F_{1,3}^{BW5} &= F_{p\gamma 1}^{V F V V}(m_{f'}^2, m_f^2, m_W^2, m_h^2, s, t; W, f, \gamma, W), \\
F_{1,4}^{BW5} &= F_{p\gamma 2}^{V F V V}(m_{f'}^2, m_f^2, m_W^2, m_h^2, s, t; W, f, \gamma, W), \\
F_\gamma^{BW5} &= F_\gamma^{V F V V}(m_{f'}^2, m_f^2, m_W^2, m_h^2, s, t; W, f, \gamma, W).
\end{aligned} \tag{D.29}$$

The coefficient of Diagram (6) is obtained by replacing $f' \rightarrow f$. Its form factors are obtained by interchanging $F_{1,3}^{BW5}$ and $F_{1,4}^{BW5}$, exchanging f' and f , and replacing $t \rightarrow u$.

[Diagram (7)]

$$\begin{aligned}
C^{BW7} &= -2a_f(v_f + a_f) \frac{g^2 g_Z^2}{\sqrt{2}} (s_W^2 + s_\beta^2) m_W c_h W W, \\
F_{1,3}^{BW7} &= F_{p\gamma}^{V F V S}(m_{f'}^2, m_f^2, m_W^2, m_h^2, s, t; W, f, Z, G^\pm), \\
F_{1,4}^{BW7} &= 0, \\
F_\gamma^{BW7} &= F_\gamma^{V F V S}(m_{f'}^2, m_f^2, m_W^2, m_h^2, s, t; W, f, Z, G^\pm).
\end{aligned} \tag{D.30}$$

The coefficient of Diagram (8) is obtained by replacing $f' \rightarrow f$. Its form factors are obtained by interchanging $F_{1,3}^{BW7}$ and $F_{1,4}^{BW7}$, exchanging f' and f , and replacing $t \rightarrow u$.

[Diagram (9)]

$$\begin{aligned}
C^{BW9} &= 2a_f Q_f \frac{e^2 g^2}{\sqrt{2}} m_W c_h W W, \\
F_{1,3}^{BW9} &= F_{p\gamma}^{V F V S}(m_{f'}^2, m_f^2, m_W^2, m_h^2, s, t; W, f, \gamma, G^\pm), \\
F_{1,4}^{BW9} &= 0, \\
F_\gamma^{BW9} &= F_\gamma^{V F V S}(m_{f'}^2, m_f^2, m_W^2, m_h^2, s, t; W, f, \gamma, G^\pm).
\end{aligned} \tag{D.31}$$

The coefficient of Diagram (10) is obtained by replacing $f' \rightarrow f$. Its form factors are obtained by interchanging $F_{1,3}^{BW9}$ and $F_{1,4}^{BW9}$, exchanging f' and f , and replacing $t \rightarrow u$.

[Diagram (11)]

$$\begin{aligned}
C^{BW11} &= -2(v_f + a_f)(v_{f'} + a_{f'}) \frac{g_Z^3 g}{\sqrt{2}} m_Z c_{hZZ}, \\
F_{1,3}^{BW11} &= F_{p\gamma 1}^{VFFV}(m_f^2, m_W^2, m_{f'}^2, m_h^2, t, u; Z, f, f', Z), \\
F_{1,4}^{BW11} &= F_{p\gamma 2}^{VFFV}(m_f^2, m_W^2, m_{f'}^2, m_h^2, t, u; Z, f, f', Z), \\
F_\gamma^{BW11} &= F_\gamma^{VFFV}(m_f^2, m_W^2, m_{f'}^2, m_h^2, t, u; Z, f, f', Z).
\end{aligned} \tag{D.32}$$

[Diagram (12)]

$$\begin{aligned}
C^{BW12} &= -2a_f(v_f + a_f) \frac{g^2 g_Z^2}{\sqrt{2}} s_\beta c_\beta m_W c_{hH^\pm W^\mp}, \\
F_{1,3}^{BW12} &= F_{p\gamma}^{VFVS}(m_{f'}^2, m_f^2, m_W^2, m_h^2, s, t; W, f, Z, H^\pm), \\
F_{1,4}^{BW12} &= 0, \\
F_\gamma^{BW12} &= F_\gamma^{VFVS}(m_{f'}^2, m_f^2, m_W^2, m_h^2, s, t; W, f, Z, H^\pm).
\end{aligned} \tag{D.33}$$

The coefficient of Diagram (13) is obtained by replacing $f' \rightarrow f$. Its form factors are obtained by interchanging $F_{1,3}^{BW12}$ and $F_{1,4}^{BW12}$, exchanging f' and f , and replacing $t \rightarrow u$.

References

- [1] T. P. Cheng and L.-F. Li, *Neutrino Masses, Mixings and Oscillations in $SU(2) \times U(1)$ Models of Electroweak Interactions*, *Phys. Rev. D* **22** (1980) 2860.
- [2] J. Schechter and J. W. F. Valle, *Neutrino Masses in $SU(2) \times U(1)$ Theories*, *Phys. Rev. D* **22** (1980) 2227.
- [3] G. Lazarides, Q. Shafi, and C. Wetterich, *Proton Lifetime and Fermion Masses in an $SO(10)$ Model*, *Nucl. Phys. B* **181** (1981) 287–300.
- [4] R. N. Mohapatra and G. Senjanovic, *Neutrino Masses and Mixings in Gauge Models with Spontaneous Parity Violation*, *Phys. Rev. D* **23** (1981) 165.
- [5] M. Magg and C. Wetterich, *Neutrino Mass Problem and Gauge Hierarchy*, *Phys. Lett. B* **94** (1980) 61–64.
- [6] P. Fileviez Perez, T. Han, G.-y. Huang, T. Li, and K. Wang, *Neutrino Masses and the CERN LHC: Testing Type II Seesaw*, *Phys. Rev. D* **78** (2008) 015018 [[arXiv:0805.3536](https://arxiv.org/abs/0805.3536)].
- [7] S. Kanemura and H. Sugiyama, *Dark matter and a suppression mechanism for neutrino masses in the Higgs triplet model*, *Phys. Rev. D* **86** (2012) 073006 [[arXiv:1202.5231](https://arxiv.org/abs/1202.5231)].
- [8] T. Nomura, H. Okada, and Y. Oriksa, *Radiative neutrino mass in alternative left-right model*, *Eur. Phys. J. C* **77** (2017) 103 [[arXiv:1602.08302](https://arxiv.org/abs/1602.08302)].
- [9] S.-Y. Guo, Z.-L. Han, and Y. Liao, *Testing the type II radiative seesaw model: From dark matter detection to LHC signatures*, *Phys. Rev. D* **94** (2016) 115014 [[arXiv:1609.01018](https://arxiv.org/abs/1609.01018)].
- [10] T. Nomura and H. Okada, *Loop induced type-II seesaw model and GeV dark matter with $U(1)_{B-L}$ gauge symmetry*, *Phys. Lett. B* **774** (2017) 575–581 [[arXiv:1704.08581](https://arxiv.org/abs/1704.08581)].
- [11] J. C. Pati and A. Salam, *Lepton Number as the Fourth Color*, *Phys. Rev. D* **10** (1974) 275–289. [Erratum: *Phys. Rev. D* 11, 703–703 (1975)].

- [12] R. N. Mohapatra and J. C. Pati, *Left-Right Gauge Symmetry and an Isoconjugate Model of CP Violation*, *Phys. Rev. D* **11** (1975) 566–571.
- [13] R. N. Mohapatra and J. C. Pati, *A Natural Left-Right Symmetry*, *Phys. Rev. D* **11** (1975) 2558.
- [14] G. Senjanovic and R. N. Mohapatra, *Exact Left-Right Symmetry and Spontaneous Violation of Parity*, *Phys. Rev. D* **12** (1975) 1502.
- [15] R. Zhou, L. Bian, and Y. Du, *Electroweak phase transition and gravitational waves in the type-II seesaw model*, *JHEP* **08** (2022) 205 [[arXiv:2203.01561](https://arxiv.org/abs/2203.01561)].
- [16] S. Jangid and H. Okada, *Electroweak phase transition with radiative symmetry breaking in a type-II seesaw model with an inert doublet*, *Phys. Rev. D* **109** (2024) 015001 [[arXiv:2310.12591](https://arxiv.org/abs/2310.12591)].
- [17] M. Aoki, S. Kanemura, M. Kikuchi, and K. Yagyu, *Renormalization of the Higgs Sector in the Triplet Model*, *Phys. Lett. B* **714** (2012) 279–285 [[arXiv:1204.1951](https://arxiv.org/abs/1204.1951)].
- [18] M. Aoki, S. Kanemura, M. Kikuchi, and K. Yagyu, *Radiative corrections to the Higgs boson couplings in the triplet model*, *Phys. Rev. D* **87** (2013) 015012 [[arXiv:1211.6029](https://arxiv.org/abs/1211.6029)].
- [19] H. Georgi and M. Machacek, *DOUBLY CHARGED HIGGS BOSONS*, *Nucl. Phys. B* **262** (1985) 463–477.
- [20] M. S. Chanowitz and M. Golden, *Higgs Boson Triplets With $M(W) = M(Z) \cos \theta \omega$* , *Phys. Lett. B* **165** (1985) 105–108.
- [21] T. Blank and W. Hollik, *Precision observables in $SU(2) \times U(1)$ models with an additional Higgs triplet*, *Nucl. Phys. B* **514** (1998) 113–134 [[hep-ph/9703392](https://arxiv.org/abs/hep-ph/9703392)].
- [22] S. Kanemura and K. Yagyu, *Radiative corrections to electroweak parameters in the Higgs triplet model and implication with the recent Higgs boson searches*, *Phys. Rev. D* **85** (2012) 115009 [[arXiv:1201.6287](https://arxiv.org/abs/1201.6287)].
- [23] A. Melfo, M. Nemevsek, F. Nesti, G. Senjanovic, and Y. Zhang, *Type II Seesaw at LHC: The Roadmap*, *Phys. Rev. D* **85** (2012) 055018 [[arXiv:1108.4416](https://arxiv.org/abs/1108.4416)].
- [24] S. Kanemura, K. Yagyu, and H. Yokoya, *First constraint on the mass of doubly-charged Higgs bosons in the same-sign diboson decay scenario at the LHC*, *Phys. Lett. B* **726** (2013) 316–319 [[arXiv:1305.2383](https://arxiv.org/abs/1305.2383)].
- [25] M. Aoki, S. Kanemura, and K. Yagyu, *Testing the Higgs triplet model with the mass difference at the LHC*, *Phys. Rev. D* **85** (2012) 055007 [[arXiv:1110.4625](https://arxiv.org/abs/1110.4625)].
- [26] S. Kanemura and K. Yagyu, *Implication of the W boson mass anomaly at CDF II in the Higgs triplet model with a mass difference*, *Phys. Lett. B* **831** (2022) 137217 [[arXiv:2204.07511](https://arxiv.org/abs/2204.07511)].
- [27] E. Asakawa and S. Kanemura, *The $H^+ - W^+ - Z^0$ vertex and single charged Higgs boson production via WZ fusion at the large hadron collider*, *Phys. Lett. B* **626** (2005) 111–119 [[hep-ph/0506310](https://arxiv.org/abs/hep-ph/0506310)].
- [28] E. Asakawa, S. Kanemura, and J. Kanzaki, *Potential for measuring the $H^+ - W^+ - Z^0$ vertex from WZ fusion at the Large Hadron Collider*, *Phys. Rev. D* **75** (2007) 075022 [[hep-ph/0612271](https://arxiv.org/abs/hep-ph/0612271)].
- [29] S. Godfrey and K. Moats, *Exploring Higgs Triplet Models via Vector Boson Scattering at the LHC*, *Phys. Rev. D* **81** (2010) 075026 [[arXiv:1003.3033](https://arxiv.org/abs/1003.3033)].

[30] J. A. Grifols and A. Mendez, *The WZH^\pm Coupling in $SU(2) \times U(1)$ Gauge Models*, *Phys. Rev. D* **22** (1980) 1725.

[31] M. Cepeda *et al.*, *Report from Working Group 2: Higgs Physics at the HL-LHC and HE-LHC*, CERN Yellow Rep. Monogr. **7** (2019) 221–584 [[arXiv:1902.00134](https://arxiv.org/abs/1902.00134)].

[32] ATLAS and CMS Collaboration, *Highlights of the HL-LHC physics projections by ATLAS and CMS*, arXiv preprint (2025) [[arXiv:2504.00672](https://arxiv.org/abs/2504.00672)].

[33] ILC Collaboration, *The International Linear Collider Technical Design Report - Volume 2: Physics*, arXiv preprint (2013) [[arXiv:1306.6352](https://arxiv.org/abs/1306.6352)].

[34] K. Fujii *et al.*, *Physics Case for the 250 GeV Stage of the International Linear Collider*, arXiv preprint (2017) [[arXiv:1710.07621](https://arxiv.org/abs/1710.07621)].

[35] S. Asai, *et al.*, *Report by the Committee on the Scientific Case of the ILC Operating at 250 GeV as a Higgs Factory*, arXiv preprint (2017) [[arXiv:1710.08639](https://arxiv.org/abs/1710.08639)].

[36] **LCC Physics Working Group** Collaboration, *Tests of the Standard Model at the International Linear Collider*, arXiv preprint (2019) [[arXiv:1908.11299](https://arxiv.org/abs/1908.11299)].

[37] M. Ahmad *et al.*, *CEPC-SPPC Preliminary Conceptual Design Report. 1. Physics and Detector*, arXiv preprint (2015) .

[38] X. Ai *et al.*, *New Physics Search at the CEPC: a General Perspective*, arXiv preprint (2025) [[arXiv:2505.24810](https://arxiv.org/abs/2505.24810)].

[39] **TLEP Design Study Working Group** Collaboration, *First Look at the Physics Case of TLEP*, JHEP **01** (2014) 164 [[arXiv:1308.6176](https://arxiv.org/abs/1308.6176)].

[40] M. B. et al. (FCC Collaboration), *Future Circular Collider Feasibility Study Report: Volume 1, Physics, Experiments, Detectors*, arXiv preprint (2025) [[arXiv:2505.00272](https://arxiv.org/abs/2505.00272)]. CERN-FCC-PHYS-2025-0002.

[41] **ATLAS** Collaboration, *A detailed map of Higgs boson interactions by the ATLAS experiment ten years after the discovery*, Nature **607** (2022) 52–59 [[arXiv:2207.00092](https://arxiv.org/abs/2207.00092)]. [Erratum: Nature 612, E24 (2022)].

[42] **CMS** Collaboration, *A portrait of the Higgs boson by the CMS experiment ten years after the discovery*, Nature **607** (2022) 60–68 [[arXiv:2207.00043](https://arxiv.org/abs/2207.00043)]. [Erratum: Nature 623, (2023)].

[43] S. Kanemura, Y. Okada, E. Senaha, and C. P. Yuan, *Higgs coupling constants as a probe of new physics*, Phys. Rev. D **70** (2004) 115002 [[hep-ph/0408364](https://arxiv.org/abs/hep-ph/0408364)].

[44] S. Kanemura, M. Kikuchi, and K. Yagyu, *Radiative corrections to the Yukawa coupling constants in two Higgs doublet models*, Phys. Lett. B **731** (2014) 27–35 [[arXiv:1401.0515](https://arxiv.org/abs/1401.0515)].

[45] S. Kanemura, M. Kikuchi, and K. Yagyu, *Fingerprinting the extended Higgs sector using one-loop corrected Higgs boson couplings and future precision measurements*, Nucl. Phys. B **896** (2015) 80–137 [[arXiv:1502.07716](https://arxiv.org/abs/1502.07716)].

[46] A. Arhrib, R. Benbrik, J. El Falaki, and A. Jueid, *Radiative corrections to the Triple Higgs Coupling in the Inert Higgs Doublet Model*, JHEP **12** (2015) 007 [[arXiv:1507.03630](https://arxiv.org/abs/1507.03630)].

[47] S. Kanemura, M. Kikuchi, and K. Sakurai, *Testing the dark matter scenario in the inert doublet model by future precision measurements of the Higgs boson couplings*, Phys. Rev. D **94** (2016) 115011 [[arXiv:1605.08520](https://arxiv.org/abs/1605.08520)].

[48] S. Kanemura, M. Kikuchi, K. Mawatari, K. Sakurai, and K. Yagyu, *Full next-to-leading-order calculations of Higgs boson decay rates in models with non-minimal scalar sectors*, *Nucl. Phys. B* **949** (2019) 114791 [[arXiv:1906.10070](https://arxiv.org/abs/1906.10070)].

[49] S. Kanemura, M. Kikuchi, K. Mawatari, K. Sakurai, and K. Yagyu, *Loop effects on the Higgs decay widths in extended Higgs models*, *Phys. Lett. B* **783** (2018) 140–149 [[arXiv:1803.01456](https://arxiv.org/abs/1803.01456)].

[50] L. Altenkamp, S. Dittmaier, and H. Rzehak, *Renormalization schemes for the Two-Higgs-Doublet Model and applications to $h \rightarrow WW/ZZ \rightarrow 4$ fermions*, *JHEP* **09** (2017) 134 [[arXiv:1704.02645](https://arxiv.org/abs/1704.02645)].

[51] M. Aiko, S. Kanemura, and K. Sakurai, *Radiative corrections to decays of charged Higgs bosons in two Higgs doublet models*, *Nucl. Phys. B* **973** (2021) 115581 [[arXiv:2108.11868](https://arxiv.org/abs/2108.11868)].

[52] S. Kanemura, M. Kikuchi, and K. Yagyu, *Next-to-leading order corrections to decays of the heavier CP-even Higgs boson in the two Higgs doublet model*, *Nucl. Phys. B* **983** (2022) 115906 [[arXiv:2203.08337](https://arxiv.org/abs/2203.08337)].

[53] M. Aiko, S. Kanemura, and K. Sakurai, *Radiative corrections to decay branching ratios of the CP-odd Higgs boson in two Higgs doublet models*, *Nucl. Phys. B* **986** (2023) 116047 [[arXiv:2207.01032](https://arxiv.org/abs/2207.01032)].

[54] M. Krause and M. Mühlleitner, *Impact of Electroweak Corrections on Neutral Higgs Boson Decays in Extended Higgs Sectors*, *JHEP* **04** (2020) 083 [[arXiv:1912.03948](https://arxiv.org/abs/1912.03948)].

[55] A. G. Akeroyd, A. Arhrib, and E.-M. Naimi, *Yukawa coupling corrections to the decay $H^+ \rightarrow W^+ A0$* , *Eur. Phys. J. C* **12** (2000) 451–460 [[hep-ph/9811431](https://arxiv.org/abs/hep-ph/9811431)]. [Erratum: *Eur. Phys. J. C* **14**, 371 (2000)].

[56] A. G. Akeroyd, A. Arhrib, and E. Naimi, *Radiative corrections to the decay $H^+ \rightarrow W^+ A0$* , *Eur. Phys. J. C* **20** (2001) 51–62 [[hep-ph/0002288](https://arxiv.org/abs/hep-ph/0002288)].

[57] M. Krause, R. Lorenz, M. Mühlleitner, R. Santos, and H. Ziesche, *Gauge-independent Renormalization of the 2-Higgs-Doublet Model*, *JHEP* **09** (2016) 143 [[arXiv:1605.04853](https://arxiv.org/abs/1605.04853)].

[58] M. Krause, M. Mühlleitner, R. Santos, and H. Ziesche, *Higgs-to-Higgs boson decays in a 2HDM at next-to-leading order*, *Phys. Rev. D* **95** (2017) 075019 [[arXiv:1609.04185](https://arxiv.org/abs/1609.04185)].

[59] F. Bojarski, G. Chalons, D. Lopez-Val, and T. Robens, *Heavy to light Higgs boson decays at NLO in the Singlet Extension of the Standard Model*, *JHEP* **02** (2016) 147 [[arXiv:1511.08120](https://arxiv.org/abs/1511.08120)].

[60] S. Kanemura, M. Kikuchi, and K. Yagyu, *Radiative corrections to the Higgs boson couplings in the model with an additional real singlet scalar field*, *Nucl. Phys. B* **907** (2016) 286–322 [[arXiv:1511.06211](https://arxiv.org/abs/1511.06211)].

[61] S. Kanemura, M. Kikuchi, and K. Yagyu, *One-loop corrections to the Higgs self-couplings in the singlet extension*, *Nucl. Phys. B* **917** (2017) 154–177 [[arXiv:1608.01582](https://arxiv.org/abs/1608.01582)].

[62] L. Altenkamp, M. Bogchia, and S. Dittmaier, *Precision calculations for $h \rightarrow WW/ZZ \rightarrow 4$ fermions in a Singlet Extension of the Standard Model with Prophecy4f*, *JHEP* **04** (2018) 062 [[arXiv:1801.07291](https://arxiv.org/abs/1801.07291)].

[63] F. Egle, M. Mühlleitner, R. Santos, and J. Viana, *Electroweak corrections to Higgs boson decays in a Complex Singlet extension of the SM and their phenomenological impact*, *JHEP* **11** (2023) 116 [[arXiv:2306.04127](https://arxiv.org/abs/2306.04127)].

[64] J. Braathen and S. Kanemura, *On two-loop corrections to the Higgs trilinear coupling in models with extended scalar sectors*, *Phys. Lett. B* **796** (2019) 38–46 [[arXiv:1903.05417](https://arxiv.org/abs/1903.05417)].

[65] J. Braathen and S. Kanemura, *Leading two-loop corrections to the Higgs boson self-couplings in models with extended scalar sectors*, *Eur. Phys. J. C* **80** (2020) 227 [[arXiv:1911.11507](https://arxiv.org/abs/1911.11507)].

[66] J. Braathen, S. Kanemura, and M. Shimoda, *Two-loop analysis of classically scale-invariant models with extended Higgs sectors*, *JHEP* **03** (2021) 297 [[arXiv:2011.07580](https://arxiv.org/abs/2011.07580)].

[67] C. Sturm, B. Summ, and S. Uccirati, *Electroweak corrections to $g + g \rightarrow H_{l,h}$ and $H_{l,h} \rightarrow \gamma + \gamma$ in the Higgs-singlet extension of the Standard model*, *JHEP* **11** (2023) 113 [[arXiv:2212.11835](https://arxiv.org/abs/2212.11835)].

[68] M. Aiko, J. Braathen, and S. Kanemura, *Leading two-loop corrections to the Higgs di-photon decay in the inert doublet model*, *Eur. Phys. J. C* **85** (2025) 489 [[arXiv:2307.14976](https://arxiv.org/abs/2307.14976)].

[69] G. Degrassi and P. Slavich, *On the two-loop BSM corrections to $h \rightarrow \gamma\gamma$ in the aligned THDM*, *Eur. Phys. J. C* **83** (2023) 941 [[arXiv:2307.02476](https://arxiv.org/abs/2307.02476)].

[70] G. Degrassi and P. Slavich, *On the two-loop BSM corrections to $h \rightarrow \gamma\gamma$ in a triplet extension of the SM*, *Eur. Phys. J. C* **85** (2025) 49 [[arXiv:2407.18185](https://arxiv.org/abs/2407.18185)].

[71] G. Degrassi, R. Gröber, and P. Slavich, *Two-loop BSM contributions to Higgs pair production in the aligned THDM*, arXiv (2025) [[arXiv:2508.11539](https://arxiv.org/abs/2508.11539)].

[72] S. Kanemura, M. Kikuchi, K. Sakurai, and K. Yagyu, *H-COUP: a program for one-loop corrected Higgs boson couplings in non-minimal Higgs sectors*, *Comput. Phys. Commun.* **233** (2018) 134–144 [[arXiv:1710.04603](https://arxiv.org/abs/1710.04603)].

[73] S. Kanemura, M. Kikuchi, K. Mawatari, K. Sakurai, and K. Yagyu, *H-COUP Version 2: a program for one-loop corrected Higgs boson decays in non-minimal Higgs sectors*, *Comput. Phys. Commun.* **257** (2020) 107512 [[arXiv:1910.12769](https://arxiv.org/abs/1910.12769)].

[74] M. Aiko, S. Kanemura, M. Kikuchi, K. Sakurai, and K. Yagyu, *H-COUP Version 3: A program for one-loop corrected decays of any Higgs bosons in non-minimal Higgs models*, *Comput. Phys. Commun.* **301** (2024) 109231 [[arXiv:2311.15892](https://arxiv.org/abs/2311.15892)].

[75] M. Krause, M. Mühlleitner, and M. Spira, *2HDECAY —A program for the calculation of electroweak one-loop corrections to Higgs decays in the Two-Higgs-Doublet Model including state-of-the-art QCD corrections*, *Comput. Phys. Commun.* **246** (2020) 106852 [[arXiv:1810.00768](https://arxiv.org/abs/1810.00768)].

[76] I. Engeln, M. Mühlleitner, and J. Wittbrodt, *N2HDECAY: Higgs Boson Decays in the Different Phases of the N2HDM*, *Comput. Phys. Commun.* **234** (2019) 256–262 [[arXiv:1805.00966](https://arxiv.org/abs/1805.00966)].

[77] A. Denner, S. Dittmaier, and A. Mück, *PROPHECY4F 3.0: A Monte Carlo program for Higgs-boson decays into four-fermion final states in and beyond the Standard Model*, *Comput. Phys. Commun.* **254** (2020) 107336 [[arXiv:1912.02010](https://arxiv.org/abs/1912.02010)].

[78] P. Athron, *et al.*, *FlexibleDecay: An automated calculator of scalar decay widths*, *Comput. Phys. Commun.* **283** (2023) 108584 [[arXiv:2106.05038](https://arxiv.org/abs/2106.05038)].

[79] Y. Yamada, *Gauge dependence of the on-shell renormalized mixing matrices*, *Phys. Rev. D* **64** (2001) 036008 [[hep-ph/0103046](https://arxiv.org/abs/hep-ph/0103046)].

[80] A. Freitas and D. Stockinger, *Gauge dependence and renormalization of tan beta in the MSSM*, *Phys. Rev. D* **66** (2002) 095014 [[hep-ph/0205281](https://arxiv.org/abs/hep-ph/0205281)].

[81] J. R. Espinosa and Y. Yamada, *Scale independent and gauge independent mixing angles for scalar particles*, *Phys. Rev. D* **67** (2003) 036003 [[hep-ph/0207351](#)].

[82] J. Papavassiliou, *Gauge independent transverse and longitudinal self energies and vertices via the pinch technique*, *Phys. Rev. D* **50** (1994) 5958–5970 [[hep-ph/9406258](#)].

[83] J. Papavassiliou, *Gauge Invariant Proper Selfenergies and Vertices in Gauge Theories with Broken Symmetry*, *Phys. Rev. D* **41** (1990) 3179.

[84] J. M. Cornwall, *Dynamical Mass Generation in Continuum QCD*, *Phys. Rev. D* **26** (1982) 1453.

[85] D. Binosi and J. Papavassiliou, *Pinch Technique: Theory and Applications*, *Phys. Rept.* **479** (2009) 1–152 [[arXiv:0909.2536](#)].

[86] G. Degrassi and A. Sirlin, *Gauge invariant selfenergies and vertex parts of the Standard Model in the pinch technique framework*, *Phys. Rev. D* **46** (1992) 3104–3116.

[87] J. M. Cornwall and J. Papavassiliou, *Gauge Invariant Three Gluon Vertex in QCD*, *Phys. Rev. D* **40** (1989) 3474.

[88] A. Denner, S. Dittmaier, and J.-N. Lang, *Renormalization of mixing angles*, *JHEP* **11** (2018) 104 [[arXiv:1808.03466](#)].

[89] S. Dittmaier and H. Rzehak, *Electroweak renormalization based on gauge-invariant vacuum expectation values of non-linear Higgs representations. Part II. Extended Higgs sectors*, *JHEP* **08** (2022) 245 [[arXiv:2206.01479](#)].

[90] P. Dey, A. Kundu, and B. Mukhopadhyaya, *Some consequences of a Higgs triplet*, *J. Phys. G* **36** (2009) 025002 [[arXiv:0802.2510](#)].

[91] **Particle Data Group** Collaboration, *Review of particle physics*, *Phys. Rev. D* **110** (2024) 030001.

[92] A. Arhrib, *et al.*, *The Higgs Potential in the Type II Seesaw Model*, *Phys. Rev. D* **84** (2011) 095005 [[arXiv:1105.1925](#)].

[93] B. W. Lee, C. Quigg, and H. B. Thacker, *The Strength of Weak Interactions at Very High-Energies and the Higgs Boson Mass*, *Phys. Rev. Lett.* **38** (1977) 883–885.

[94] B. W. Lee, C. Quigg, and H. B. Thacker, *Weak Interactions at Very High-Energies: The Role of the Higgs Boson Mass*, *Phys. Rev. D* **16** (1977) 1519.

[95] M. Luscher and P. Weisz, *Is There a Strong Interaction Sector in the Standard Lattice Higgs Model?* *Phys. Lett. B* **212** (1988) 472–478.

[96] W. J. Marciano, G. Valencia, and S. Willenbrock, *Renormalization Group Improved Unitarity Bounds on the Higgs Boson and Top Quark Masses*, *Phys. Rev. D* **40** (1989) 1725.

[97] M. Aoki and S. Kanemura, *Unitarity bounds in the Higgs model including triplet fields with custodial symmetry*, *Phys. Rev. D* **77** (2008) 095009 [[arXiv:0712.4053](#)]. [Erratum: *Phys. Rev. D* 89, 059902 (2014)].

[98] M. Bohm, H. Spiesberger, and W. Hollik, *On the One Loop Renormalization of the Electroweak Standard Model and Its Application to Leptonic Processes*, *Fortsch. Phys.* **34** (1986) 687–751.

[99] W. F. L. Hollik, *Radiative Corrections in the Standard Model and their Role for Precision Tests of the Electroweak Theory*, *Fortsch. Phys.* **38** (1990) 165–260.

[100] M.-C. Chen, S. Dawson, and T. Krupovnickas, *Constraining new models with precision electroweak data*, *Int. J. Mod. Phys. A* **21** (2006) 4045–4070 [[hep-ph/0504286](#)].

[101] M.-C. Chen, S. Dawson, and T. Krupovnickas, *Higgs triplets and limits from precision measurements*, *Phys. Rev. D* **74** (2006) 035001 [[hep-ph/0604102](#)].

[102] P. H. Chankowski, S. Pokorski, and J. Wagner, *(Non)decoupling of the Higgs triplet effects*, *Eur. Phys. J. C* **50** (2007) 919–933 [[hep-ph/0605302](#)].

[103] M.-C. Chen, S. Dawson, and C. B. Jackson, *Higgs Triplets, Decoupling, and Precision Measurements*, *Phys. Rev. D* **78** (2008) 093001 [[arXiv:0809.4185](#)].

[104] C.-W. Chiang, A.-L. Kuo, and K. Yagyu, *One-loop renormalized Higgs boson vertices in the Georgi-Machacek model*, *Phys. Rev. D* **98** (2018) 013008 [[arXiv:1804.02633](#)].

[105] S. Kanemura, M. Kikuchi, and K. Yagyu, *New renormalization scheme in the two Higgs doublet models*, *Phys. Lett. B* **858** (2024) 139050 [[arXiv:2408.08033](#)].

[106] A. Denner, *Techniques for calculation of electroweak radiative corrections at the one loop level and results for W physics at LEP-200*, *Fortsch. Phys.* **41** (1993) 307–420 [[arXiv:0709.1075](#)].

[107] J. Fleischer and F. Jegerlehner, *Radiative Corrections to Higgs Decays in the Extended Weinberg-Salam Model*, *Phys. Rev. D* **23** (1981) 2001–2026.

[108] S. Kanemura, M. Kikuchi, K. Sakurai, and K. Yagyu, *Gauge invariant one-loop corrections to Higgs boson couplings in non-minimal Higgs models*, *Phys. Rev. D* **96** (2017) 035014 [[arXiv:1705.05399](#)].

[109] A. Sirlin, *Radiative Corrections in the $SU(2)$ - L \times $U(1)$ Theory: A Simple Renormalization Framework*, *Phys. Rev. D* **22** (1980) 971–981.

[110] N. K. Nielsen, *On the Gauge Dependence of Spontaneous Symmetry Breaking in Gauge Theories*, *Nucl. Phys. B* **101** (1975) 173–188.

[111] G. Passarino and M. J. G. Veltman, *One Loop Corrections for $e^+ e^-$ Annihilation Into $\mu^+ \mu^-$ in the Weinberg Model*, *Nucl. Phys. B* **160** (1979) 151–207.

[112] Aidan Randle-Conde, *Feynman Diagram Tutorial*, <https://www.aidansean.com/feynman/> (2010) .

[113] J. Ellis, *TikZ-Feynman: Feynman diagrams with TikZ*, *Comput. Phys. Commun.* **210** (2017) 103–123 [[arXiv:1601.05437](#)].

[114] M. Dohse.

[115] M. D. Goodsell, S. Liebler, and F. Staub, *Generic calculation of two-body partial decay widths at the full one-loop level*, *Eur. Phys. J. C* **77** (2017) 758 [[arXiv:1703.09237](#)].

[116] E. Braaten and J. P. Leveille, *Higgs Boson Decay and the Running Mass*, *Phys. Rev. D* **22** (1980) 715.

[117] S. G. Gorishnii, A. L. Kataev, S. A. Larin, and L. R. Surguladze, *Scheme dependence of the next to next-to-leading QCD corrections to $\Gamma(\text{tot})$ ($H \rightarrow \text{hadrons}$) and the spurious QCD infrared fixed point*, *Phys. Rev. D* **43** (1991) 1633–1640.

[118] K. G. Chetyrkin and A. Kwiatkowski, *Second order QCD corrections to scalar and pseudoscalar Higgs decays into massive bottom quarks*, *Nucl. Phys. B* **461** (1996) 3–18 [[hep-ph/9505358](#)].

[119] S. A. Larin, T. van Ritbergen, and J. A. M. Vermaasen, *The Large top quark mass expansion for Higgs boson decays into bottom quarks and into gluons*, *Phys. Lett. B* **362** (1995) 134–140 [[hep-ph/9506465](#)].

[120] M. Aiko, *et al.*, *Probing extended Higgs sectors by the synergy between direct searches at the LHC and precision tests at future lepton colliders*, *Nucl. Phys. B* **966** (2021) 115375 [[arXiv:2010.15057](#)].

[121] W.-Y. Keung and W. J. Marciano, *HIGGS SCALAR DECAYS: $H \rightarrow W^- X$* , *Phys. Rev. D* **30** (1984) 248.

[122] B. A. Kniehl, *Higgs phenomenology at one loop in the standard model*, *Phys. Rept.* **240** (1994) 211–300.

[123] S. Dawson and R. Kauffman, *QCD corrections to Higgs boson production: nonleading terms in the heavy quark limit*, *Phys. Rev. D* **49** (1994) 2298–2309 [[hep-ph/9310281](#)].

[124] M. Spira, A. Djouadi, D. Graudenz, and P. M. Zerwas, *Higgs boson production at the LHC*, *Nucl. Phys. B* **453** (1995) 17–82 [[hep-ph/9504378](#)].

[125] K. G. Chetyrkin, B. A. Kniehl, and M. Steinhauser, *Hadronic Higgs decay to order α_s^{**4}* , *Phys. Rev. Lett.* **79** (1997) 353–356 [[hep-ph/9705240](#)].

[126] A. Djouadi, *The Anatomy of electro-weak symmetry breaking. I: The Higgs boson in the standard model*, *Phys. Rept.* **457** (2008) 1–216 [[hep-ph/0503172](#)].

[127] A. Djouadi, *The Anatomy of electro-weak symmetry breaking. II. The Higgs bosons in the minimal supersymmetric model*, *Phys. Rept.* **459** (2008) 1–241 [[hep-ph/0503173](#)].

[128] E. J. Chun, H. M. Lee, and P. Sharma, *Vacuum Stability, Perturbativity, EWPD and Higgs-to-diphoton rate in Type II Seesaw Models*, *JHEP* **11** (2012) 106 [[arXiv:1209.1303](#)].

[129] P. S. Bhupal Dev, D. K. Ghosh, N. Okada, and I. Saha, *125 GeV Higgs Boson and the Type-II Seesaw Model*, *JHEP* **03** (2013) 150 [[arXiv:1301.3453](#)]. [Erratum: *JHEP* 05, 049 (2013)].

[130] F. Arbabifar, S. Bahrami, and M. Frank, *Neutral Higgs Bosons in the Higgs Triplet Model with nontrivial mixing*, *Phys. Rev. D* **87** (2013) 015020 [[arXiv:1211.6797](#)].

[131] C.-S. Chen, C.-Q. Geng, D. Huang, and L.-H. Tsai, *$h \rightarrow Z\gamma$ in Type-II seesaw neutrino model*, *Phys. Lett. B* **723** (2013) 156–160 [[arXiv:1302.0502](#)].

[132] S. Ashanujjaman and K. Ghosh, *Revisiting type-II see-saw: present limits and future prospects at LHC*, *JHEP* **03** (2022) 195 [[arXiv:2108.10952](#)].

[133] **ATLAS** Collaboration, *Measurement of the properties of Higgs boson production at $\sqrt{s} = 13$ TeV in the $H \rightarrow \gamma\gamma$ channel using 139 fb^{-1} of pp collision data with the ATLAS experiment*, *JHEP* **07** (2023) 088 [[arXiv:2207.00348](#)].

[134] **CMS** Collaboration, *Measurements of Higgs boson production cross sections and couplings in the diphoton decay channel at $\sqrt{s} = 13$ TeV*, *JHEP* **07** (2021) 027 [[arXiv:2103.06956](#)].

[135] M. Misiak and M. Steinhauser, *Weak radiative decays of the B meson and bounds on M_{H^\pm} in the Two-Higgs-Doublet Model*, *Eur. Phys. J. C* **77** (2017) 201 [[arXiv:1702.04571](#)].

[136] M. Misiak, A. Rehman, and M. Steinhauser, *Towards $\bar{B} \rightarrow X_s \gamma$ at the NNLO in QCD without interpolation in m_c* , *JHEP* **06** (2020) 175 [[arXiv:2002.01548](#)].

[137] **CMS** Collaboration, *Combined measurements and interpretations of Higgs boson production and decay at $\sqrt{s}=13$ TeV*, CMS-PAS-HIG-21-018 (2025) .

- [138] S. Kanemura, M. Kikuchi, and K. Yagyu, *Probing exotic Higgs sectors from the precise measurement of Higgs boson couplings*, *Phys. Rev. D* **88** (2013) 015020 [[arXiv:1301.7303](https://arxiv.org/abs/1301.7303)].
- [139] S. Kanemura, K. Tsumura, K. Yagyu, and H. Yokoya, *Fingerprinting nonminimal Higgs sectors*, *Phys. Rev. D* **90** (2014) 075001 [[arXiv:1406.3294](https://arxiv.org/abs/1406.3294)].
- [140] D. Jurčiukonis and L. Lavoura, *On the extension of the SM through a scalar quadruplet*, [arXiv:2406.01628](https://arxiv.org/abs/2406.01628).
- [141] M. Aiko, S. Kanemura, and K. Mawatari, *Next-to-leading-order corrections to the Higgs strahlung process from electron–positron collisions in extended Higgs models*, *Eur. Phys. J. C* **81** (2021) 1000 [[arXiv:2109.02884](https://arxiv.org/abs/2109.02884)].
- [142] J. de Blas *et al.*, *Higgs Boson Studies at Future Particle Colliders*, *JHEP* **01** (2020) 139 [[arXiv:1905.03764](https://arxiv.org/abs/1905.03764)].